

Response to referee 1

Interactive comment on “Carbon monoxide climatology derived from the trajectory mapping of global MOZAIC-IAGOS data” by M. Osman et al.

Anonymous Referee #1

Received and published: 24 November 2015

Reviewer’s comments on: "Carbon monoxide climatology derived from the trajectory mapping of global MOZAIC-IAGOS data" by M. Osman, et al.

General Comments

This manuscript by Osman et al. reports a novel use of MOZAIC/IAGOS (or 'M/I') measurements to construct a global, 3D, time-varying climatology for CO. The method relies on the HYSPLIT trajectory model and NCAR/NCEP reanalysis wind fields to 'project' measured CO concentrations to regions and altitudes lacking actual measurements.

The resulting climatology is evaluated first by comparing CO climatology maps generated with forward and backward trajectories separately. The method is then validated by comparing M/I CO statistics at a number of airports with trajectory-mapped climatologies calculated after withholding M/I measurements at each of those airports.

Finally, the CO climatology is compared with MOPITT satellite results, where MOPITT Level 3 CO values have been re-gridded to a 5-by-5 degree grid, matching the resolution of the trajectory-mapped climatology.

While the general method described in the manuscript is novel, the significance of the new climatology product is very unclear. The manuscript includes very little in the way of an error analysis that would permit an understanding of the limitations of the climatology. This analysis should be presented separately from the validation of the method. At a minimum, such an analysis should include (1) a clear description of the underlying assumptions of the method, and the impact of these assumptions on the accuracy of the climatology, and (2) a statistical analysis of the 'robustness' of the climatology (based on the variability of the CO values that are averaged together in each 'bin'). An important assumption that is only vaguely mentioned in the manuscript is that measurements of CO near source regions (e.g., urban regions surrounding airports) are directly useful for estimating CO concentrations large distances both upwind and downwind of the airport. This 'airport effect' would seem to result in a significant positive bias in the trajectory-mapped CO values. A statistical analysis of the variability of the trajectory-mapped CO values is necessary to distinguish regions where the CO climatology is 'statistically robust' from those regions where the uncertainty is very large.

Following the reviewer's suggestion, sample plots of number of samples per grid cell and the standard error of the mean associated with the trajectory-mapping have been added. These are available for each month/year/decade and level in the climatology. We have added text discussing these results as well. We thank the reviewer for drawing our attention to this oversight.

The manuscript does not include a true validation section, which would involve comparing the trajectory-mapped CO climatology with an existing product with known error characteristics. The presented methods for evaluating the climatology are mostly qualitative.

These methods have some value but are rather indirect and inconclusive. For example, since all airports are located near major urban centers, the biasing effects of urban sources of CO may well be similar at different airports. So, the trajectory-mapped climatology may generally represent CO profiles near urban regions better than in rural areas far from sources. If so, the experiments in which trajectory-mapped climatologies are calculated after withholding observations at one airport are still not indicative of the accuracy of the climatology away from urban regions. A more conclusive validation would be based on independent in-situ data from aircraft deployed during some field campaign, where the issue of local sources was known to be unimportant.

The effects of urban sources of CO are indeed observed in the boundary layer. This is an important point that should have been better emphasized and we thank the reviewer for drawing it to our attention. However, the urban effect decreases above the boundary layer since the aircraft travels up to 200-400 km before reaching its cruise altitude, which considerably reduces the effect of urban sources of CO. The following figure shows the comparison between NOAA in-situ data (Novelli et al., 1992; Lang et al., 1992; and Conway et al., 1994; Emmons et al., 2004; Emmons et al., 2009; Deeter et al., 2010) and the trajectory-mapped CO climatology. Individual NOAA CO measurements were compared with the monthly mean trajectory-mapped CO climatology, or if the monthly mean was unavailable, the seasonal mean climatology for that particular location. The total number of NOAA aircraft field campaign CO profiles from for the period 2001-2012 is 1940.

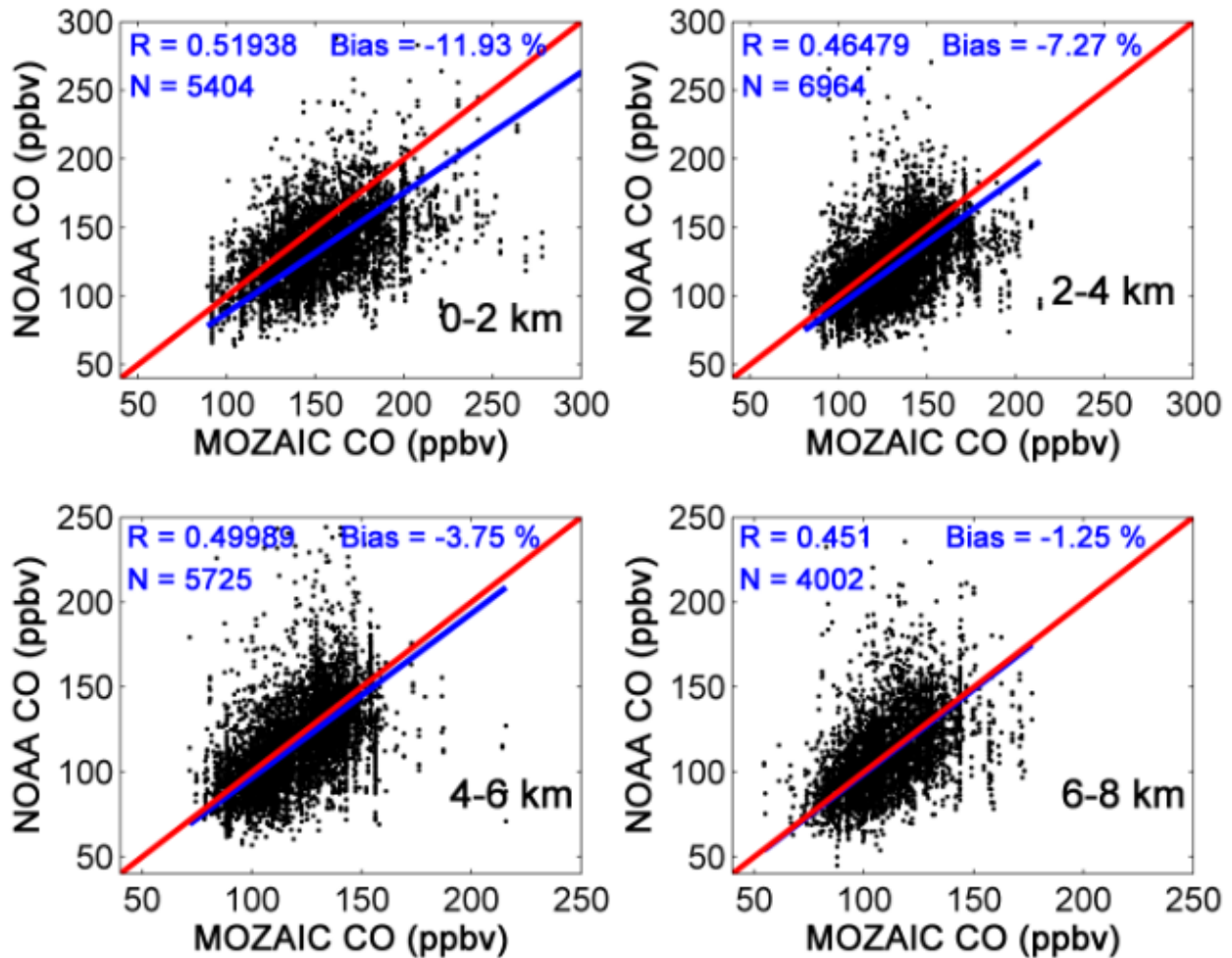
The text has been revised to discuss these points.

Added references:

Conway, T. J., P. P. Tans, L. S. Waterman, K. W. Thoning, D. R. Kitzis, K. A. Masarie, and N. Zhang, Evidence for interannual variability of the carbon cycle from the NOAA/CMDL global air sampling network, *J. Geophys. Res.*, 99, 22,831-22,855, 1994.

Lang, P.M., L. P. Steele, L. S. Waterman, R. C. Martin, K. A. Masarie, and E. J. Dlugokencky
NOAA/CMDL atmospheric methane data for the period 1983-1990 from shipboard flask
sampling NOAA Tech. Memo., ERL CMDL-4, 88 pp., 1992.

Novelli, P. C., L. P. Steele, and P. P. Tans, Mixing ratios of carbon monoxide in the troposphere.
J. Geophys. Res., 97, 20,731-20,750, 1992.



Comparison between NOAA flask profiles and the monthly trajectory-mapped CO climatology for the period from 2001-2012. MOZAIC CO measurements are biased high in the boundary layer as CO values near airports are typically above background.

The comparisons of the trajectory-mapped climatology with MOPITT Level 3 products re-gridded at 5-degree resolution have only qualitative value due to several effects. First, the trajectory-mapped CO values are based on in-situ measurements near urban regions (esp. in the lower troposphere), whereas MOPITT Level 3 products at 5-degree resolution represent a mix of urban and mostly rural atmospheric conditions. This effect would very likely result in a positive bias in the trajectory-mapped climatology. Second, because of the significant variability of MOPITT retrieval performance with respect to various geophysical parameters (surface type, CO

loading, thermal contrast), the validity of MOPITT averaging kernels averaged over large regions is unclear. All previous published MOPITT validation papers have exploited MOPITT Level 2 data averaged over much smaller regions.

Major Revisions

1. Most readers will find this paper unreasonably long and it should therefore be shortened. I believe the paper should be split into a 'methodology and validation' paper (based on Sections 1-4) and a separate 'analysis' paper (based on Sections 5 and 6). Given that some parts of the methodology need to be lengthened (see below), reducing the paper's length is even more important.

Following the reviewer's comments, the O₃-CO subsection (6.2) has been removed from the paper in order to reduce its size. Other reductions have been made as well.

2. The paper should include a section specifically addressing errors in the trajectory mapped CO climatology product. In addition to other sources of potential error (e.g., chemistry and trajectory errors), this quantitative error analysis should estimate the magnitude of systematic errors due to the fact that the M/I CO measurements in the lower-troposphere (e.g., 800 hPa to 1000 hPa) are likely biased towards CO concentrations observed over urban regions near airports. The error analysis should also provide information on the statistical robustness of the climatology product in relation to the variability of the trajectory-mapped CO values which are averaged together in each climatology bin. This statistical analysis should then be used to assess the expected geographical variability of the uncertainties of the trajectory-mapped CO climatology.

As suggested by the reviewer, we added plots and discussion of the standard errors of the mean and number of sample per grid point associated with the trajectory mapping. These maps are available on the FTP site for each month/year/decade and level in the climatology. We have added some discussion of these to the text. We have also added discussion of the "airport effect".

Standard errors associated with the trajectory mapping:

Figure X2 shows the standard errors associated with trajectory mapping and the number of samples per grid cell for monthly, seasonal and annual averages at 4.5 km. Similar figures for other levels are included with the climatology on the FTP site. The largest number of samples per grid cell and the lowest standard errors are found over North America and Europe as there are more frequent MOZAIC-IAGOS aircraft flights in this region. The standard error is computed using all data points found inside a grid cell. This is probably biased somewhat low since some grid cells may contain more than one value from a particular trajectory. This bias is likely not more than a factor of 2, based on typical trajectory lengths.

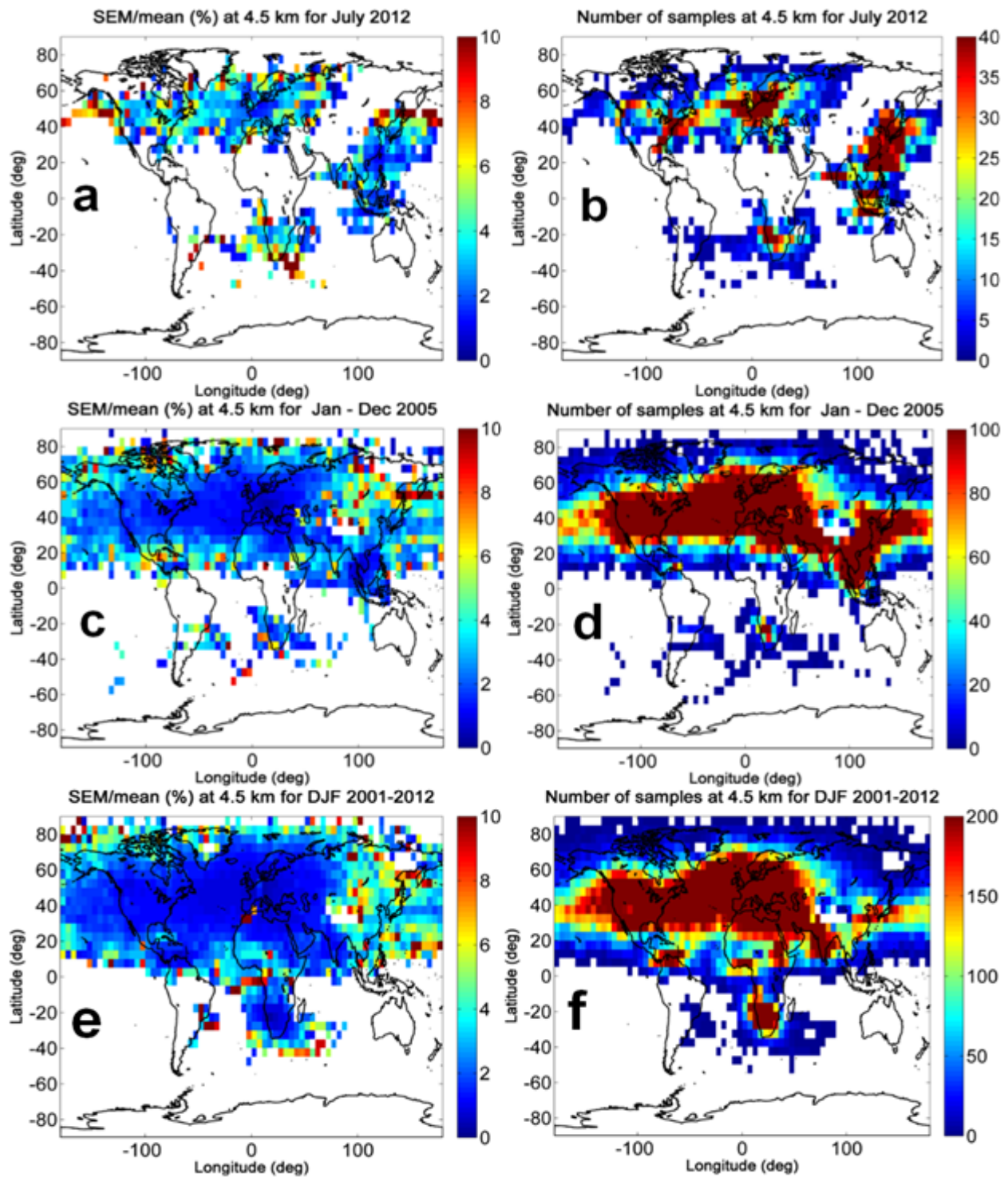


Fig. X2. The standard error of the mean (left panels) and number of samples (right panels) for monthly (July 2012), annual (2005), seasonal (DJF 2001-2012) means at 4.5 km altitude above sea level. The month and year shown are chosen as typical; other months and years show similar patterns. The data are binned on a $5^\circ \times 5^\circ$ latitude and longitude grid.

3. The purpose of the comparisons with MOPITT Level 3 products is unclear. Is the intent to use MOPITT products to validate the MOZAIC-based CO climatology, or is it the other way around? Statements on pages 18, 19, and 20 suggest that the trajectory mapped CO climatology reveals biases in the MOPITT V6 product, despite the fact that this product has already been thoroughly validated against in-situ data obtained from NOAA aircraft and the HIPPO field campaign. True validation involves comparisons of a new product with an established product with known error characteristics.

In this case, it seems that the error characteristics of the MOPITT product are better understood and better quantified than the errors associated with the trajectory-mapped climatology. Thus, it seems more reasonable to conclude that the MOPITT V6 product reveals biases in the trajectory-mapped CO climatology (than the other way around).

The main purpose of the comparison of the trajectory mapped CO climatology with MOPITT is simply to show that trajectory mapping produces global maps that look reasonable, and that the mapping product agrees fairly well with MOPITT even far from airports. The difference at higher altitudes is surprising, however, and we felt that it was important to note this in the paper. Since it is not our intent to validate MOPITT, we merely show, by showing that we get similar differences with unmapped MOZAIC data (using Frankfurt as an example), that the differences are not due somehow to the mapping procedure. This, of course, we considered unlikely beforehand, as trajectory errors are found to be typically random; we have observed no biases in our work to date. Such biases would have to stem from the NCEP meteorological reanalyses used as input, which have themselves been extensively validated.

4. The comparisons with MOPITT total column values (Section 4.2) appear to be based on incorrect assumptions regarding the MOPITT layering scheme, and should be repeated and reanalyzed. Specifically, the assumed layer boundaries (at the midpoints between the MOPITT retrieval levels) do not agree with the layering scheme discussed in Deeter et al., (2013) and in the MOPITT V5 User's Guide.

Indeed. Corrected, and description corrected in the text.

Minor Revisions and Technical Corrections

p. 2, l. 16 - 'comparison' should be 'comparing'

Done.

p. 2, l. 22 - Are the results really conclusive that MOPITT is biased, or are the authors really just stating that there is some bias between MOPITT and the trajectory-mapped climatology?

No, it is not our intent to validate MOPITT. We have rephrased the text to make our conclusions less definitive. We do see a puzzling difference at higher altitudes, but that could of course be some unknown problem with the aircraft measurements at lower pressures.

p. 2, Abstract - Should be some brief statement about the limitations of the climatology, e.g. primarily for Northern Hemisphere.

We have noted this, and also the urban effect in the boundary layer. In areas where there are few profiles or even none, most of the information comes through relatively long range transport with associated larger uncertainties.

p. 5, l. 9 - The meaning of the sentence "Background CO levels are found ..." is unclear.

We replaced the sentence in p. 5 l. 9-10 by:

Long range atmospheric transport redistributes CO widely due to its relatively long lifetime. Typical tropospheric background CO levels range between 50 and 120 ppbv (WHO, 2000).

We've added the reference:

WHO, Air quality guidelines for Europe, 2nd ed. Copenhagen, World Health Organization Regional Office for Europe, 2000 (WHO Regional Publications, European Series No. 91), 2000

p. 5, l. 13 - There is insufficient evidence for this claim.

Replaced by: "CO values as high as 1800 ppbv have been reported over Beijing (Zbinden, et al., 2013).

p. 6, l. 25 - What are these 'obvious advantages'?

The trajectory approach takes into account known atmospheric motions from the NCEP meteorological wind fields. The advantage over linear or quadratic interpolation is that it uses additional information about the atmosphere, and therefore can be expected to give a better estimate of the redistribution of CO. Using linear or quadratic interpolation is the default best estimate in the absence of such knowledge. Text revised.

p. 6, l. 28 - This statement is premature, since no data have yet been presented in the manuscript.

The trajectory-mapped MOZAIC-IAGOS CO climatology is publicly available at ftp://es-ee.tor.ec.gc.ca/pub/ftpd/MOZAIC_output_CO/. We removed the text that discusses about O3-CO correlations in p. 7 to shorten the manuscript.

p. 7, l. 13 - typo in 'transformation'

Corrected.

p. 7, l. 20 - There is no clear reason for dividing the MOPITT-related material into Sections 2.4 and 4; they should be combined in a single section.

We agree and have moved the first part of Section 4 as suggested.

p. 8, l. 21 - what fraction of the airports (or MOZAIC profiles) are located in the Southern Hemisphere?

Nearly 9 % of the airports are located in the SH and 6% of MOZAIC-IAGOS profiles are from the SH.

p. 9, l. 1 - This is incorrect; MOPITT retrievals do not rely on thermal contrast between the surface and atmosphere (but do rely on a temperature gradient within the atmosphere).

Corrected as p.9 l.1-2: "thermal contrast between the Earth's surface and atmosphere" replaced by "a temperature gradient within the atmosphere"

p. 9, l. 6 - Which MOPITT product is exploited in this paper, the TIR-only, NIR-only, or TIR/NIR?

Added p. 9, l. 1- added: TIR/NIR

p. 9, l. 19-26 - MOPITT validation results vary widely from one version to another; only V6 validation results should be listed here since results for other versions are irrelevant.

We agree and have removed the irrelevant sections as suggested by the reviewer. We thank the referee for identifying this.

p. 10, l. 4 - Why were the M/I cruise data not used?

The cruise data are less useful for our purposes since they are all near the tropopause. However, we have used them for validation (see Fig. 6, now Fig. 7).

p. 11, l. 3 - A thorough discussion of the potential effects of source regions on the trajectory-mapped climatology is needed here; It is not conclusive that qualitative comparisons of maps based separately on backward or forward trajectories prove that source regions have an insignificant effect.

The issue with sources is that while forward trajectories should redistribute the CO correctly, backward trajectories will (erroneously) map the CO to places upwind of where it was generated. We have expanded the text on this point.

p. 12, l. 19 - Add reference to Worden et al (Atmos. Meas. Tech., 6(7), 1633–1646, doi:10.5194/amt-6-1633-2013) regarding the variables which affect MOPITT averaging kernels.

Added:

Worden, H. M., Edwards, D. P., Deeter, M. N., Fu, D., Kulawik, S. S., Worden, J. R., and Arellano, A.: Averaging kernel prediction from atmospheric and surface state parameters based on multiple regression for nadir-viewing satellite measurements of carbon monoxide and ozone, Atmos. Meas. Tech., 6, 1633-1646, doi:10.5194/amt-6-1633-2013, 2013.

p. 13, l. 22 - Here the manuscript lacks important details. Exactly how were the CO concentrations at the 'missing' MOPITT levels (above the maximum MOZAIC aircraft altitude) determined? How many levels in the vertical grid are actually affected by this?

Note that the described strategy of using MOPITT a priori profiles is inconsistent with methods used in MOPITT validation papers and might lead to unphysical discontinuities in the CO profile. Does the chosen method of filling in these high levels affect the results?

If the top of the monthly mean trajectory-mapped MOZAIC-IAGOS CO vertical profile (that is interpolated to MOPITT pressure levels) is below 100 hPa, we use the corresponding MOPITT monthly a priori profile for the missing CO data above the highest trajectory-mapped altitude. However, most of the trajectory-mapped CO profiles reach up to altitude 200-100 hPa, which is about 14 km above sea level. Thus for extending the trajectory-mapped MOZAIC-IAGOS CO profiles to the highest MOPITT level, we have utilized the MOPITT a priori profile mostly for 100 hPa and sometimes for 200 hPa. The same procedure has been used in previous work. de Laate et al. (2012) have shown robust results by using MOPITT a priori profiles for the missing MOZAIC-IAGOS in situ measurements above the maximum MOZAIC-IAGOS aircraft altitude. The authors found the errors as a result of using the MOPITT a priori profile for the missing MOZAIC-IAGOS in situ measurements above the maximum MOZAIC-IAGOS aircraft altitude to be about 5 % or less. Since the maximum altitude of the top of the trajectory-mapped data (i.e., ~14 km) is greater than the maximum altitude reached by the MOZAIC-IAGOS aircraft (i.e., ~12 km), the error in our comparison can be expected to be smaller yet.

p. 14, l. 17 - Why exclude airports in the Southern Hemisphere from the validation study?

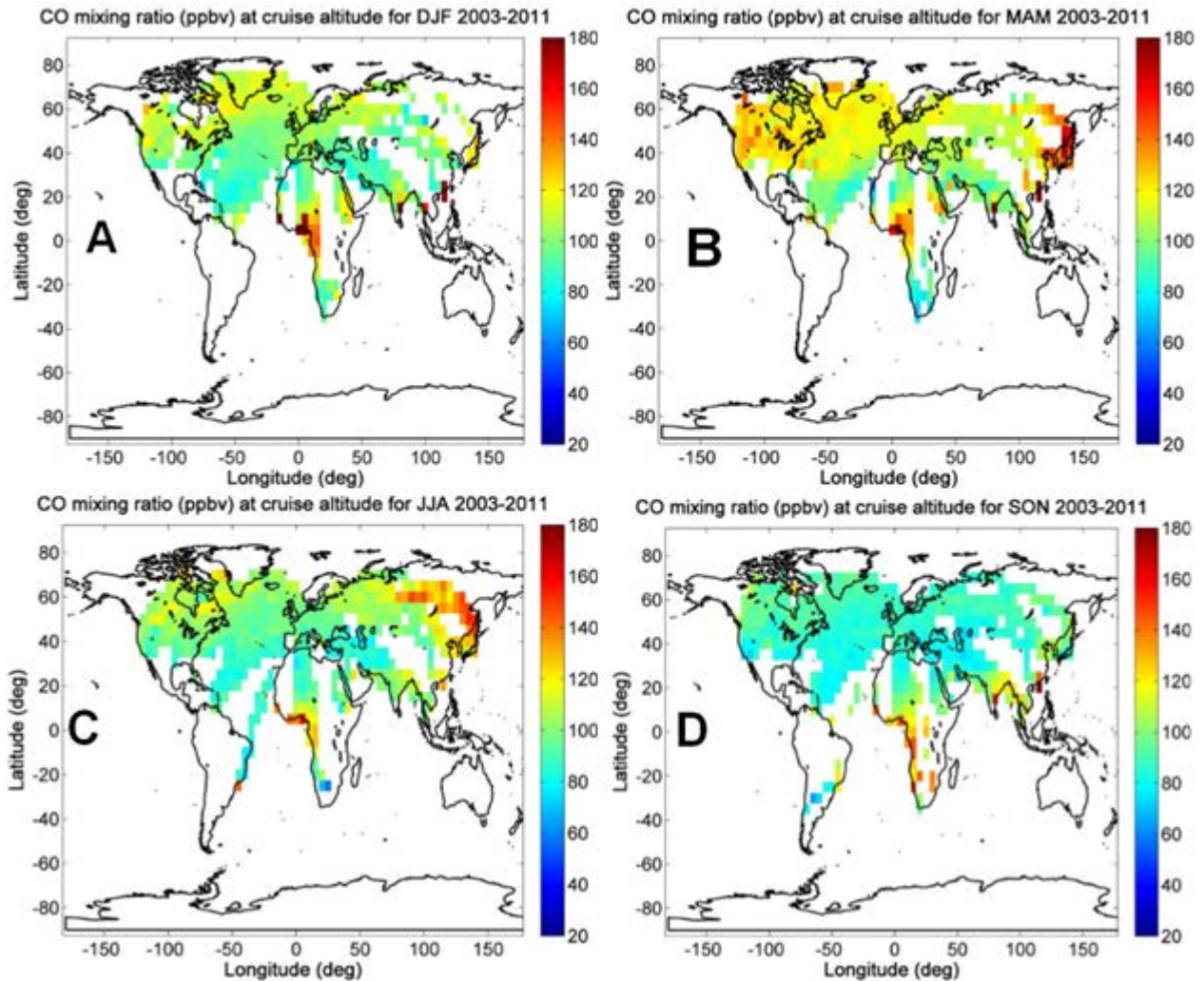
Unfortunately, there are limited MOZAIC-IAGOS data in the SH. Consequently, if an airport in the SH excluded from the trajectory-mapped calculation for the validation, most of the information comes via relatively long trajectories, which are associated with larger uncertainties, and the comparison becomes uncertain as well.

p. 15, l. 25 - All of the listed airports are located in the Northern Hemisphere. Should include several from the Southern Hemisphere, where the climatology might be more challenged.

Please see above.

p. 16, l. 15 - For readers' convenience, online M/I CO maps should be reproduced in the manuscript (with permission) to compare against Fig. 6.

The following figure is reproduced and added in the manuscript (now shown in Fig. 7).



p. 17, l. 22 - Both the shapes and magnitudes (or areas) of the averaging kernels are significant.

Done. In p. 17, l. 22 - shapes replaced by shapes and magnitudes (or areas)

p. 17, l. 7 - It is unclear if the analysis of Fig. 2 is included just as an example, or if it supposedly illustrates overall bias in MOPITT. Any conclusions about MOPITT retrieval bias should compare findings to MOPITT validation papers; possible reasons for any discrepancies in validation results (relative to published results) should be discussed.

Figure 2 (now Figure 3) is included as an illustration and it reveals the discrepancy between trajectory-mapped and MOPITT CO. Possible reasons are noted.

p. 18, l. 10 - Which MOPITT product was used: TIR-only, NIR-only or TIR/NIR?

TIR/NIR

p. 18, l. 10 - Emphasize that standard MOPITT L3 retrievals have been regridded to 5-degree resolution for this analysis.

Added in p18, l 11 : The standard MOPITT V6L3 retrievals have been regridded to 5-degree resolution for this analysis.

p. 18, l. 27 - Are the authors suggesting that the trajectory-mapped CO climatology can be used to validate MOPITT, or are the MOPITT data being used to validate the MOZAIC CO climatology? This sentence observes that there is a difference between the two products ("reveals significant biases between MOPITT and the trajectory-mapped ..."), while the first sentence in the next paragraph ("MOPITT seems to underestimate ...") suggests that the trajectory-mapped CO climatology can be used to determine biases in MOPITT products.

No, it is not our intent to validate MOPITT. We have rephrased the text to make our conclusions less definitive. We do see a puzzling difference at higher altitudes, but that could of course be some unknown problem with the aircraft measurements at lower pressures.

p. 19, l. 5 - This is incorrect; all previous MOPITT validation work was performed with MOPITT Level 2 products, not Level 3 products. This may be related to the significant discrepancies in the validation results reported in this manuscript compared to previously Corrected. We thank the referee for identifying the error.

p. 19, l.9 - It is not true that all published MOPITT validation results have been based on NOAA flask sampling.

Corrected.

p. 19, l. 10-19 - Comparisons of MOPITT L3 data (w/ 5-degree resolution) and M/I profiles for one airport (Frankfurt) do not provide convincing evidence of a general negative bias in the MOPITT retrievals, especially given that MOPITT V6 validation results have been previously reported for a large number of NOAA sites and for the HIPPO field campaign (Deeter et al., 2014).

The comparison of MOZAIC-IAGOS in situ profiles at Frankfurt against MOPITT is intended only to show that the differences are not due somehow to the mapping procedure, since we get similar differences with unmapped MOZAIC data (using Frankfurt as an example),

p. 19, l. 12 - It is unclear if these comparisons are based on standard MOPITT L3 data, or the regridded 5-degree resolution L3 data.

Added: the comparison is based on the regridded 5-degree resolution MOPITT V6L3 data

p. 20, l. 12 - It is unclear why MOPITT retrievals in the lower troposphere would only yield a lower-bound (although it is true that such retrievals are often highly constrained by the a priori).

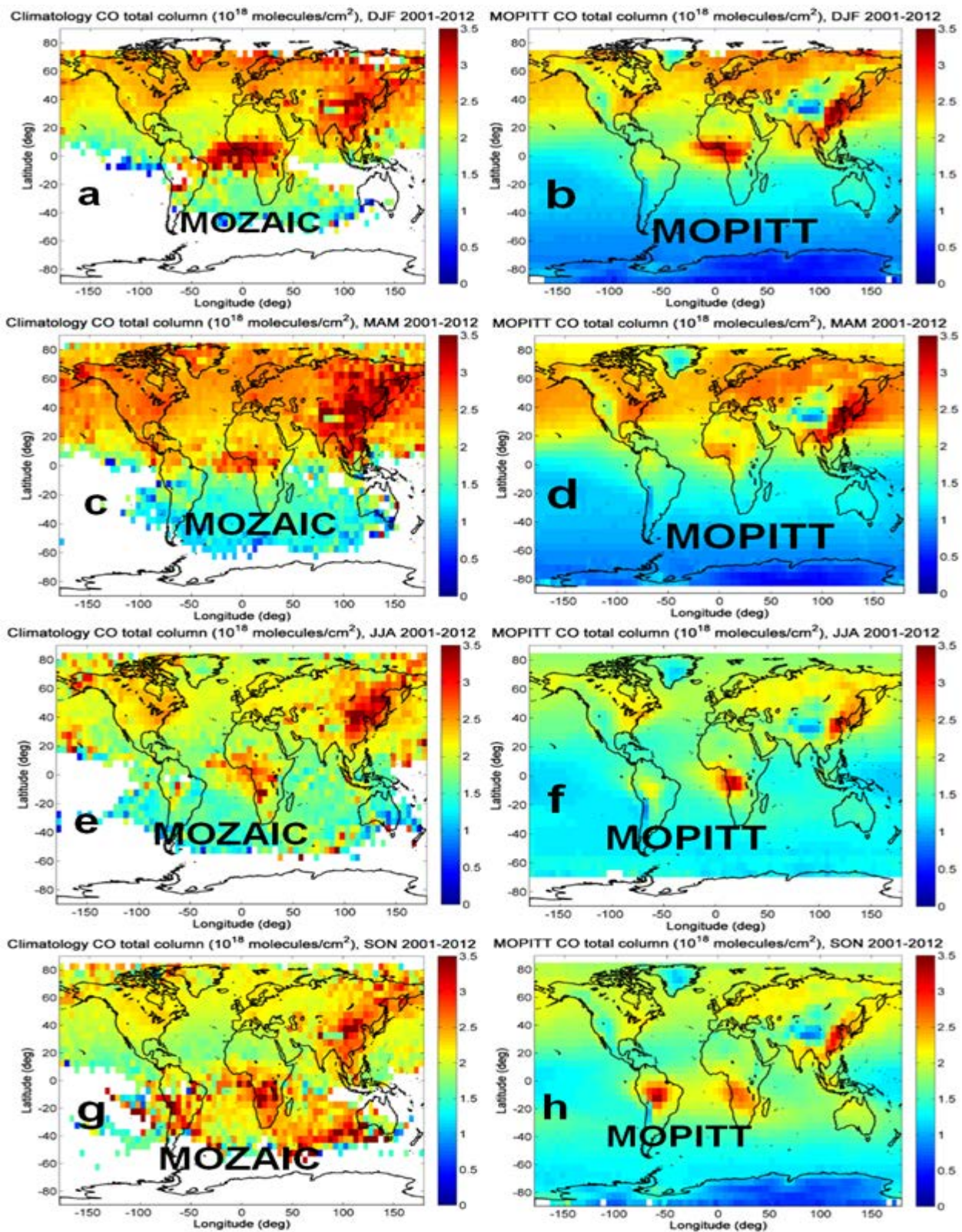
We were citing an observation by Liu et al. (2005), who noted that MOPITT has low sensitivity to CO in the lower troposphere. However, we have removed those remarks in the current version.

p. 21 - References are needed for the text and equations presented in Section 4.2.

added p21. 16:: Deeter 2002 and Emmons et al. (2004)

added p21. 113: Deeter 2002 and Emmons et al. (2004)

added p22 15: Deeter 2002 and Emmons et al. (2004)



August 2002 to DJF, December 2005 to MAM, December 2011 to JJA and August 2012 to SON 2001-2012. Total column values correcting the MOPITT layering scheme.

=====

Deeter, M. N. (2009), MOPITT (Measurements of Pollution in the Troposphere) Validated Version 4 Product User's Guide, National Center for Atmospheric Research. Available at http://web3.acd.ucar.edu/mopitt/v4_users_guide_val.pdf.

Deeter, M. N. (2011), MOPITT (Measurements of Pollution in the Troposphere) Validated Version 5 Product User's Guide, National Center for Atmospheric Research. Available at http://www.acom.ucar.edu/mopitt/v5_users_guide_beta.pdf

Deeter, M. N. (2013), MOPITT (Measurements of Pollution in the Troposphere) Validated Version 6 Product User's Guide, National Center for Atmospheric Research. Available at https://www2.acom.ucar.edu/sites/default/files/mopitt/v6_users_guide_201309.pdf

Deeter, M. N. (2002), Calculation and Application of MOPITT (Measurements of Pollution in the Troposphere) Averaging Kernels, Available at http://www.acom.ucar.edu/mopitt/data/avg_krnls_app.pdf

We thank the referee for his/her careful review and very helpful remarks.

Response to referee 2

Interactive comment on “Carbon monoxide climatology derived from the trajectory mapping of global MOZAIC-IAGOS data” by M. Osman et al.

Anonymous Referee #2

Received and published: 30 November 2015

General Comments

The paper of Osman et al. presents a global, height-resolved climatology of tropospheric carbon monoxide (CO) from MOZAIC-IAGOS data. A trajectory mapping approach was used to inter- and extrapolate the aircraft data to a regular spatial grid.

Several evaluation and validation efforts of the new climatology are presented. This includes detailed comparisons with MOPITT satellite measurements. Furthermore, horizontal and vertical distributions and trends of the CO distributions from the climatology as well as correlations with ozone distributions are discussed.

I found that the paper is well written and interesting to read. It fits in the scope of ACP. Most of the analyses presented here appear to be scientifically sound. The new data set will be of interest for atmospheric modellers looking for CO data sets to initialize and validate their simulations. It will be also helpful to retrieval scientists that could use it as a priori information and for regularization of the retrievals. My main concern is that the paper is very long. In the revision I would suggest to try to shorten and condense the information as much as possible. Specific comments and technical corrections for the author’s consideration are given below.

[We thank the referee for his thoughtful remarks. All the referees felt this way, so we have removed some sections and figures and tried to reduce the text as well.](#)

Specific Comments

p29874, 18-p29875, 12: Such detailed background information on CO photochemistry might not be needed in this observational paper.

[We've reduced the discussion of CO photochemistry.](#)

p29876, 18-10: It seems your climatology is in fact four-dimensional, taking the time domain into account?

[That's correct, if we consider time as a dimension.](#)

p29878, 17: Does the 5% calibration error count as "accuracy" rather than "precision" error of the measurements?

It is described as a calibration uncertainty by Nédélec et al., (2003), so it can be regarded as a systematic uncertainty.

p29878, 123: Is there a general reference for MOPITT?

Drummond and Mand, 1996.

p29881, 111-12: How large are the typical vertical errors of your trajectory calculations?

That is discussed briefly on page 29881, and more thoroughly in our previous work. Also, Draxler et al. (1997) suggest that the total error accompanying a HYSPLIT generated trajectory to be anywhere from 15-30% of the travel distance. We have expanded slightly on this in the revised text.

p29881, 124-25: Is there a smooth transition of the correlation length between the troposphere and stratosphere?

Not likely --- based on ozone correlation lengths, (Figs. 5a & 5b of Liu et al., 2009) the transition is not smooth.

p29882, 116: Vectors (\mathbf{x} , \mathbf{x}_a ,...) should appear in bold face, I think. You might add an additional term (+ $G \epsilon$) in Eq. (2) to remind the reader that retrieval is also influenced by measurement errors (e.g., retrieval noise).

Done.

$$\mathbf{x}_{\text{ret}} = \mathbf{x}_a + \mathbf{A}(\mathbf{x} + \mathbf{x}_a) = \mathbf{A}\mathbf{x} + (\mathbf{I} + \mathbf{A})\mathbf{x}_a + \boldsymbol{\epsilon} \text{ (or } \mathbf{G}\boldsymbol{\epsilon})$$

where $\boldsymbol{\epsilon}$ is the retrieval error due to random errors in the measurement and systematic errors in the forward model (e.g., the error in the atmospheric temperature retrieval) and where G is a gain matrix and where e is the measurement error vector.

p29883, 19-10: How large are the areas of the averaging kernels? Are they close to one? Another interesting quantity would be the FWHM of the averaging kernels, providing a measure of the vertical resolution of the retrievals.

The computed mean area of the averaging kernels is close to unity, but they vary considerably, as can be seen from Figure 2 (now Figure 3). The value of the number of degrees of freedom for the signal (DFS), which is calculated as the diagonal element sum of the averaging kernels, is typically 1.5 to 2. DFS provides an estimate of the number of independent pieces of information contained in the measurements. The full-width at half maximum (FWHM) in Fig. 2a (now Fig. 3a) of the 200-1000 hPa curves is approximately 5-6 km and the largest value of about 7.5 km is seen for the 500 hPa curve. In Fig. 2b (now Fig. 3b), the averaging kernels between 300 and 500 hPa are reasonably sharply peaked with their FWHM about 6 km.

p29891, 12-23: This text might better fit into the method/theory section (Sect. 2.4)?

We agree and have moved it as suggested.

p29892, 11-5: Vectors should be printed in bold face, I think.

$$c_{ret} = c_a + a(x + x_a)$$

$$c_a = t^T x_a$$

Done.

p29902, 114-15: I would also expect that the trajectory approach performs better than linear/quadratic interpolation, but this was not shown the paper.

Strictly speaking, that is true. We have removed this statement from the Conclusions. Instead, we note that the trajectory approach takes into account known atmospheric motions from the NCEP meteorological wind fields, and therefore can be expected to give a better estimate of the redistribution of CO than linear or quadratic interpolation, as it uses additional information about the atmosphere.

Using linear or quadratic interpolation is the default best estimate in the absence of such knowledge, so the worst case of trajectory mapping should be equivalent to linear/quadratic interpolation.

p29904, 14-9: Perhaps mention (once more) how the climatology data can be accessed?

Added on p29904,19: The data set is publically available at

ftp://es-ee.tor.ec.gc.ca/pub/ftpd/MOZAIC_output_CO/

Figures: Some figures (e.g., Fig. 2, 3, 15) have very small font sizes and low quality and resolution, making it difficult to read labels.

Done.

Technical Corrections

p29879, 112: "southward local equator" -> "southward equator" (?)

Done.

p29880, 17: remove brackets around url

Done.

p29886, 122: reveals _that_

Done.

p29886, 124: _an_ increasing number

Done.

p29888, 119-20: reword "a very few" (?)

Replaced by "a very small number"

p29890, 119: remove "also"

Done.

p29890, 119: except _for a_ few

Done.

p29892, 113: which _is_ not

Done.

p29892, 121: African -> Africa

Done.

We thank the referee for his/her careful review and very useful remarks.

Response to referee 3

Interactive comment on “Carbon monoxide climatology derived from the trajectory mapping of global MOZAIC-IAGOS data” by M. Osman et al.

Anonymous Referee #3

Received and published: 10 December 2015

General comments

The authors present a new climatology based on the unique dataset of CO profile observations from MOZAIC and IAGOS measured since 2001. This data is an invaluable complement to the existing global observations from surface stations and satellite retrievals, particularly for the free troposphere and UT/LS regions. An attempt is made to widen the unevenly distributed observations by calculating forward and backward trajectories. As can be seen from the comparison with MOPITT retrievals this works out quite well in most parts of the Northern Hemisphere and the Tropics, while the lack of flight data in the Southern Hemisphere hampers the climatology completeness and probably also its correctness there. The paper structure is sound and the data and methods used for this study are relevant and of importance for global chemistry and air quality monitoring. I'd like to see the manuscript published, if the following basic items will be addressed:

We thank the referee for his thoughtful remarks.

- The influence of the available number of MOZAIC/IAGOS observations on your climatology should be examined in more detail. Particularly for the southern edges of the MOZAIC flight corridors the agreement of forward and backward trajectories and the comparisons to MOPITT seem to be weak as also pointed out in my specific comments.

Can you give an error estimate for each grid box of the climatology simply based on the number of trajectories calculated or give at least a (map) overview of the number of trajectories used in each grid box?

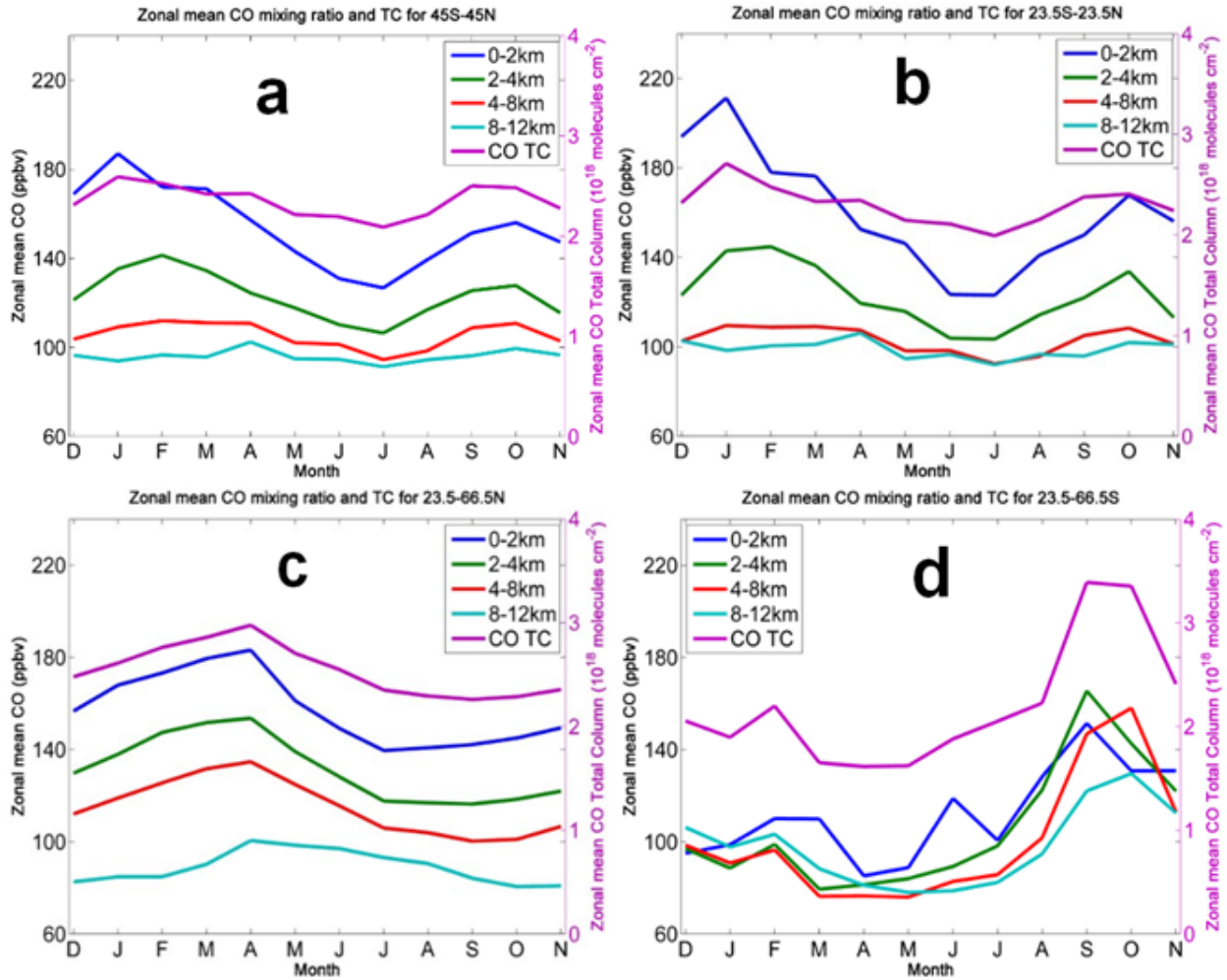
Following the reviewer's suggestion, sample plots of number of samples per grid cell and the standard error of the mean associated with the trajectory-mapping have been added. These are available for each month/year/decade and level in the climatology. We have added text discussing these results as well. We thank the reviewer for drawing our attention to this oversight.

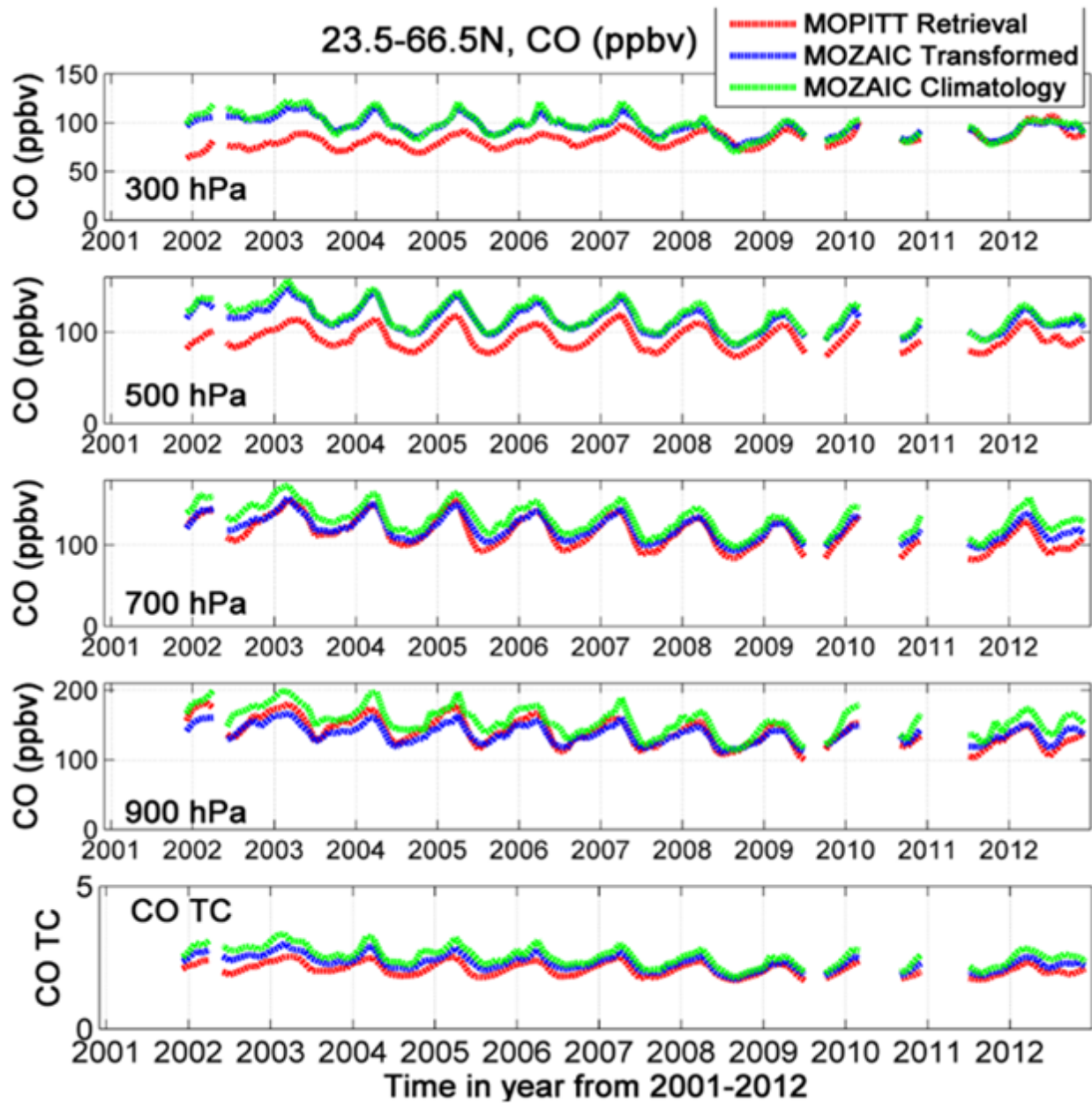
- In several cases it would be more comprehensive to compare zonal averages instead of maps. Moreover the chosen months and years in the Figures often look arbitrary.

We changed Figs. 10 and 11 (now Figs. 12 & 13) to seasonal CO column mean, but have kept Fig. 7 (now Fig. 9) as it is, noting in the text that other months show similar distributions.

Please stick to seasonal climatologies or to a few same examples wherever possible. Total column comparisons to MOPITT could be added to Figures 13 and 17.

Done.





- The manuscript is too long which can be seen most prominently in the number of Figures. I propose to shorten section 6.1 (including Figures S4-S6) significantly as well as the discussion of Figures 19-21, skipping Figures 19-20. Figures 2 and 9 can be minimized and Figures 4 and 5 can be combined into one Figure.

In order to reduce the size of the paper, section 6.2 has been removed from the manuscript. As suggested by the referee, several figures were reduced or removed.

Specific comments

p.29875, 1.10-14: You could give upper limits of observed values for these polluted regions. Values can be higher than 1000 ppb (see e.g. Wang et al., 2004)

Added. p.29875, 1.10-14: We found the seasonal mean maximum of 1516 ppbv during Fall 2001-2012 in the same region.

p.29877, 1.3-5: The sentence only repeats your statement on p.29876, l. 25-28. Please combine.

Done.

p.29877, 1.5-7: Please give some short information (or reference) here on how the source distribution of CO can be derived from the O3-CO correlations.

This section has been removed from the paper to reduce the size of the manuscript.

p.29878, 1.13: Please insert here that you are using only profile data from takeoff and landing.

OK.

p.29879, 1.6-8: Are there any references available for these MOPITT products? What is the version of the total column product?

Deeter et al. (2014) is a reference for MOPITT V6L3.

p.29879, 1.19-29: To which versions of the MOPITT retrievals do these bias estimates refer to? What is the expected or reported difference of version 6 retrievals to those products?

As they refer to versions of MOPITT other than V6, we have removed from them from the manuscript as suggested by Referee.#1.

p.29880, 1.3: In the abstract you limit the maximum altitude to 14 km. Please clarify.

The maximum altitude of the aircraft at cruise height is about 12 km and the number of advected air parcels reaching altitudes above 14 km is very small. Consequently, we report our data for a maximum altitude of 14 km. In fact, our upper limit is 20 km, but only a few parcels are seen above 14 km.

p.29880, 1.2-6: Did you use the exact horizontal position of the airplane during ascent/descent to start the trajectories or did you always start from the airport geographical location? The aircraft position can deviate considerably from the airport position, particularly for higher flight altitudes.

We used the exact location of the aircraft to start the trajectories. Text revised to note this.

p.29882, 1.2: Please give the exact path to the CO data. On the given ftp server, several directories would fit.

ftp://es-ee.tor.ec.gc.ca/pub/ftpd/MOZAIC_output_CO/

p.29883, 1.25-26: I don't understand why a horizontal mapping from 1x1 to 5x5 needs a linearity in log pressure and CO mixing ratio. Please expand or omit. Figure 2 could be shortened to one example.

This was an error. We have corrected the text.

p.29884, 1.24 – p.29885, 1.3: From Figures 3 and S1 I can see quite large differences for many occasions, e.g. regions in Northern Asia or the tropical Atlantic ocean, where differences are higher than 50%. The quality of Figure 3 needs to be improved.

As suggested by the referee, Figure 3 (now Figure 4) has been replotted and the quality improved.

p.29885, 1.13: Why did you choose the month of May?

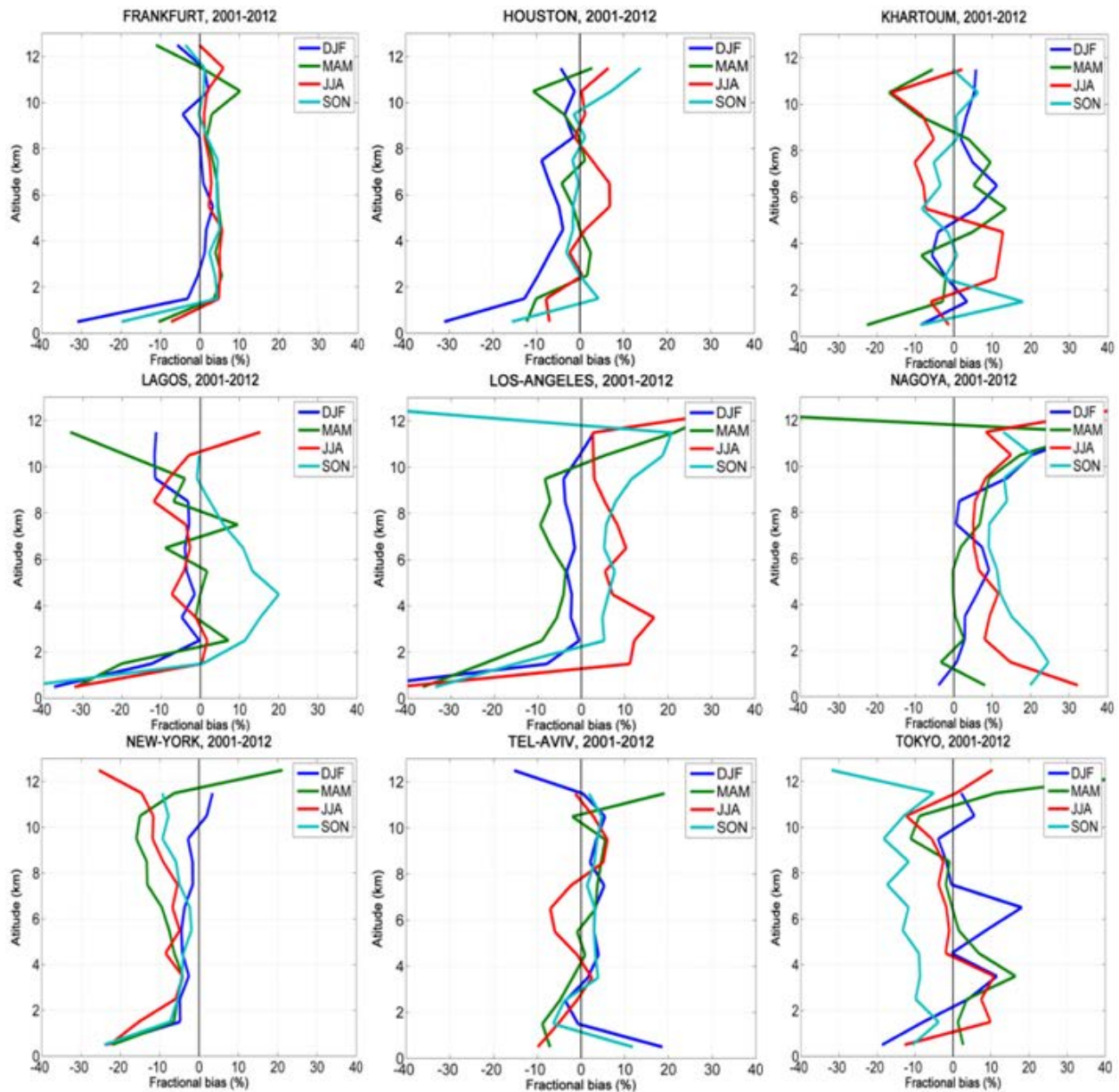
The bias calculations have been done for all months. It does not seem to show seasonal dependence and this can be seen in Fig. 5 (now Fig. 6). As a result, we chose May as an example to show the bias between the trajectory-mapped and the in situ measurement.

p.29885, 1.14 – p.29886, 1.11 and Figures 4-5: You should consider to combine Figures 4 and 5 to one Figure with less examples. Please give total numbers of profiles which contribute to the mean MOZAIC-IAGOS profiles from the airports shown in the Figures. Airports shown here can be marked additionally in Figure 1. I doubt that all selected airports represent basically different conditions (e.g. Cairo / Tel Aviv or Atlanta / Houston).

Following the reviewer's suggestion, we reduced the number of figures in Fig. 5 (now Fig. 6) to 9 (from 12) by removing those airports which do not represent different atmospheric conditions. We have removed Atlanta, Cairo, and New Delhi.

Airport	latitude	Longitude	Number of profiles
Frankfurt	50.04	8.51	12324
Houston	29.97	-95.35	130
Khartoum	15.59	32.55	118
Lagos	6.57	3.31	265
Los Angeles	33.94	-118.41	280
Nagoya	34.88	136.8	439
New York	40.63	-73.78	978
Tel Aviv	32.02	34.88	341
Tokyo	35.77	140.37	929

Selected airports used in the validations.



p.29886, 1.18-20: You should emphasize that the MOZAIC data for the Southern Hemisphere is almost entirely related to flight tracks over the land surfaces. The higher SON values could be mostly related to biomass burning events and the values over the southern oceans may be much lower.

Done.

p.29887, 1.12: Which product? V6L3?

That is correct. MOPITT V6L3

p.29888, 1.25-27: Correlations in Figure 7 are only shown for January, land and ocean are not distinguished. Even then you report a correlation coefficient of 0.68 for 300 hPa. Thus I can't believe that correlation coefficients of 0.7 are always reached.

Figures 9 and 10 (now Figures 11 & 12) suggest that the mapping does a pretty good job over the oceans, too, as CO is advected long distances in four days (which is also short compared to its lifetime).

p.29888, 1.28: Do you mean for height levels above 700 hPa or for levels with pressures above 700 hPa?

We mean (geometric) altitudes above the 700 hPa pressure level. Text revised.

p.29889, 1.9-14: What exactly is compared in Figure 8? Is it monthly means of in-situ profiles which afterwards have been transformed using the averaging kernels against monthly means of MOPITT retrievals or was the transformation being done with the single profiles?

The former, monthly means of in-situ profiles have been transformed using the MOPITT averaging kernels and plotted against monthly means of MOPITT retrievals.

p.29889, 1.3-19: What are the conclusions you draw from this paragraph?

We have added: |”This implies that the differences at 500 and 300 hPa are not a result of the trajectory mapping.”

p.29889, 1.24-28: I cannot see the dispersion towards the Arabian peninsula from Figure 9.

Indeed, the transport toward South America is much clearer. We have revised the text.

p.29889, 1.28-29: Which region exactly?

In southern Africa. Text corrected.

p. 29890, 1.1-14: There is not much new insight for the CO comparison from this paragraph. Also your comments on the MOPITT retrieval refer to an older version. You can skip this.

Agreed.

p.29890, 1.17-20: I don't agree with this statement. From Figure S2, there are many regions where MOPITT is lower than MOZAIC. Showing zonal averages instead of maps could help here to quantify.

The statement is quoting the results of averaging the maps shown.

p.29891. Eq. 5: How did you derive this equation? Is there any reference?

It is described in Deeter (2002).

Deeter, M. N. (2002), Calculation and Application of MOPITT (Measurements of Pollution in the Troposphere) Averaging Kernels. Available at http://www.acom.ucar.edu/mopitt/data/avg_krnls_app.pdf. Citation added.

p.29891, 1.13-23: Skip the section “The interface . . . column retrievals.” or explain why this information is necessary here.

Removed lines 13-23.

p.29892, 1.26- p.29893, 1.2: Your findings are hard to see from Figure 10. It would be more elucidating to see a climatology of zonal mean values for both data products.

We've replaced this figure with one of seasonal means.

p.29893, 1.20-22: Figure 12 shows monthly patterns. Seasonal maps eventually would be sufficient.

We would like to keep it.

p.29893, 1.20- p. 29894, 1.19: Section 5.1. needs to be reworked. NH concentrations are not higher than SH concentrations for all months, NH biomass burning is negligible in winter. Moreover it is not explained why you find so much CO over the southern oceans, far away from the sources. How strong is your observational basis (even together with trajectory modeling) for these regions? Over Australia and South America there are very few measurements.

We have rewritten this section to be clearer. There are limited MOZAIC-IAGOS data in the SH. The CO over the southern oceans comes from relatively long trajectories as the observations (airports) are far away, and so the associated uncertainties are larger. However, CO has a long lifetime, so it is not unreasonable to find a lot of CO over the southern oceans, far away from the sources. We have compared with global maps of MOPITT CO data, averaged over the same period, and we do not see larger differences in those maps between land and sea. We do see a bias between our results and MOPITT (our values are larger. One puzzling difference is that MOPITT does not show the high values we see between Australia and the southern tip of Africa; MOPITT values are elevated there but not as much as ours. A possible explanation, which we have not investigated, is that MOZAIC-IAGOS data are not evenly distributed in time; if the aircraft sampled some large biomass-burning events these could bias the averages.

p.29894, 1.22-24: You can skip either Figure 13a or 13b, basically it shows the same information. Alternatively you could show only one Figure with a comparison to total column CO from MOPITT, but for different latitude bands.

Following the reviewer's suggestion, we have added total CO column for different latitude bands to Fig. 13 (now Fig. 15).

p.28896, 1.15-21: As can be seen from the previous figures, large regions of the extratropical SH are not covered by the MOZAIC/IAGOS climatology. It is thus misleading to interpret a zonal average profile from this part of the world. I cannot trust the conclusions you draw from this section.

That is true. It is now noted in the manuscript that the trajectory-mapped CO in the SH extratropics is mainly representative of the tropics, unlike in the NH extratropics.

p.29897, 1.5-8: It would be intriguing to add a total column comparison to this interesting Figure 17.

Done.

p.39898, 1.1 – p.29899, 1.2: Given the length of the manuscript and the limited information content of the section, I'd propose to skip the section completely or at least to shorten it significantly.

We have shortened this somewhat, and we have removed section 6.2 entirely, to reduce the size of the manuscript.

p.29900, 1.8-9: Maximum monthly mean values of about 80 ppbv for ozone at 4.5 km seem to be quite high. Is this supported by the literature?

Yes, such values are common at northern mid-latitudes. For example, Liu et al. (2013) have shown monthly mean CO values of about 80 ppbv at 4.5 km. This section has been removed, however.

p.29900, 1.12 – p.29901, 1.24: This section can be condensed considerably. Your main conclusions can be drawn from Figure 21, without showing Figure 19 and 20.

Agreed. We have removed p.29900, 1.12 – p.29901, 1.24 since section 6.2 has been removed entirely.

p.29901, 1.26: Insert: “as well as interannual variability”.

Done.

p.29901, 1.29 – p.29902, 1.5: Skip the sentence referring to Figure 21. The rest of this paragraph belongs to the conclusions section.

Done. we thank the referee for thoughtful comments.

p.29902, 1.17-20: I have problems to agree with this conclusion about the SH maximum. I don't think your results are based on a solid fundament of observations for this region.

Text has been added to reflect the fact that our results in the SH are derived from limited data in the region.

Figure 1: Airports from which profiles are shown later on could be marked here.

O.K.

Figure 2: Show only one example (max. two).

Done.

Figure 4: Combine with Figure 5.

We have reduced Fig. 4 (now Fig 5).

Figure 7: Blue line is missing. The last sentence of the Figure caption can be skipped.

Removed "the blue line is the line of best fit," from the Fig. 7 (now Fig. 9) captions.

Figure 8: mention Frankfurt in the Figure caption.

Done.

Figure 9: e)-f) can be skipped.

These show comparisons in the mid-troposphere.

Figure 11: Why you do not show here a climatology for e. JAN/JUL? Blue line is not explained.

Now the monthly plot is replaced by a seasonal climatology. The blue line is the line of best fit, which is forced to pass through (0,0).

Figure 13: The last sentence of the Figure caption can be skipped.

OK.

Figure 14: How well are the data on the southern edge constrained. Can you compare to MOPITT?

In the SH MOZAIC-IAGOS data are limited. As a result a clear CO trend in the region cannot be observed, unlike the NH. However, the trajectory-mapped CO climatology reflects the major features of the region seen in MOPITT maps, for example, in Fig. 9 (now Fig. 11). However, we cannot compare with higher SH latitudes since there are no available MOZAIC-IAGOS data in that region.

Figures S4-S6 can be skipped when rewriting section 6.1.

Figures S4 & S5 have been removed from the manuscript, but we have kept Fig. S6 (now Fig. S4).

Technical corrections

p.29875, 1.2: Give a reference for IPCC AR5.

IPCC, 2013 (IPCC AR5): Climate Change 2013: The Physical Science Basis. Contribution of Working Group I to the Fifth Assessment Report of the Intergovernmental Panel on Climate Change [Stocker, T.F., D. Qin, G.-K. Plattner, M. Tignor, S.K. Allen, J. Boschung, A. Nauels, Y. Xia, V. Bex and P.M. Midgley (eds.)]. Cambridge University Press, Cambridge, United Kingdom and New York, NY, USA, 1535 pp.

p.29875, 1.14: The reference Zbinden et al., 2013 is missing in the reference section.

Done.

Zbinden, R. M., V. Thouret, P. Ricaud, F. Carminati¹, J.-P. Cammas, P. Nédélec, Climatology of pure tropospheric profiles and column contents of ozone and carbon monoxide using MOZAIC in the mid-northern latitudes (24° N to 50° N) from 1994 to 2009, doi:10.5194/acp-13-12363-2013, 2013.

p.29875, 1.29: NO_y is not explained.

NO_y refers to the sum of NO_x plus all compounds that are the products of atmospheric oxidation of NO_x. Text added.

oxidation products p.29879, 1.16: The reference Worden et al., 2010 is missing in the reference section.

Done.

Worden, H. M., Deeter, M. N., Edwards, D. P., Gille, J. C., Drummond, J. R., and Ned'elec, P. P.: Observations of near-surface carbon monoxide from space using MOPITT multispectral retrievals, *J. Geophys. Res.*, 115, D18314, doi:10.1029/2010JD014242, 2010.

p.29879, 1.16-17: The reference Deeter et al., 2012 is missing in the reference section.

Done.

Worden, H. M., M. N. Deeter, D. P. Edwards, J. C. Gille, J. R. Drummond, and P. P. Nedelec, Observations of near-surface carbon monoxide from space using MOPITT multispectral retrievals, *J. Geophys. Res.*, 115, doi:10.1029/2010JD014242, 2012.

p.29879, 1.19: "Lou et al., 2007" should be "Luo et al, 2007".

Done. Luo et al, 2007

p.29884, l.14: skip “with”.

Done.

p.29884, l.13-14: skip “Eq.” (two times).

Done.

p.29886, l.24: Replace “ a increasing” by “an increasing”.

Done.

p.29889, l.5: The reference Deeter et al., 2010 is missing in the reference section.

Done.

Deeter, M. N., Edwards, D. P., Gille, J. C., Emmons, L. K., Francis, G., Ho, S.-P., Mao, D., Masters, D., Worden, H., Drummond, J. R., and Novelli, P.: The MOPITT Version 4 CO Product: Algorithm Enhancements, Validation, and Long-Term Stability, *J. Geophys. Res.*, 115, D07306, doi:10.1029/2009JD013005, 2010.

p. 29891, l.6: Replace “total column vectors” by “total column operator”.

Done.

p. 29892, l.8: Replace “times” by “time intervals”.

Done.

p. 29892, l.13: Insert “is” in between “which” and “not”.

Done.

p. 29892, l.21: Replace “African” by “Africa”.

Done.

p. 29893, l.20: Skip “As an example,”.

Done.

p. 29899, l.6: Please update this reference in the reference section.

Manuscript is still under preparation and modified to Osman et al., 2016

p. 29899, l.20: Replace “correlation” by “positive correlation”.

Done.

p.29901, 1.6: Replace “Bowman” by “Bowman et al.”.

Done.

p.29902, 1.25-26: Skip parantheses.

Done.

Figure 2: The quality of the Figure needs to be improved.

Done.

Figure 3: The quality of the Figure needs to be improved.

Done.

Figure 12: The quality of the Figure needs to be improved.

Done.

Figure 14: Add “km” in the Figure caption.

Done.

Figure 15: The quality of the Figure needs to be improved.

Done.

Figure 18: Replace “winter” by “summer” in the Figure caption.

Done.

We thank the referee for his/her careful review and very helpful comments.

The figure numbers were renumbered since some figures have been added and removed from the manuscript. The following table shows the current figure numbers vs. previous ones.

Current Figure #	Previous Figure #
Fig. 1	Fig. 1
Fig. 2	Newly added
Fig. 3	Fig. 2
Fig. 4	Fig. 3
Fig. 5	Fig. 4
Fig. 6	Fig. 5
Fig. 7	Fig. 6
Fig. 8	Newly added
Fig. 9	Fig. 7
Fig. 10	Fig. 8
Fig. 11	Fig. 9
Fig. 12	Fig. 10
Fig. 13	Fig. 11
Fig. 14	Fig. 12
Fig. 15	Fig. 13
Fig. 16	Fig. 14
Fig. 17	Fig. 15
Fig. 18	Fig. 16
Fig. 19	Fig. 17
Fig. S1	Fig. S1
Fig. S2	Fig. S2
Fig. S3	Fig. S3
Fig. S4	Fig. S6

***Figs. 18-21, S4 & S5 have been removed from the manuscript in order to reduce the size of the paper.**

1 Carbon Monoxide Climatology derived from the Trajectory Mapping of 2 Global MOZAIC-IAGOS Data

3 | M. [K. Osman](#)^{1,*}, D.W. Tarasick¹, J. Liu², O. Moeini¹, V. Thouret³, V. E. Fioletov¹, M.
4 | Parrington⁴, P. Nédélec³

5 | ¹Environment Canada, 4905 Dufferin Street, Downsview, ON, M3H 5T4 Canada

6 | ²Department of Geography and Program in Planning, University of Toronto, 100 St. George
7 | Street, Toronto, Ontario, M5S 3G3, Canada

8 | ³Laboratoire d'Aérodologie, UMR5560, CNRS and Université de Toulouse, Toulouse, France

9 | ⁴European Centre for Medium-Range Weather Forecasts, Shinfield Park, Reading, RG2 9AX,
10 | UK

11 | [*now at: Cooperative Institute for Mesoscale Meteorological Studies, The University of](#)
12 | [Oklahoma, and NOAA/National Severe Storms Laboratory, Norman, Oklahoma, USA](#)

13 Abstract

14 A three-dimensional gridded climatology of carbon monoxide (CO) has been developed by
15 trajectory mapping of global MOZAIC-IAGOS in situ measurements from commercial aircraft
16 data. CO measurements made during aircraft ascent and descent, comprising nearly 41,200
17 profiles at 148 airports worldwide from December 2001 to December 2012 are used. Forward
18 and backward trajectories are calculated from meteorological reanalysis data in order to map the
19 CO measurements to other locations, and so to fill in the spatial domain. This domain-filling
20 technique employs 15,800,000 calculated trajectories to map otherwise sparse MOZAIC-IAGOS
21 data into a quasi-global field. The resulting trajectory-mapped CO dataset is archived monthly
22 from 2001-2012 on a grid of 5° longitude×5° latitude×1 km altitude, from the surface to 14 km
23 altitude.

24 | The mapping product has been carefully evaluated, [first](#) by comparing maps constructed using
25 only forward trajectories and using only backward trajectories. The two methods show similar
26 global CO distribution patterns. The magnitude of their differences is most commonly 10% or
27 less, and found to be less than 30% for almost all cases. The ~~trajectory-mapped CO~~
28 ~~dataset~~[method](#) has also been validated by ~~comparison~~[comparing](#) profiles for individual airports
29 with those produced by the mapping method when data from that site are excluded. While there
30 are larger differences below 2 km, the two methods agree very well between 2 and 10 km with
31 the magnitude of biases within 20%. [Finally, the mapping product is compared with global](#)
32 [MOZAIC-IAGOS cruise-level data, which were not included in the trajectory-mapped dataset,](#)
33 [and with independent data from the NOAA aircraft flask sampling program.](#)

1 Maps are also compared with Version 6 data from the Measurements Of Pollution In The
2 Troposphere (MOPITT) satellite instrument. Both data sets clearly show major regional CO
3 sources such as biomass burning in central and southern Africa and anthropogenic emissions in
4 eastern China. While the maps show similar features and patterns, and agreement is good
5 relative biases are small in the lowermost troposphere, the MOPITT CO profile shows negative biases we
6 find differences of ~20% in CO volume mixing ratios between 500 hPa and 300 hPa. These
7 upper troposphere biases are not related to the mapping procedure, as almost identical
8 differences are found with the original in situ MOZAIC-IAGOS data. The total CO trajectory-
9 mapped MOZAIC-IAGOS ~~climatology~~-column agrees with ~~is also higher than~~ the MOPITT CO
10 total column, by within ±5-12-16%, which is consistent with previous reports.

11 ~~The maps clearly show major regional CO sources such as biomass burning in the central and~~
12 ~~southern Africa and anthropogenic emissions in eastern China.~~ The dataset shows the seasonal
13 CO cycle over different latitude bands and altitude ranges ~~that are representative of the regions~~
14 as well as long-term trends over different latitude bands. We observe a decline in CO over the
15 northern hemisphere extratropics and the tropics consistent with that reported by previous studies
16 using other data sources.

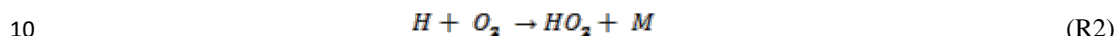
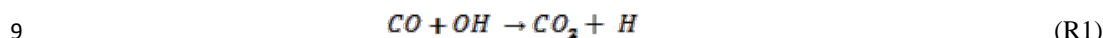
17 ~~Similar maps have been made using the concurrent O₃ measurements by MOZAIC-IAGOS, as~~
18 ~~the global variation of O₃-CO correlations can be a useful tool for the evaluation of ozone~~
19 ~~sources and transport in chemical transport models.~~ We anticipate ~~use~~ of the trajectory-mapped
20 MOZAIC-IAGOS CO dataset as an a priori climatology for satellite retrieval, and for air quality
21 model validation and initialization.

22 **1 Introduction**

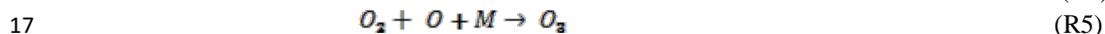
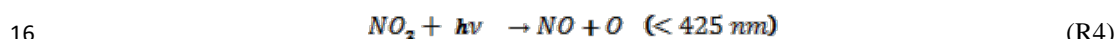
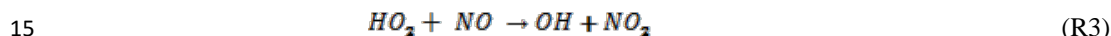
23 Atmospheric carbon monoxide (CO) is an important global air pollutant and trace gas. Due to its
24 relatively long lifetime of 1-4 months (Hubler et al., 1992; Law and Pyle, 1993), it is an ideal
25 tracer for long range atmospheric transport (Logan et al., 1981; Lelieveld et al., 2001; Shindell et
26 al., 2006). Moreover, in the tropics, it is an important tracer of upward transport during
27 convective events (e.g., Pommrich et al., 2014). Consequently, it has been employed to facilitate
28 interpretations of chemical measurements (Jaffe et al., 1996; Parrish et al., 1991, 1998; Wang et
29 al., 1996, 1997) and in validating chemical transport models (Carmichael et al, 2003; Liu et al.,
30 2003; Tan et al., 2004; Wang et al., 2004). The main sources of atmospheric CO are relatively
31 well understood (Galanter et al., 2000; Granier et al., 2011; Holloway et al., 2000); however, the
32 magnitude of individual sources and their seasonal variability, especially of biomass burning, are
33 not well quantified. Stein et al. (2014) also reported that models are also generally biased low
34 due to either an underestimation of CO sources or an overestimation of its sinks. There are
35 differences in the emission densities of anthropogenic and natural sources, despite the fact that
36 the anthropogenic and natural sources are of similar magnitude on a global scale (Granier et al.,
37 2011; Logan et al., 1981). The anthropogenic sources are primarily associated with large
38 industrial centers or major biomass burning regions while the natural sources, such as oxidation

1 of methane (CH₄) and non-methane hydrocarbons (NMHCs) are much more diffuse. This makes
2 CO a good atmospheric tracer gas for anthropogenic emissions as its lifetime allows it to be used
3 as an indicator of how large-scale atmospheric transport redistributes pollutants on a global scale.

4 CO plays a vital role in the chemistry of the atmosphere. This significance mainly comes from
5 the influence of CO on the concentrations and distributions of the atmospheric oxidants, ozone
6 (O₃), the hydroperoxy (HO₂) and hydroxyl radicals (OH) (e.g. Novelli et al., 1994, 1998).
7 Reaction (R1) between CO and OH represents 90-95% of the CO sink (Logan et al., 1981), and
8 about 75% of the removal of OH (Thompson, 1992) in the troposphere:



11 In areas with sufficient NO_x (=NO + NO₂), HO₂ formed in reaction (R2) leads to photochemical
12 reactions (R3)-(R5) which bring about net O₃ production. In urban areas and regions of biomass
13 burning, large amounts of these O₃ precursors will be produced, and O₃ can be formed in, and
14 downwind of, the source region (Crutzen, 1973; Fishman and Seiler, 1983):



18 O₃ is associated with respiratory problems and decreased crop yields (e.g., McKee, 1993;
19 Chameides et al., 1994). Since CO and OH are principal reaction partners, CO concentrations in
20 the atmosphere have important climatological implications. OH is also responsible for the
21 removal of greenhouse gases such as CH₄, and other volatile organic compounds in the
22 atmosphere. Via these interactions with OH, O₃ and CH₄, CO has an indirect radiative forcing of
23 about 0.25 W m⁻² (IPCC AR5).

24 Global atmospheric chemistry models require accurate CO concentrations on a global scale in
25 order to define spatial and temporal variations of atmospheric oxidants and CO. For this reason
26 measurements of CO are made by different kinds of remote sensing and in situ instruments, in
27 ground-based networks, aircraft programmes and from space (Novelli et al., 1994, 1998;
28 Rinsland and Levine, 1985; Zander et al., 1989; Brook et al., 2014; Reichle et al., 1990; 1999;
29 Worden et al., 2013; Petzold et al., 2015). [Long range atmospheric transport redistributes CO widely due to its relatively long lifetime. Typical tropospheric background CO levels range between 50 and 120 ppbv \(WHO, 2000\). Background CO levels are found in all regions of the troposphere, where mixing ratios between 45 and 250 ppbv have been reported \(Novelli et al., 1994\). Extreme m](#)
30 [Mixing ratios much higher than 250 ppb have been observed in the upper](#)
31 [troposphere over Asia \(Nédélec et al., 2005\) or over the Pacific \(Clark et al., 2015\) in biomass](#)
32 [burning plumes of boreal biomass burning. CO values as high as 1800 ppbv have been reported](#)
33
34
35

1 [over Beijing \(Zbinden, et al., 2013\)](#)~~The largest values in the lower troposphere have been~~
2 ~~observed over Beijing (Zbinden et al., 2013).~~

3 Early studies of ground-based observations showed increasing trends in global CO before 1980
4 (Khalil and Rasmussen, 1988; Rinsland and Levine, 1985; Zander et al., 1989), followed by a
5 modest decline in the 1990s (Novelli et al. 1994; 2003; Khalil and Rasmussen, 1994). More
6 recently satellite observations have shown that the decline has continued: Worden et al. (2013)
7 report a global trend from 2000-2011 of ~10% per decade on column CO in the northern
8 hemisphere. Petetin et al. (2015) show a similar decrease of about 2 ppb per year over Frankfurt
9 throughout the troposphere from 2002 to 2012. The decrease is at least partly due to a decrease in
10 global anthropogenic CO emissions (Granier et al., 2011).

11 In-service Aircraft for a Global Observing System (IAGOS), and its predecessor Measurement
12 of Ozone and water vapor by Airbus in-service aircraft (MOZAIC), have been making
13 automatic and regular measurements of O₃, water vapour and standard meteorological
14 parameters onboard long-range commercial Airbus A340 aircraft since August 1994 (Marengo et
15 al., 1998, Petzold et al., 2015). Measurements of CO (Nédélec et al., 2003) and NO_y [\(the sum of](#)
16 [NO_x plus its atmospheric oxidation products\)](#) (Volz-Thomas et al., 2005) were added in late
17 2001. The MOZAIC database currently contains data from more than ~~71,900 vertical profiles of~~
18 ~~O₃ and~~ 41,200 vertical profiles of CO, measured during takeoff and landing from 148 airports
19 around the world. MOZAIC measurements show the general features of the atmospheric CO
20 distribution (Zbinden et al., 2013; Petzold et al., 2015 and references therein), capturing major
21 regional features (e.g., strong CO emissions from biomass burning or anthropogenic sources).

22 The objective of this paper is to present a three-dimensional (i.e., latitude, longitude, altitude)
23 gridded climatology of carbon monoxide that has been developed by trajectory mapping of
24 global MOZAIC-IAGOS CO data from 2001-2012. We employ a domain-filling technique,
25 using approximately 15,800,000 calculated trajectories to map otherwise sparse MOZAIC-
26 IAGOS CO data into a global field.

27 This is a technique that has been used successfully with tropospheric and stratospheric
28 ozonesonde data (G. Liu et al., 2013; J. Liu et al., 2013). Stohl et al. (2001) used trajectory
29 statistics to extend one year of MOZAIC O₃ measurements into a 4-season O₃ climatology at 10°
30 longitude by 6° latitude and three vertical heights. Tarasick et al. (2010) developed high
31 resolution (1°×1°×1 km in latitude, longitude, and altitude) tropospheric O₃ fields for North
32 America from ozonesonde data from the INTEX (Intercontinental Transport Experiment) and
33 ARCTAS (Arctic Research of the Composition of the Troposphere from Aircraft and Satellites)
34 campaigns, and this was extended to global tropospheric ozonesonde data by G. Liu et al. (2013).
35 It is possible to apply this technique to CO because the lifetime of CO in the troposphere, as
36 noted above, is generally of the order of weeks or months. This physically-based [interpolation](#)
37 method, using the reanalysis meteorological data from the National Centers for Environmental
38 Prediction/National Center for Atmospheric Research (NCEP/NCAR) (Kalnay et al., 1996) [to, in](#)

1 [effect, interpolate data based on knowledge of atmospheric transport](#), offers obvious advantages
2 over typical statistical interpolation methods. [Indeed, it is expected to improve global models and](#)
3 [satellite data validation and it can also be used as a priori for satellite data retrieval.](#)

4 ~~Major regional features of the global CO distribution are clearly evident in the global maps thus~~
5 ~~produced, especially regions of intense biomass burning or anthropogenic pollution. The 3D~~
6 ~~global trajectory mapped CO climatology facilitates visualization and comparison of different~~
7 ~~years, decades, and seasons, and offers insight into the global variation of CO. Moreover, it will~~
8 ~~be useful for climate and air quality model initialization and validation, and can be used as an a~~
9 ~~priori climatology for satellite data retrievals. Comparison with similar maps made using the~~
10 ~~concurrent O₃ measurements by MOZAIC-IAGOS allow us to examine the global variation of~~
11 ~~O₃-CO correlations, which convey information about the source distribution of CO. O₃-CO~~
12 ~~correlations are also of great interest around the tropopause region since such correlations~~
13 ~~provide information on mixing processes (e.g., Hoor et al., 2004; Pan et al., 2006; Vogel et al.,~~
14 ~~2011) besides of the source regions. This paper is organized in the following order. Following~~
15 ~~discussion of the MOZAIC-IAGOS and MOPITT instruments in Sect. 2.1 and 2.2, respectively,~~
16 ~~we describe trajectory mapping calculation via HYSPLIT model in Sect. 2.3. The transformation~~
17 ~~of MOZAIC-IAGOS data by applying the MOPITT a priori profile and averaging kernels is~~
18 ~~presented in Sect. 2.4. The validation of the trajectory mapped dataset against MOZAIC-IAGOS~~
19 ~~in situ data will be presented in Sect. 3. The same section assesses the differences between the~~
20 ~~CO mapping produced using only backward and only forward trajectories, and also compares~~
21 ~~with in situ global CO data at cruise altitudes between 8 and 12 km. Subsequently, the~~
22 ~~comparison of the trajectory mapped MOZAIC-IAGOS CO with MOPITT CO retrievals is~~
23 ~~presented in Sect. 4. Section 5 discusses the results obtained from the global 3D trajectory-~~
24 ~~mapped climatology data. After pointing out the potential applications of the trajectory mapped~~
25 ~~MOZAIC-IAGOS CO climatology (i.e., O₃-CO relationship and global variation and trends of~~
26 ~~CO) and data coverage and the associated standard errors in Sect. 6, we make concluding~~
27 ~~remarks about the results we obtain from this study in Sect. 7.~~

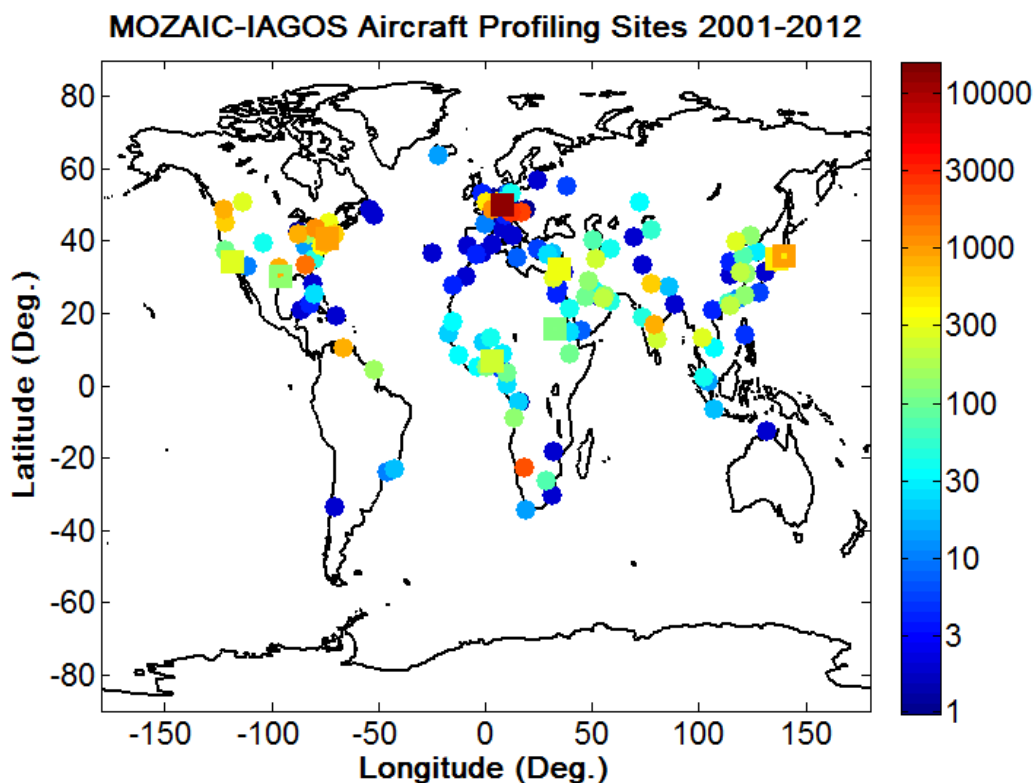
28 **2 Measurements of CO**

29 **2.1 MOZAIC-IAGOS**

30 CO measurements were made by an improved version of a commercial Model 48CTL CO
31 Analyzer from Thermo Environmental Instruments employing the Gas Filter Correlation
32 technique. The Model 48CTL is based on the principle that CO absorbs infrared radiation at a
33 wavelength of 4.67 microns. For 30 s integration time (the response time of the instrument) the
34 precision achieved is 5 ppb (noise) or 5% (calibration) CO, with minimum detection limit of 10
35 ppb. The analyzer samples at a horizontal resolution of about 7 km (since the maximum cruise
36 speed of the Airbus A340 aircraft is nearly 250 m/s) and the vertical resolution during ascents
37 and descents is nearly 300 m. Nedelec et al. (2003 for MOZAIC, 2015 for IAGOS) give detailed

1 descriptions of the CO analyzer, measurement technique, instrument validation and quality
2 testing.

3 The airports visited by aircraft equipped with MOZAIC-IAGOS instrumentation are shown in
4 Fig. 1. Further details are available at <http://www.iagos.fr>.



5
6
7 **Fig. 1.** Airports ~~stations~~ visited by MOZAIC-IAGOS aircraft from 2001-2012. The color bar
8 indicates the number of profiles available from each airport. The squares show the locations of
9 the selected airports used for the validation in this study.

10 The sampled data from these airports are unevenly distributed ~~both~~ spatially, and also temporally
11 because the frequency of visits to airports by aircraft that take part in MOZAIC-IAGOS varies
12 considerably depending on commercial airlines' operational constraints. ~~This-Thus means that~~ at
13 ~~airports such as~~ Frankfurt, Germany we find ~~as many as~~ 12,324 CO profiles while from
14 Dammam, Saudi Arabia we have only 2 ~~CO profiles~~ during the period 2001-2012. The
15 trajectory-mapping method is valuable for filling the sparse and variable spatial domain.

1 2.2 MOPITT

2 MOPITT is a nadir-viewing gas correlation radiometer which provides global atmospheric
3 profiles of CO volume mixing ratio (VMR) and CO total column values using near-infrared
4 radiation at 2.3 μm and thermal-infrared radiation at 4.7 μm (Drummond and Mand, 1996). CO
5 columns and profiles are retrieved from the IR emission channels (4.6 μm) for all cloud-free
6 scenes. The MOPITT measurement technique relies on [a temperature gradient within the
7 atmosphere](#)~~thermal contrast between the Earth's surface and atmosphere~~, leading to a retrieval
8 dependence on surface temperature, and little sensitivity to CO in the boundary layer. The
9 retrieval uses a priori profiles that vary geographically and temporally. MOPITT-derived CO
10 VMR profiles reflect the vertical sensitivity of the measurement as defined by the retrieval
11 averaging kernel (e.g. Fig. 23) and a priori profile. In this study, we have used Level 3, Version
12 6 monthly CO mixing ratio profile data, reported on 10 pressure levels, as well as CO total
13 column. [Nighttime CO observations of MOPITT have not been validated and appear subject to
14 larger bias \(Heald et al., 2004\). Hence, we use the daytime data for comparison.](#) MOPITT data
15 are publicly available at the NASA Langley Research Center Atmospheric Science Data Center:
16 https://eosweb.larc.nasa.gov/project/mopitt/mopitt_table.

17 MOPITT was launched in 1999 into sun-synchronous polar orbit with a 1030 local time (LT)
18 northward or southward ~~local~~-equator cross-over time. The instrument field of view is 22x22
19 km^2 . Cross-track scanning with a 612 km swath provides near complete coverage of the surface
20 of the Earth approximately every 3 days. MOPITT retrievals have gone through intensive
21 validation against in situ measurements from aircraft on a regular basis since the start of the
22 mission (Worden et al., 2010; Deeter et al., 2012, 2013, 2014; Emmons et al., 2004, 2007, 2009;
23 Jacob et al., 2003). MOPITT CO retrievals have also been validated by comparing to ground-
24 based and TES satellite measurements (Jacob et al., 2003 and ~~Loe-Luo~~ Luo et al., 2007). [Deeter et al.
25 \(2014\) employ the MOPITT L3 V6 product and showed biases to vary from -5.2% at 400 hPa to
26 8.9% at the surface. However, most of pPrevious studies focused on the earlier versions of the
27 MOPITT product. In the lower troposphere a mean positive bias of 6-8% against in situ
28 validation profiles has been reported, and a mean bias and standard deviation for the retrieved
29 CO column of \$5 \pm 11\%\$ and \$0.5 \pm 12.1\%\$ for periods, respectively, March 2000–May 2001 and
30 August 2001–December 2002 \(Emmons et al., 2004\). Jacob et al. \(2003\) reported the CO bias
31 to be \$6 \pm 2\%\$, where as Emmons et al. \(2007\) found approximately \$7 \pm 8\%\$ bias for summer
32 2004 measurements. Deeter et al. \(2013\) also show a total column retrieval bias of about \$0.08 \times\$
33 \$10^{18}\$ molecules/ \$\text{cm}^2\$ \(-4%\) against in situ profiles. Furthermore, Deeter et al. \(2012\) reported a
34 positive bias of surface level CO concentrations on the order of a few percent against in situ
35 profiles.](#)

36 2.3 Trajectory calculation and global CO mapping via HYSPLIT

37 For each CO profile of the MOZAIC-IAGOS data set presented here, the mean CO VMR was
38 calculated for 1-km intervals from sea level up to 12 km (the maximum altitude of the aircraft).

1 Cruise data were not used. The HYSPLIT (Hybrid Single-Particle Lagrangian Integrated
2 Trajectory) model version 4.9 (Draxler and Hess, 1998, Draxler, 1999) was employed to
3 calculate trajectories for each level of each profile. ~~We used~~ The exact location of the aircraft
4 was used to start the trajectories. HYSPLIT, publicly accessible at
5 (<http://ready.arl.noaa.gov/HYSPLIT.php>), uses the reanalysis meteorological wind fields from the
6 National Centers for Environmental Prediction/National Center for Atmospheric Research
7 (NCEP/NCAR) (Kalnay et al., 1996) as an input to describe the transport of CO in the
8 atmosphere. The reanalysis data are ~~readily~~ available from 1948 until the present. Both forward
9 and backward trajectories for 4 days at 6-hour intervals (32 positions for each level) were
10 calculated for 41,200 CO profiles, and the mean CO mixing ratios from each level (i.e.,
11 tropospheric and lower stratospheric air masses) of each profile were assigned to the
12 corresponding trajectory positions along the forward and backward paths. Trajectories only move
13 upward and downward with the meteorological vertical velocity fields since the HYSPLIT
14 kinematic trajectory model employs vertical motions supplied with the NCEP reanalysis
15 meteorological data set. Numerous studies show that the choice of vertical wind velocity has
16 significant impact on the transport of tracers (e.g., Schoeberl et al. 2003; Ploeger et al., 2010,
17 2012). Kinematic models show excessive dispersion for tracers with strong gradients (e.g., O₃ in
18 the vicinity of the tropopause), particularly for trajectories of 7 days or more. ~~We limit~~ Here
19 trajectories were limited to a maximum ~~of~~ 4 days in length. Moreover, unlike O₃, CO does not
20 have a strong vertical gradient in the upper troposphere. Trajectories that reach the ~~bottom~~
21 ~~boundary (i.e., ground)~~ continue at the surface where ~~the~~ trajectory robustness ~~grows to be is~~
22 more uncertain. Trajectories that reach the top height of the model (20,000 m above sea level)
23 ~~will~~ terminate. Although HYSPLIT is capable of generating a trajectory every hour (i.e., 24
24 trajectories per day), the ~~average available~~ typical maximum frequency of CO measurements ~~(if~~
25 ~~the MOZAIC IAGOS aircraft visits the airports)~~ is around 2 profiles per day (with the exception
26 of Frankfurt where we can get up to 6 profiles per day). In this ~~version, trajectory-mapped~~
27 ~~MOZAIC IAGOS CO climatology, we did not~~ no attempt was made to exclude-identify major
28 individual anthropogenic CO sources; however, the climatology could in principle be refined by
29 excluding backtrajectories from ~~sources identified via emission inventories~~. We note, however,
30 that if major anthropogenic sources were a significant source of error, we would see differences
31 between the CO mapping produced using only backward and only forward trajectories (see Sect.
32 3.1).

33 This mapping implicitly assumes that CO chemistry may be neglected over a timescale of 4 days.
34 Except near major ~~anthropogenic~~ sources, this assumption should be valid, as the lifetime of CO
35 is much longer. However, trajectories have significant errors over such timescales. Stohl (1998)
36 in a comprehensive review, quotes typical errors of about 100-200 km/day in the troposphere.
37 This can be combined with an estimate of the correlation length in the troposphere to yield an
38 estimate for the information value of a mapped measurement. Liu et al. (2009) find that O₃
39 measurements in the troposphere correlate with an exponential dependence of approximately

1 $e^{-(r/R)^{1.5}}$, where r shown in Eq. (1) is distance and R is a correlation length of 500-1000 km
 2 in the troposphere, and 1000-2000 km in the stratosphere. ~~The means that the horizontal distance~~
 3 ~~for the correlation coefficient to decrease by a factor of e is 500-1000 km in the troposphere and~~
 4 ~~1000-2000 km in the stratosphere.~~ As the CO lifetime is even longer than the ozone lifetime, the
 5 correlation length for CO should be at least as large. Therefore, the trajectory-mapped data were
 6 binned at intervals of 5° latitude and 5° longitude, at every 1-km altitude, and averaged with a
 7 weighting, w , assigned according to the formula:

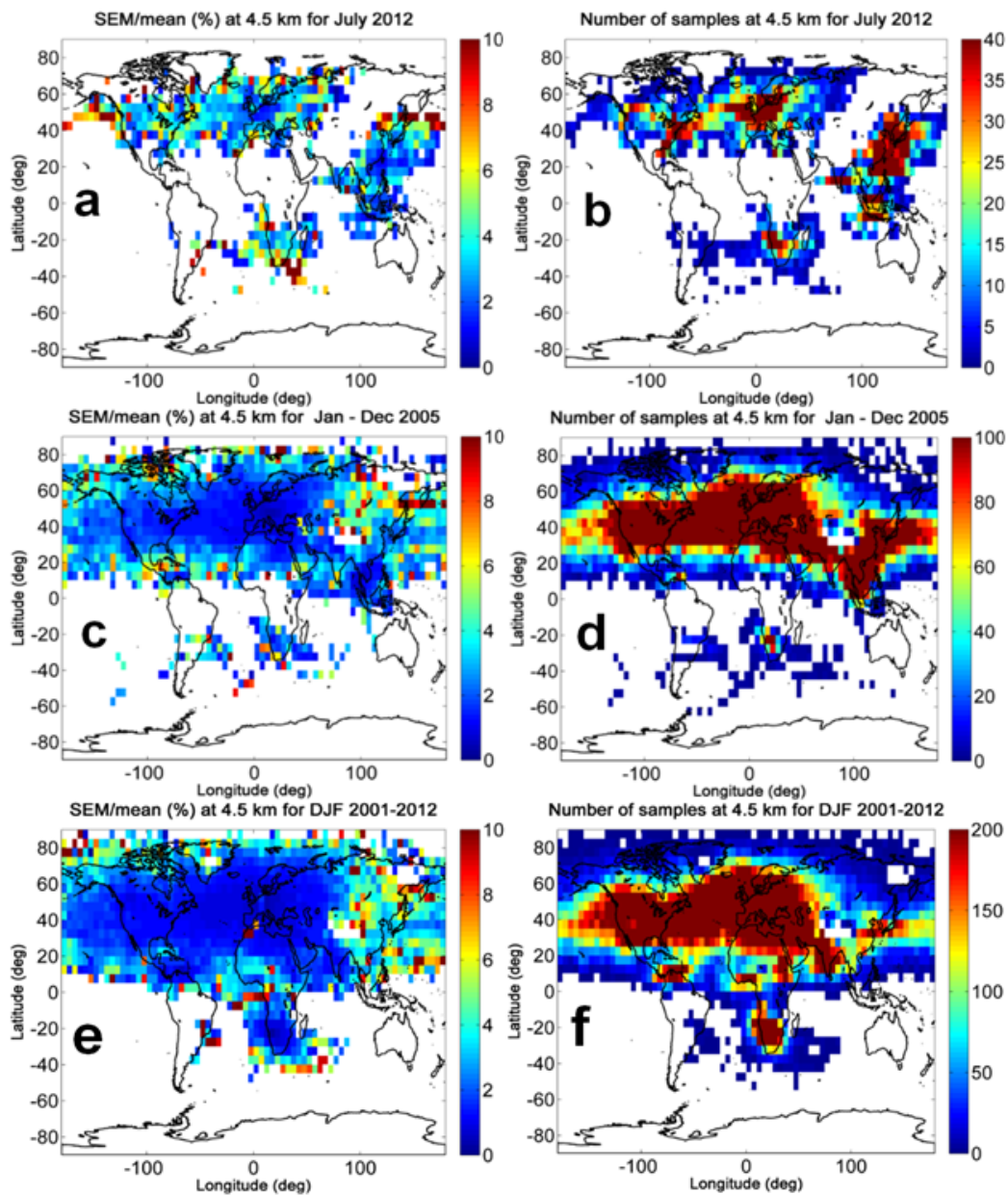
$$8 \quad w = e^{-(150t/R)^{1.5}} \quad (1)$$

9 where R is the correlation length (taken as 700 km ~~and 1500 km~~ in the troposphere and 1500 km
 10 and in the stratosphere, ~~respectively~~), and t is the age of the trajectory in days.

11 The trajectory mapping greatly spreads out the in situ CO information along the trajectory paths,
 12 increasing the spatial domain to include much of the globe. Two different vertical coordinate
 13 systems were utilized for the binning, and hence the maps were generated for elevations above
 14 sea level and above ground level. Data are available publicly at [ftp://es-
 15 ee.tor.ec.gc.ca/pub/ftpd/MOZAIC_output_CO/ftp://es-ee.tor.ec.gc.ca/pub/ftpd/](ftp://es-ee.tor.ec.gc.ca/pub/ftpd/MOZAIC_output_CO/ftp://es-ee.tor.ec.gc.ca/pub/ftpd/). In this work, we
 16 present global CO maps generated for elevations above sea level. Global maps of monthly,
 17 annual, seasonal and decadal means are presented, for each altitude, from 2001-2012.

18 2.4 Distribution of data and uncertainties associated with trajectory mapping

19 Figure 4A2 shows typical standard errors of the mapping product and the number of samples per
 20 grid cell, for typical monthly, annual and decadal maps at 4.5 km altitude above sea level.
 21 Similar figures for other levels are included with the climatology on the FTP site. As can be
 22 seen, the largest number of samples per grid cell and the lowest standard errors are found over
 23 North America and Europe as there are more frequent MOZAIC-IAGOS aircraft flights in this
 24 region. Higher standard errors are found at NH high latitudes and much of the SH, where airports
 25 visits by MOZAIC-IAGOS-equipped aircraft are much fewer. The standard error is computed
 26 using all data points found inside a grid cell. This is probably biased low, since some grid cells
 27 may contain more than one value from a particular trajectory. This bias is likely not more than a
 28 factor of 2, based on typical trajectory lengths. These maps present a visual interpretation that
 29 distinguishes regions where the CO climatology is 'statistically robust' (for example, North
 30 America and Europe) from those regions where the uncertainty is larger. The average number of
 31 samples is approximately 20, 90, and 140 per grid cell for the monthly, annual and decadal maps,
 32 and this number does not vary greatly among layers. The average standard error is generally
 33 between 3 and 4% of the mean at 4.5 km for all three averaging periods. The monthly mean
 34 shows the highest error and the lowest number of samples per grid cell.



1
2
3
4
5
6

[Fig. 4A2](#) The standard error of the mean (left panels) and number of samples (right panels) for monthly (July 2012), annual (2005), seasonal (DJF 2001-2012) means at 4.5 km altitude above sea level. The month and year shown are chosen as typical; other months and years show similar patterns. The data are binned on a 5°x5° latitude and longitude grid.

2.4.5 MOZAIC-IAGOS Comparison with MOPITT

When comparing the MOPITT retrievals with in situ data, it is necessary to take into account the sensitivity of the retrievals to the true profiles. The method used by MOPITT to retrieve tropospheric CO profiles follows that of Rodgers (2000). In order to perform the most meaningful and accurate comparison, the in situ data to be compared must be transformed using the averaging kernel matrix, A , and a priori profile, x_a , as shown by Eq. (2). A “retrieved” comparison profile, x_{ret} , is calculated by using the in situ profile, x , as the “true” profile in Eq. (2) which is interpolated to the lower resolution of MOPITT. As described by Emmons et al. (2004), the in situ profile (x) is transformed with averaging kernel matrix (A) and the a priori CO profile (x_a) to get a profile (x_{ret}), the appropriate quantity to compare with the MOPITT retrievals:

$$x_{ret} = x_a + A(x - x_a) + \varepsilon = Ax + (I - A)x_a + \varepsilon \quad (2)$$

where I is the identity matrix and ε is the retrieval error due to random errors in the measurement and systematic errors in the forward model (e.g., the error in the atmospheric temperature retrieval). x_{ret} , x , and x_a are expressed in terms of the logarithm of the VMR. The averaging kernels provide the relative weighting between the true and a priori profiles and reflect the sensitivity of the retrieval to the measurement (Worden et al., 2013). They are very sensitive to the surface temperature and will be different for each point on the globe. The matrix A describes the sensitivity of the retrieved CO log(VMR) profile to perturbations applied at each level of the “true” log(VMR) profile. The quantity x_{ret} , the transformed in situ profile, represents the result of applying a linear transformation to the in-situ profile in the same way that the remote sensing retrieval process is believed to transform the true profile. Thus, x_{ret} can be directly compared against the MOPITT retrieved CO profile in a manner that is not affected by varying vertical resolution or a priori dependence. x_{ret} , x , and x_a are expressed in terms of the natural/common logarithm of the volume mixing ratio (VMR), i.e., $\log_e(\text{VMR})/\log_{10}(\text{VMR})$.

The vertical resolution of the retrieved profile is described by the shapes of the averaging kernels. Figure 2-3 shows that the kernels are broad except at pressure levels between 400-300 hPa and exhibit a large degree of overlap. The overlap of the averaging kernels peaking in the boundary layer and those at the top of the atmosphere indicates a significant correlation for the retrieved values at these levels. Typical full-width at half maximum (FWHM) of these curves is approximately 5-8 km. The retrieved CO values at these levels both top and bottom are also influenced by CO at mid levels, and by the a priori CO profile at all pressure levels. The averaging kernels also describe the relative contributions, to the CO VMR retrieved at a given level, of the true and a priori (via $I - A$) CO profiles at all pressure levels (Eq. (2)). Where the area under the averaging kernel is smaller, the a priori information in the retrieved CO profile is relatively larger. MOPITT CO averaging kernels exhibit variability from month to month, season

1 to season as well as nighttime to daytime, depending on the atmospheric temperature profile,
2 surface pressure and the CO profile itself.

3 The vertical coordinate of the MOZAIC-IAGOS climatology profile is kilometers above sea
4 level, while the MOPITT a priori profile and averaging kernels are on pressure levels in hPa.
5 Therefore, before applying the MOPITT averaging kernels the climatology data were
6 interpolated using NCEP global pressure profiles that vary as a function of time (month) and
7 latitude, to the 10 vertical pressure grid levels (1000, 900, 800, 700, 600, 500, 400, 300, 200, and
8 100 hPa) used by MOPITT. The interpolated profile was then convolved with the a priori profile
9 and the averaging kernels following Eq. (2) (Emmons et al., 2004). For the atmospheric residual
10 above the maximum MOZAIC-IAGOS profile altitude, the MOPITT a priori profiles were used.

11 In order to compare with these transformed CO profiles, the MOPITT CO profiles, averaging
12 kernels, and a priori profiles were mapped down from the original horizontal resolution of $1^\circ \times 1^\circ$
13 in latitude and longitude to a reduced $5^\circ \times 5^\circ$ grid. ~~The mapping was linear in log pressure and~~
14 ~~volume mixing ratio of CO. An Two~~ examples of comparisons of trajectory-mapped MOZAIC-
15 IAGOS CO profiles with ~~an~~ individual (reduced) $5^\circ \times 5^\circ$ MOPITT CO profiles ~~is~~ are shown in Fig.
16 ~~23. The original trajectory-mapped MOZAIC-IAGOS CO profile, the a priori profile, and the~~
17 ~~transformed trajectory-mapped MOZAIC-IAGOS CO profile are shown along with the MOPITT~~
18 ~~retrieved CO profile.~~ The application of the averaging kernels to the MOZAIC-IAGOS CO
19 profile results in significant a vertical transformation, which can shift mixing ratios significantly
20 at some levels. The averaging kernel, for example, identified as "1000" (i.e., surface) shows
21 how changes to the true CO mixing ratio at all ten retrieval levels would each contribute to a
22 change in the retrieved value at the surface at 1000 mbar. The original trajectory-mapped
23 MOZAIC-IAGOS climatology profile is quite different from the transformed climatology profile
24 and ~~as seen from the same figure~~ the departures of the transformed CO mixing ratio from the true
25 mixing ratios can be as large as 60 ppb at some pressure levels.

26 CO total column amounts are retrieved from the MOPITT observations in addition to the profile
27 retrievals. The retrieved CO total column c_{ret} (a scalar) is related to the retrieved profile x_{ret} (a
28 vector) through the linear relation

$$29 \quad c_{ret} = \mathbf{t}^T \mathbf{x}_{ret} \quad (3)$$

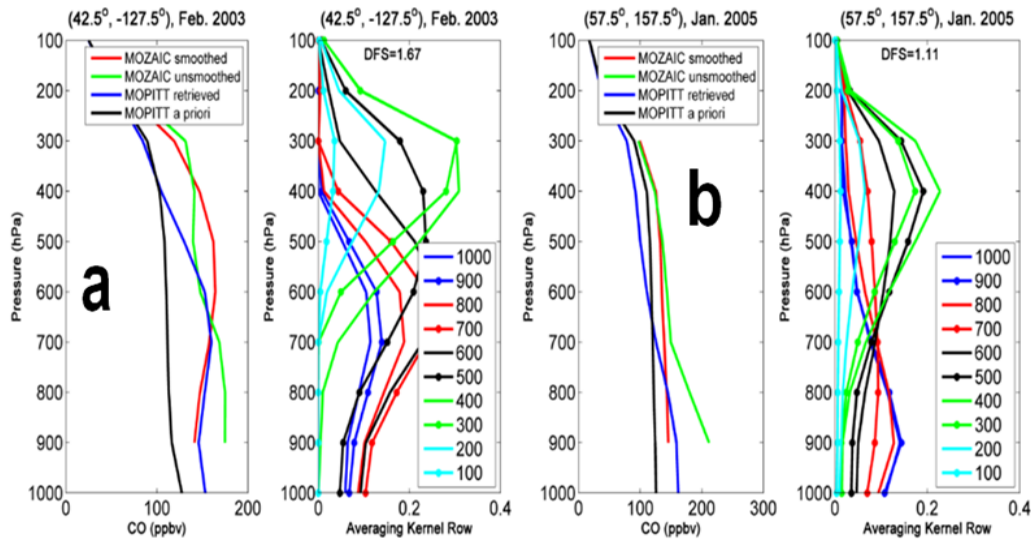
30 where T indicates the transpose operation and t is the total column vectors. The CO total column
31 averaging kernel can be calculated from the profile averaging kernels by

$$32 \quad \mathbf{a} = \mathbf{t}^T \mathbf{A} \quad (4)$$

33 The column operator simply converts the mixing ratio for each retrieval level to a partial column
34 amount. Using the hydrostatic relation, the operator \mathbf{t} is expressed as

$$35 \quad \mathbf{t} = 2.120 \cdot 10^{13} \Delta p \quad (5)$$

1 [Equation \(5\)](#) is expressed in molecules/cm²/ppbv and Δp is the vector of the thicknesses of the
 2 [retrieval pressure levels](#) (in hPa).



3
 4 **Fig. 23.** Examples of comparisons of monthly means of the trajectory-mapped MOZAIC-IAGOS
 5 CO profiles, with the corresponding MOPITT's averaging kernels, a priori and retrievals. The
 6 left panels of each subplot show the original trajectory-mapped MOZAIC-IAGOS climatology
 7 profile (green, i.e. unsmoothed ~~in the caption~~), the a priori profile (black), the transformed
 8 trajectory-mapped MOZAIC-IAGOS climatology profile (red, i.e. smoothed ~~in the caption~~), and
 9 the MOPITT retrieved CO profile (blue). The right panels ~~of each subplot~~ shows the mean
 10 averaging kernels, [for different pressure levels](#), obtained by averaging all daytime averaging
 11 kernels in the 5°x5° latitude-longitude box centered on the coordinates indicated.

12 ~~The different colors of the averaging kernel curves indicate the different pressure levels.~~

13 3 Validation

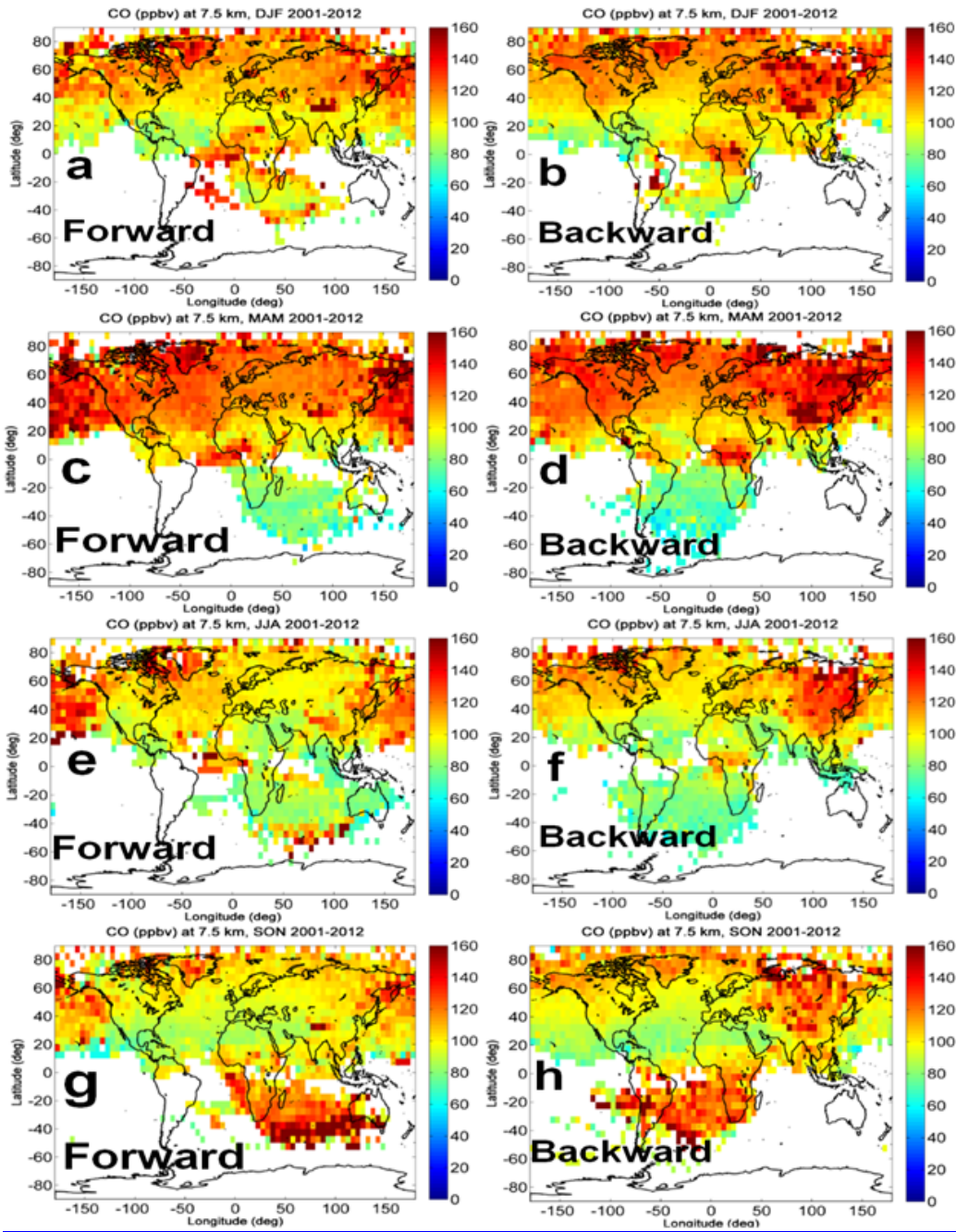
14 Validation of the trajectory-mapped MOZAIC-IAGOS CO dataset product has been performed
 15 by ~~Eq. (1)~~ comparing maps constructed using only forward trajectories against ~~with~~ those
 16 constructed using only backward trajectories; ~~and Eq. (2)~~ comparing profiles for individual
 17 airports against those produced by the mapping method when data from that site are excluded;
 18 [\(3\) comparing with global MOZAIC-IAGOS cruise-level data, which were not included in the](#)
 19 [trajectory-mapped dataset, and \(4\) comparing with independent data from the NOAA aircraft](#)
 20 [flask sampling program.](#) ~~The airport stations that have been selected in this validation study~~
 21 ~~represent tropical and northern hemisphere midlatitude locations that are subject to different~~
 22 ~~meteorological and CO source conditions.~~

1 3.1 Comparison of trajectory-mapped MOZAIC-IAGOS CO profiles

2 | As a first step in validation of the trajectory-mapped climatology, Figs. 3-4 and S1 (in the
3 | Supplement) assess the differences between the CO mapping produced using only backward and
4 | only forward trajectories for different seasons using the 7.5 km level as an example. If chemistry
5 | (i.e. local sources or sinks) were a significant source of error then one would expect to see
6 | differences between these maps. In fact, the CO distribution patterns are very similar (Fig. 34).
7 | Differences are most commonly 10% or less, and found to be less than 30% for almost all cases.
8 | They are typically less than 10% at northern mid-latitudes and less than 20% in the tropics
9 | between $\pm 30^\circ$ latitude, except in the Pacific and Atlantic oceans where they can be as large as
10 | 30%. As Fig. S1 illustrates, differences (Fig. S1) also show no distinct pattern, except for some
11 | clustering in areas where the trajectories are longest, and therefore least reliable. As differences
12 | between the two distributions are comparable with the uncertainties of the mean value estimates
13 | and not systematic, it is reasonable to combine forward and backward mapped values to produce
14 | an averaged CO map.

15

16



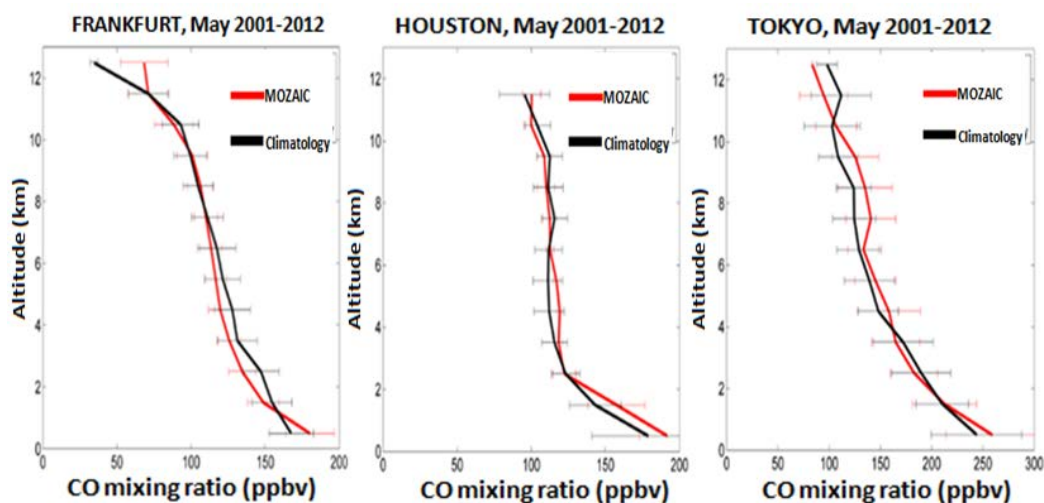
1
 2 **Fig. 34.** Examples of the global distribution, 2001-2012, of trajectory-mapped MOZAIC-IAGOS
 3 CO (ppbv) produced using only backward (right panels) and only forward (left panels)

1 trajectories at 7.5 km a.s.l. ~~The panels correspond to different seasons:~~ (a, b) December-
2 February, (c, d) March-May, (e, f) June-August and (g, h) September-November ~~2001-2012~~.

3 3.2 Comparison between trajectory-mapped and in situ profiles

4 A good test of an interpolation model is to examine how it performs in areas where no data are
5 available. Figure 4-5 compares the trajectory-mapped climatology profiles at three airport sites
6 (Frankfurt, Germany; Houston, USA; and Tokyo, Japan) with the average of the MOZAIC-
7 IAGOS data from each of these sites for May of 2001-2012. ~~However, since the sampling~~
8 ~~frequency varies from airport to airport,~~ Houston and Tokyo are not as well sampled as Frankfurt
9 ~~throughout the period~~(Figure 1). The climatology profiles for each location were produced by
10 excluding data from that location, but using all other MOZAIC-IAGOS data.

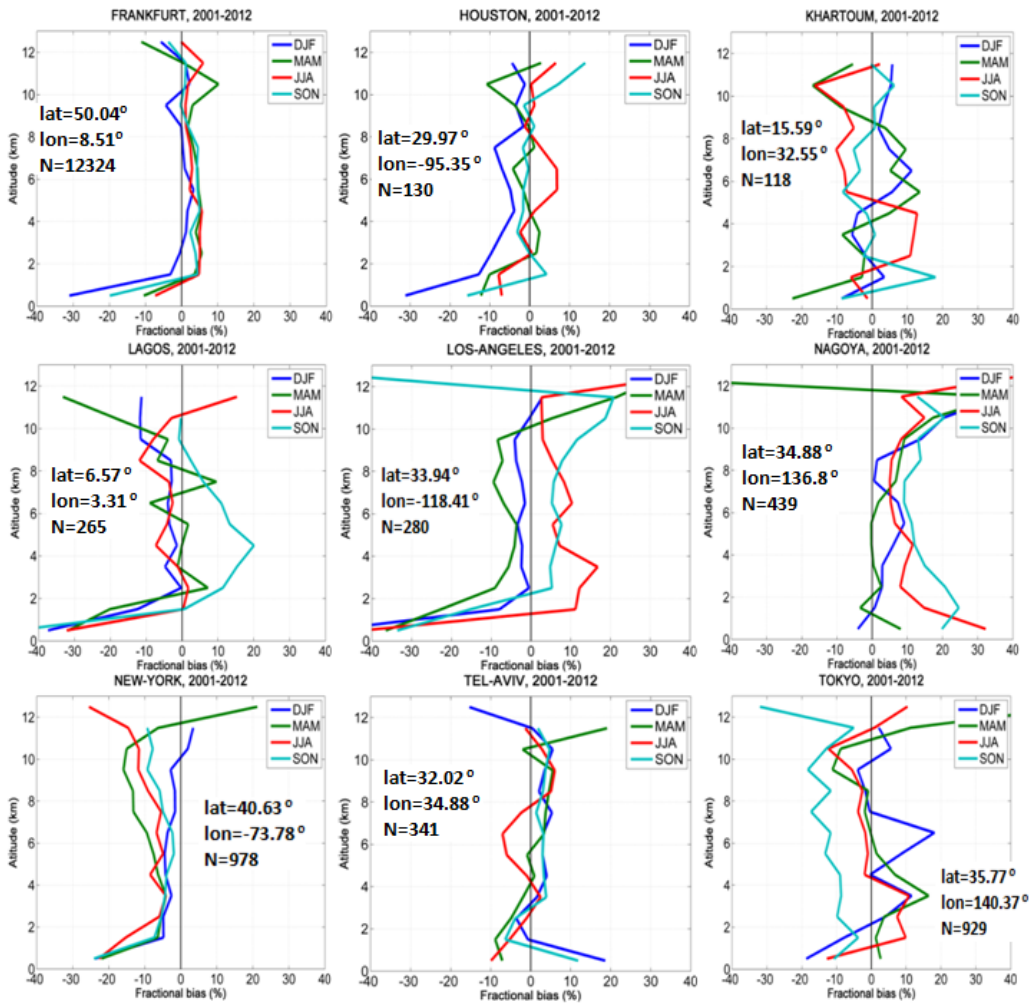
11 Generally, the profiles from the two methods agree very well and the agreement is especially
12 good in the free troposphere, at altitudes between 2 and 10 km. Referring to the bottom panels of
13 Fig. 45, the magnitude of the differences for most altitudes is well under 20%.



14
15 **Fig. 45.** Comparisons of trajectory-mapped MOZAIC-IAGOS CO climatology and MOZAIC-
16 IAGOS profiles at ~~Frankfurt, Germany (left panels), Houston, TX (middle panels), Tokyo, Japan~~
17 ~~(right panels)three sites. The top left, middle and right panels show MOZAIC-IAGOS CO~~
18 ~~climatology profiles (black) and the corresponding MOZAIC-IAGOS in situ profiles (red) of~~
19 ~~Frankfurt (Germany), Houston (TX, USA) and Tokyo (Japan) respectively for May 2001-2012.~~
20 The climatology profiles for each location were produced by excluding data from that location,
21 but using all other MOZAIC-IAGOS data. The horizontal error bar half-length is twice the
22 standard error of the mean (equivalent to 95% confidence limits on the averages when the
23 number of data points is large). ~~Bottom left, middle and right panels indicate the relative~~
24 ~~difference $[2*(Clim - MOZAIC)/(Clim + MOZAIC)]$, expressed in %, between the trajectory-mapped~~

1 ~~MOZAIC IAGOS climatology and MOZAIC IAGOS in situ profiles from Frankfurt (Germany),~~
2 ~~Houston (USA) and Tokyo (Japan) respectively for May 2001-2012. The actual MOZAIC-~~
3 ~~IAGOS profiles are labeled as MOZAIC, while the profiles from trajectories without input from~~
4 ~~the airport station being tested are labeled as Climatology.~~

5 ~~In Fig. 5-6 we extend the shows seasonally-averaged comparisons shown in Fig. 4 for other~~
6 ~~seasons as well as for another airports that represent different meteorological and source~~
7 ~~conditions differences, using this method, for a number of airports with different characteristics.~~
8 ~~The airport stations that have been selected in this validation study represent tropical and~~
9 ~~northern hemisphere midlatitude locations that are subject to different meteorological and CO~~
10 ~~source conditions. The selected airports are Atlanta (USA), Cairo (Egypt), Frankfurt (Germany),~~
11 ~~Houston (USA), Khartoum (Sudan), Lagos (Nigeria), Los Angeles (USA), Nagoya (Japan), New~~
12 ~~Delhi (India), New York (USA), Tel Aviv (Israel) and Tokyo (Japan). Again, the sampling~~
13 ~~frequency among the airports is not the same throughout the period. Similar to the results shown~~
14 ~~in Fig. 4, in Fig. 5 we notice good agreement between the trajectory-mapped and the~~
15 ~~in situ measurements for different locations and seasons across the globe is generally good in the~~
16 ~~free troposphere. There are larger differences below 2 km where trajectories have larger errors~~
17 ~~predominantly due to complex dispersion and turbulence in the planetary boundary layer [Stohl~~
18 ~~and Seibert, 1998] . However, the overall agreement between 2 and 10 km is very good with~~
19 ~~biases again within 20%. As in previous studies using this method, the largest differences are~~
20 ~~seen where other sources of data are distant. The smallest overall bias is seen at Frankfurt, even~~
21 ~~though the exclusion of Frankfurt data removes nearly 1/3 of the total number of profiles.~~
22 ~~Apparently data from nearby airports such as Munich (Germany) and Brussels (Belgium) map~~
23 ~~accurately to the Frankfurt location. The consistency of these validation tests suggests that the~~
24 ~~trajectory-mapped dataset provides a reliable picture of the tropospheric CO distribution.~~

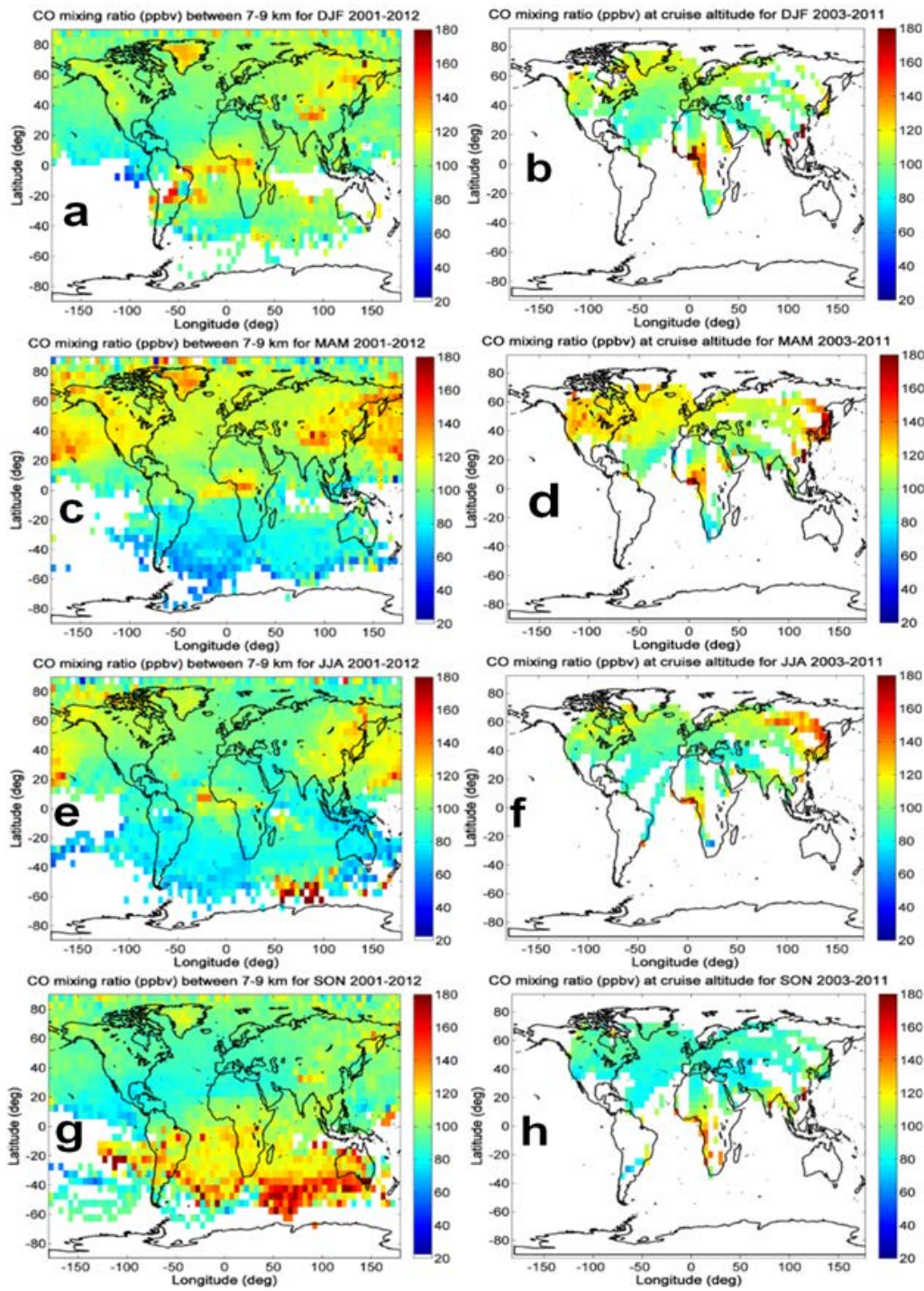


1
2
3 **Fig. 56.** Similar to Fig. 4 (lower panels) but for the seasonal Seasonal mean relative biases
4 $[2(\text{Clim-MOZAIC})/(\text{Clim}+\text{MOZAIC})]$, expressed in %, between trajectory-mapped and
5 MOZAIC-IAGOS in situ profiles for the period from 2001 to 2012. In each panel, different
6 colors indicate different seasons: December-February (blue), March-May (green), June-August
7 (red) and September-November (cyan). The selected airports are representative of different
8 meteorological and source conditions across the globe. N , lat and lon are the number of profiles,
9 latitude and longitude of each airports.

10 **3.3 Comparison with the MOZAIC-IAGOS in-situ for Upper Troposphere**

1 We can also compare the trajectory-mapped profile data and MOZAIC-IAGOS in situ global CO
2 data at cruise altitudes between 8 and 12 km. ~~The right panels of Fig. 67 The maps found at~~
3 ~~http://www.iagos.fr/mace/reanalysis_climatology_CO.php~~ show the global seasonal mean
4 (December-February, March-May, June-August and September-November) distribution of CO in
5 the upper troposphere (within 60 hPa below the tropopause) for the period from 2003 to 2011.
6 ~~The figure clearly shows the seasonal cycle of CO with seasonal maximum in the northern~~
7 ~~hemisphere (NH) spring (MAM) and peak CO values in the southern hemisphere (SH) spring~~
8 ~~(SON).~~ Elevated CO levels in the upper troposphere are generally seen over the areas where
9 there is strong biomass burning (~~central Africa, southern Africa and South America~~). ~~The figure~~
10 ~~also reveals that h~~High CO emissions are observed over eastern China in MAM primarily due to
11 a rise in coal use (Boden et al., 2009; Gregg et al., 2008; Tie et al., 2006) and ~~an~~ increasing
12 number of vehicles (Cai and Xie, 2007).

13 ~~The left panels of Fig. 67 Figure-6 shows the trajectory-mapped global seasonal variation of CO~~
14 ~~for December-February, March-May, June-August and September-November climatology~~ 2001-
15 2012 at altitudes between 7 and 9 km above sea level. The trajectory-mapping yields more data
16 over the oceans and NH high latitudes ~~in Fig. 6 than is seen in CO maps cited above~~. However,
17 ~~major regional features of the global CO distributions for different seasons are clearly evident in~~
18 ~~both figures.~~ The figures show ~~seasonal~~ high CO values in spring in both hemispheres and
19 elevated CO levels over regions where there ~~is intensive biomass burning (central Africa,~~
20 ~~southern Africa and South America) and anthropogenic emissions (eastern China are strong~~
21 ~~sources)~~. Comparable CO values are noticeable from the figures over the Northern Atlantic
22 Ocean, ~~although the trajectory-mapped data appear high over as well high-elevation areas as like~~
23 ~~Greenland and the Himalayas.~~ ~~This may be due to over-correction of trajectories for terrain~~
24 ~~differences.~~ ~~Such an o~~Overall, ~~the good~~ qualitative agreement between the trajectory-mapped
25 CO and MOZAIC-IAGOS in situ CO cruise data ~~result suggests that the trajectory-mapped CO~~
26 ~~dataset performs well appears very good, even~~ in remote areas ~~as well~~.



1 **Fig. 67.** Global distribution of seasonal mean trajectory-mapped MOZAIC-IAGOS CO between
2 7-9 km altitudes above sea level for the period from 2001 to 2012. Left: Panels (MOZAIC-
3 IAGOS trajectory). Right: and right (MOZAIC-IAGOS cruise altitude.

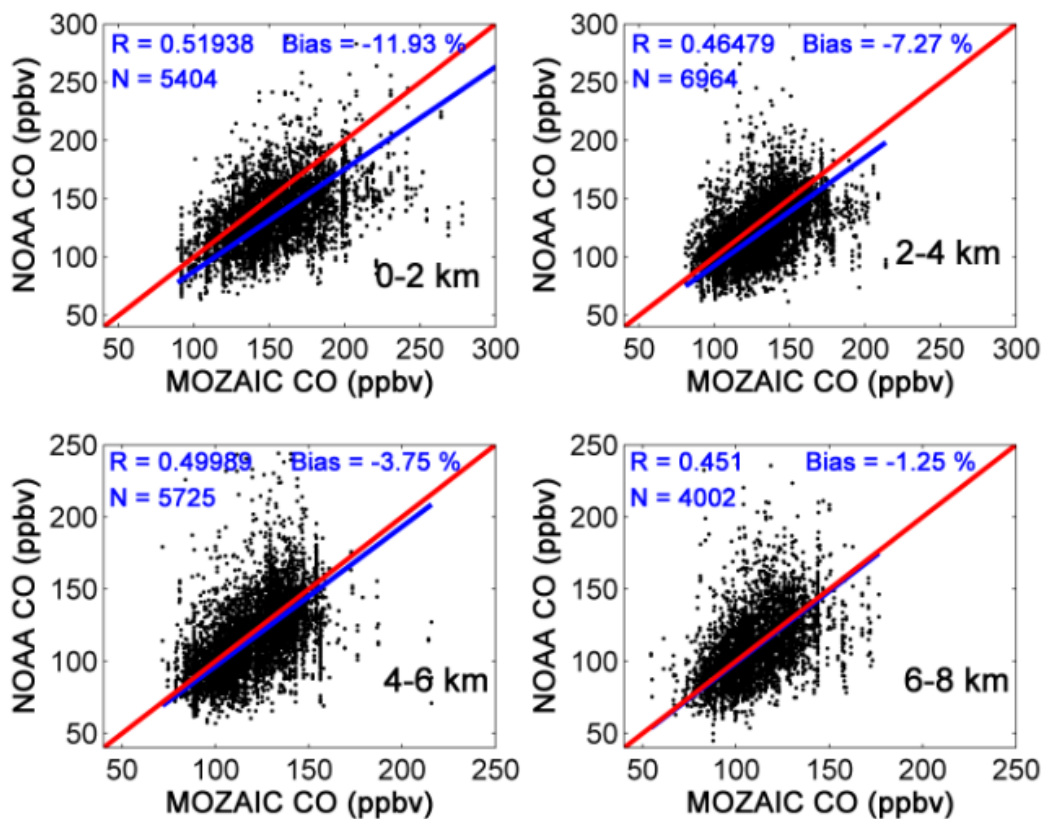
4) panels a, b, c, and d show the seasonal mean of CO for December February, March May, June-
5 August and September November from top to down, respectively.

6 3.4 NOAA CO vertical profiles

7 The vertical in situ CO profiles acquired through NOAA’s flask sampling program have been
8 extensively utilized previously for validations of CO measurements of MOPITT [Emmons et al.,
9 2004; Emmons et al., 2009; Deeter et al., 2010; Deeter et al., 2013]. Typically 12–15 flask
10 samples are utilized to derive an in situ profile and a single flask is used to sample air at a unique
11 altitude, providing in situ measurements from near the ground up to about 300–350 hPa. The
12 flasks are shipped to the Global Monitoring Division of NOAA’s Earth System Research
13 Laboratory (ESRL) for trace gas analysis. Details on procedures of sample collection are found
14 in Novelli et al. [1992], Lang et al. [1992], and Conway et al. [1994].

15 Figure 6A8 shows comparisons between NOAA in-situ data and the trajectory-mapped
16 MOZAIC-IAGOS CO climatology, for altitude ranges of 0-2, 2-4, 4-6 and 6-8 km The
17 comparison uses for all available flask data (1940 profiles for the period from 2001-2012).
18 NOAA CO data points are matched with the corresponding grid cell ($5^{\circ} \times 5^{\circ} \times 1$ km) of the
19 monthly climatology, for the same year and month. If the monthly CO value for a particular grid
20 cell is missing, the seasonal mean (if it exists) of the trajectory-mapped CO climatology- (2001-
21 2012) is used for the comparison. Above 2 km agreement is fairly good, considering that the
22 comparison is between point measurements and monthly averages over a large volume. The
23 positive bias below 2 km is probably due to the effect of urban sources of CO since airports are
24 located close to cities. In general, MOZAIC-IAGOS CO measurements at takeoff and landing
25 are above background. Their “airport effects” decreases rapidly as can be from the figure for
26 higher altitudes. Their decrease is not only because the aircraft ascends above the boundary
27 layer,s but also samples over 150-400 km in distance as the aircraft ascends to, or descends
28 from, cruise altitude.

29



1
 2 [Fig. 6A8 CO mixing ratio comparison between trajectory-derived and NOAA flask data for the](#)
 3 [period from 2001-2012, for four altitude ranges. Bias is calculated as the mean of the differences](#)
 4 [in %, \$\[2\(\text{NOAA}-\text{Clim}\)/\(\text{Clim}+\text{NOAA}\)\]\$, of all data points. The blue line is the line of best fit, the](#)
 5 [red line is the 1:1 line, N is number of data pairs, and R is the correlation coefficient. Monthly](#)
 6 [trajectory mapped CO data are used for the comparison, or seasonal mean values if the monthly](#)
 7 [mean value for a particular grid cell is not available.](#)

8 **4 Trajectory-mapped MOZAIC-IAGOS Versus MOPITT**

9 This section is devoted to comparing the trajectory-mapped MOZAIC-IAGOS CO dataset with
 10 the extensively validated product from the MOPITT instrument onboard the NASA Terra
 11 satellite, which has been operating continuously since March 2000 (Drummond and Mand, 1996;
 12 Edwards et al., 1999). Global comparison ~~was is~~ made for both CO profiles and CO total column
 13 for different time periods.

14 **4.1 Comparison with MOPITT CO profiles**

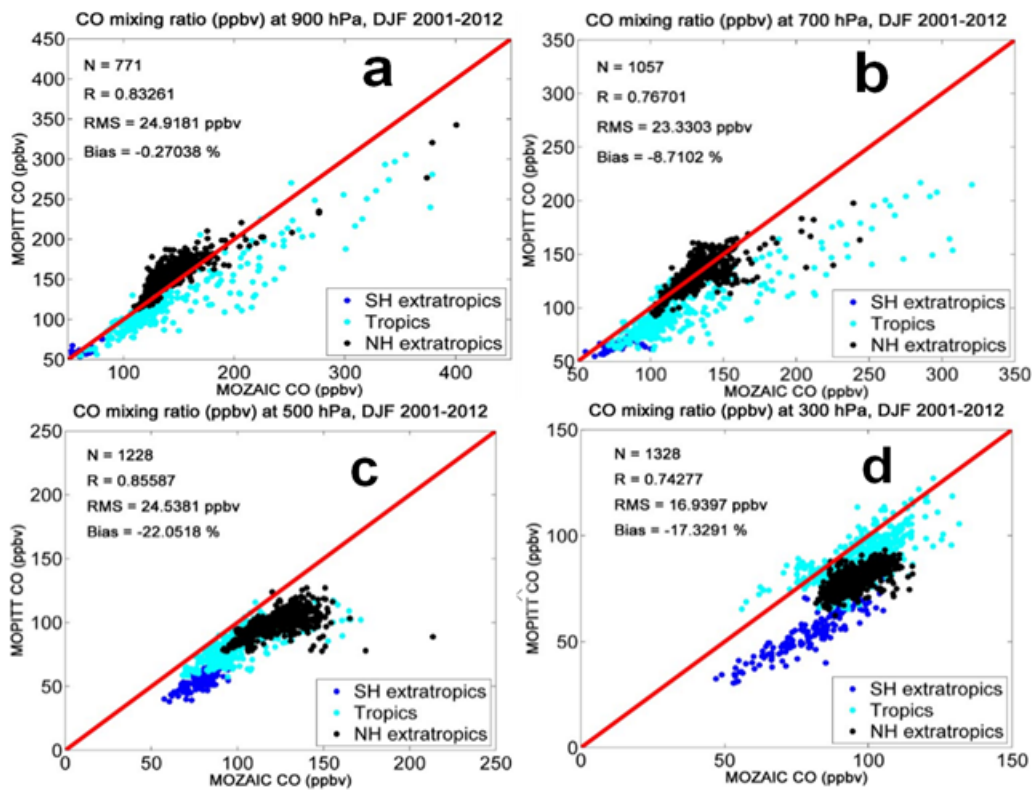
1 As described in Section 2.4, in order to make a rigorous comparison with MOPITT data, the
2 climatology profiles are first transformed using the corresponding MOPITT a priori profiles and
3 averaging kernels via Eq. (2). Figure 2-3 shows examples of retrieved CO profiles (x_{ret}),
4 together with the original climatology (x) and the a priori profiles (x_a).

5 When ~~examining the comparison between the~~ MOPITT CO retrievals and the trajectory-
6 mapped CO profile it is useful to keep in mind the ~~shapes and magnitudes (or areas)~~ shapes of the
7 averaging kernels. For example, ~~the 100 and 1000 mbar kernels are typically less peaked than the~~
8 ~~other pressure levels. Consequently,~~ the generally broad and weak averaging kernels ~~for the 100~~
9 ~~and 1000 mbar levels demonstrate~~ that a significant fraction of the information ~~used~~ in the
10 retrieval is from the a priori profile ~~or CO~~ and from other ~~layers altitudes or both~~. Figure 2-3 also
11 cautions that the transformed trajectory-mapped MOZAIC-IAGOS CO is closer to both the
12 MOPITT CO retrievals and a priori profiles when there is less information from the
13 measurement. ~~Furthermore, as can be seen from Fig. 2, the MOPITT retrievals are not able to~~
14 ~~resolve the finer scale vertical structure of the trajectory mapped CO profiles. The departures of~~
15 ~~the retrieved CO VMR from the trajectory mapped VMRs at some pressure levels are as large as~~
16 ~~60 ppb.~~ In the lower troposphere the MOPITT CO retrieval profile is positively biased (Deeter et
17 al., 2014), whereas the bias is negative in the upper troposphere. In Fig. 23, we have used only
18 the dayside retrievals from MOPITT as the dayside retrievals have the maximum information
19 content (Deeter et al., 2004). ~~The MOPITT V6 L3 retrievals, which have been regridded to 5°~~
20 ~~resolution, are used in this analysis.~~

21
22 Figure 7-9 shows ~~profile~~ comparisons between MOPITT retrievals and the MOZAIC-IAGOS
23 climatology for global CO data at pressure levels 900 hPa, 700 hPa, 500 hPa, and 300 hPa. The
24 ~~slopes biases~~ and correlations between MOPITT CO ~~retrievals VMR~~ and the CO climatology
25 (after applying the averaging kernels and the a priori profiles) ~~for different levels~~ are indicated in
26 ~~the each figure plot. The different dot colors shown in Fig. 7 stand for different latitude bands:~~
27 ~~23.5-66.5° S (SH extratropics), 23.5° S-23.5° N (tropics), 23.5-66.5° N (NH extratropics).~~ The
28 ~~same figure shows that there~~ are clearly two distinct clusters of dots in Fig. 7a-9a and 7b-9b, and
29 the high CO VMRs values seen here are from ~~the~~ tropics, with ~~a a very few~~ very little small
30 ~~number~~ from the NH extratropics. ~~The enhanced CO values may have originated from~~
31 ~~anthropogenic sources and/or biomass burning; however, identifying individual sources is~~
32 ~~beyond the scope of this paper.~~ Recent work by Ding et al. (2015) shows the association of
33 enhanced CO in the free troposphere with the uplifting of CO from biomass burning and
34 anthropogenic sources.

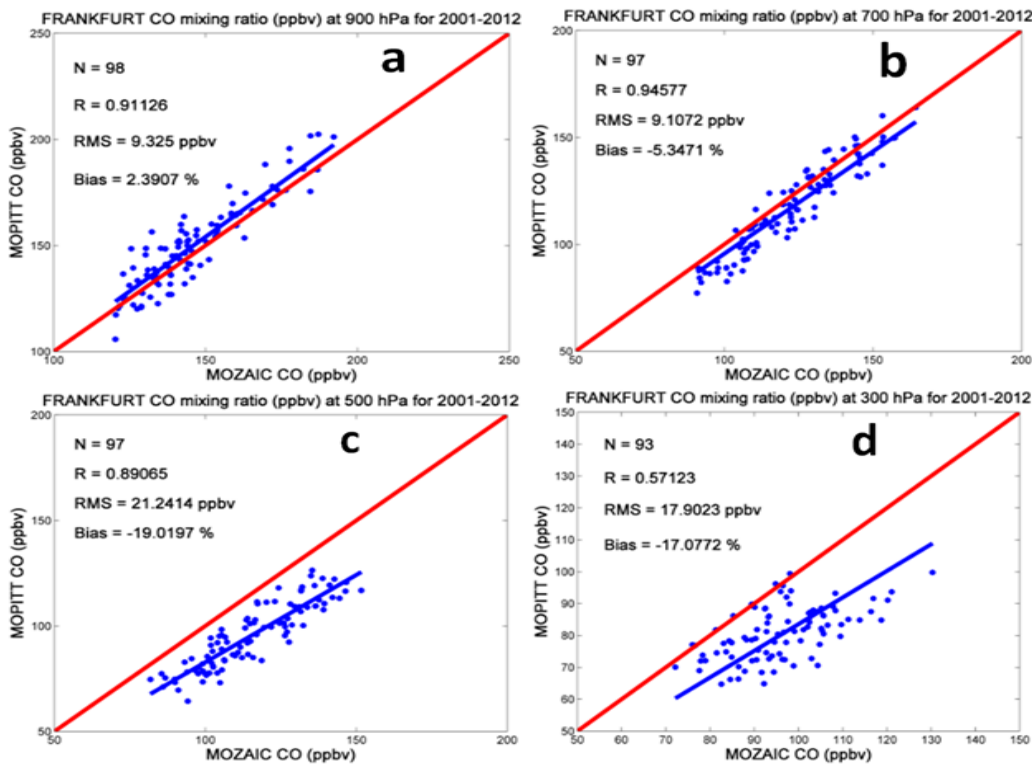
35 MOPITT and trajectory-mapped MOZAIC-IAGOS CO climatology mixing ratios are well-
36 correlated with correlation coefficients of 0.7 or higher, for daytime data over both land and
37 ocean. However, Fig. 7-9 also reveals significant biases between MOPITT retrievals and the
38 trajectory-mapped MOZAIC-IAGOS CO climatology (geometric) altitudes above the 700 hPa

1 [pressure level above 700 hPa](#). Although in Fig. [7-9](#) we have chosen to show biases for [January](#)
 2 [DJF winter](#) 2001-2012, the same analysis for other [months and time periods/seasons](#) yields similar
 3 results.



4
 5
 6 **Fig. 79.** Comparison results for [January-DJF \(December, January, February\)](#) 2001-2012.
 7 MOPITT CO retrievals at 900 [\(a\)](#), 700 [\(b\)](#), 500 [\(c\)](#) and 300 [\(d\)](#)-hPa are plotted against trajectory-
 8 mapped MOZAIC-IAGOS CO climatology profiles that have been transformed using the
 9 MOPITT averaging kernels and a priori data. The red line is the 1:1 line, [the blue line is the line](#)
 10 [of best fit](#), N denotes the total number of data points, R is the correlation coefficient, RMS is root
 11 mean square error in ppbv and $Bias$ is the relative bias between them in %. In each panel, the
 12 different color dots [show for latitude bands: tropics \(cyan\), NH extratropics \(black\) and SH](#)
 13 [extratropics \(blue\)](#). [group different latitude bands: 23.5-66.5° S \(SH extratropics\), 23.5° S - 23.5°](#)
 14 [N \(tropics\) and 23.5-66.5° N \(NH extratropics\)](#). [In this study, we have used the monthly](#)
 15 [MOPITT V6 L3 TIR/NIR daytime product](#).

1 These large differences are surprising, MOPITT seems to underestimate CO VMR by as much as
2 21% against the trajectory mapped MOZAIC IAGOS CO climatology at 500 hPa. This result is
3 significantly different from~~since~~ previous work such as Deeter et al. (2014, 2013, 2010) and
4 Emmons et al. (2004, 2007, 2009). Most of these examined earlier versions of the MOPITT L3
5 L2 product, although Deeter et al. (2014), who also use the MOPITT L3 V6 product, and
6 NOAA flask data (among other sources), and reported biases -varying from -5.2% at 400 hPa to
7 8.9% at the surface. These results are not dissimilar to our comparison in Figure 6A8, and would
8 suggest a difference of about 5% between MOPITT and the trajectory-mapped climatology, with
9 the climatology being higher primarily due to the airport effect. Although the validation data sets
10 are not identical (owing primarily to incomplete global coverage of the MOZAIC-IAGOS
11 product), the relative bias of 22% at 500 hPa seems excessive. In all cases the validation data
12 consisted of flask samples taken by NOAA aircraft. In order to eliminate the possibility that
13 trajectory errors might be contributing to ~~the this~~ bias ~~we find with the MOZAIC IAGOS CO~~
14 ~~dataset~~, we have also compared MOZAIC-IAGOS in situ CO profiles against MOPITT
15 retrievals. As an example in Fig. 810, we display the comparison between MOZAIC-IAGOS in
16 situ CO profiles at Frankfurt (Germany) and MOPITT CO retrievals, which have been regridded
17 to 5° resolution, over Frankfurt from MOPITT overpasses. The MOZAIC-IAGOS in situ aircraft
18 CO values have been transformed using the MOPITT averaging kernels and a priori data, for the
19 period from December 2001- December 2012. MOPITT and MOZAIC-IAGOS are again
20 strongly correlated, and biases at 500 hPa and 300 hPa are large, and in fact very similar in
21 magnitude to those with respect to the trajectory-mapped MOZAIC-IAGOS CO dataset. This
22 implies that the differences at 500 and 300 hPa are not a result of the trajectory mapping.

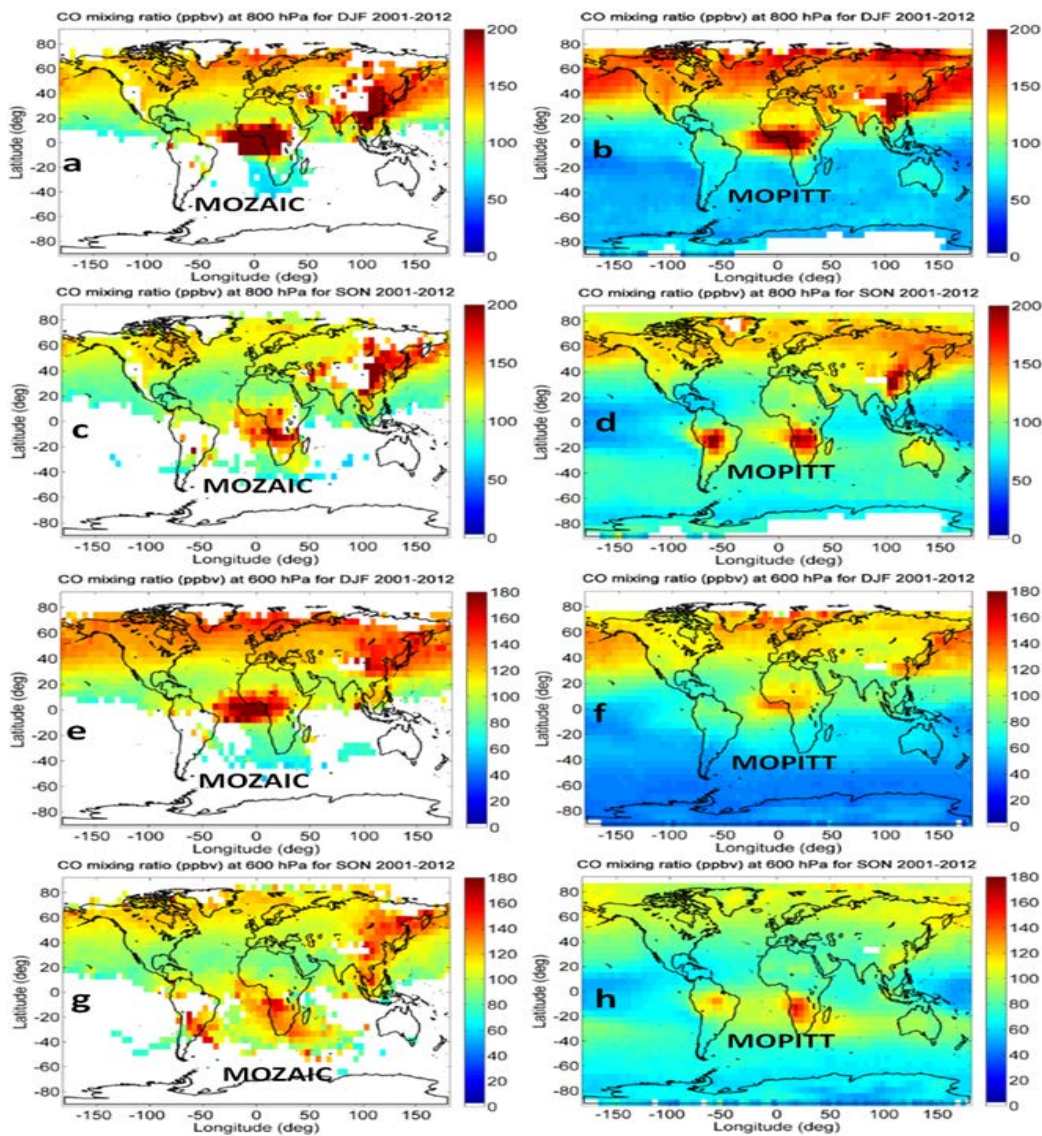


1
 2 **Fig. 810.** Same as Fig. 7-9 but MOPITT CO retrievals at 900 hPa (a), 700 hPa (b), 500 hPa (c),
 3 ~~and 300 (e) hPa~~ are plotted against MOZAIC-IAGOS CO in situ profiles that have been
 4 transformed using the MOPITT averaging kernels and a priori data. The in situ profiles are
 5 monthly means from 2001-2012 (Frankfurt, Germany). Outliers (CO mixing ratios more than 1.5
 6 standard deviations from the mean at each pressure level) have been removed, which improves
 7 the correlation coefficient at 300 hPa but makes no significant change in other derived
 8 parameters.

9 A global comparison between the trajectory-mapped MOZAIC-IAGOS climatology and
 10 MOPITT at 600 hPa is displayed in Fig. 911. As can be seen, ~~from the same figure~~ both datasets
 11 capture major features of the CO distribution, particularly anthropogenically polluted (i.e.,
 12 northeast China) and biomass burning (i.e., west Africa, central Africa, South Africa and central
 13 America) regions. The CO-rich air in the lower troposphere over west Africa, where biomass
 14 burning fires are active, is convectively lifted ~~vertically upward~~ to the upper troposphere where it
 15 disperses over the African tropics towards the east coast of South America ~~and the south Arabian~~
 16 ~~peninsula~~ (Edwards et al., 2003). ~~Indeed, the transport toward South America is much clearer.~~
 17 ~~In Over southern Africa and southeast Asia, where there are strong sources, In this region, and in~~

1 general at 600 hPa, higher CO VMRs are measured ~~found~~ by the MOZAIC-IAGOS mapping
2 than by MOPITT.

3 ~~Over southeast Asia, MOZAIC-IAGOS detects highly polluted air masses. In these areas~~
4 ~~MOZAIC-IAGOS also measures higher CO than MOPITT. Comparison of the panels for DJF~~
5 ~~with those for SON of Fig. 9 also show that the NH CO VMRs are much higher during~~
6 ~~December-February than September-November (a result of the difference in OH, as noted above)~~
7 ~~and the latitude gradient in December-February is higher than in September-November. This is~~
8 ~~because in the SH the seasonal peak in CO occurs in September-November. This comparison~~
9 ~~also reveals a shift of the biomass burning from central Africa to South Africa and central~~
10 ~~America. Both datasets capture this, although the TIR/NIR product offers the greatest sensitivity~~
11 ~~to CO in the lower troposphere (Deeter et al., 2014). MOZAIC-IAGOS shows higher CO~~
12 ~~concentrations in these regions than MOPITT. On the other hand, Liu et al. (2005) suggested that~~
13 ~~since MOPITT (V3-L2) has low sensitivity to CO in the lower troposphere, the CO VMR~~
14 ~~estimated may only be a lower bound. The same authors noted that fires can be missed if not~~
15 ~~large enough or if they do not coincide with the MOPITT overpass time, or both. The presence~~
16 ~~of clouds is also another limitation for missing data.~~



1

2 **Fig. 911.** Global distribution of the seasonal mean trajectory-mapped MOZAIC-IAGOS CO
 3 climatology (left panels), after transformation with the MOPITT a priori profiles and averaging
 4 kernels matrix, and MOPITT CO retrievals (right panels). CO mixing ratio (ppbv) as a function
 5 of latitude and longitude at 800 (a-d) and 600 (e-h) hPa pressure levels. Data are binned at $5^{\circ} \times 5^{\circ}$
 6 in latitude and longitude for the period from 2001-2012. The CO mixing ratios shown in panels:
 7 (a, b) at 800 hPa for DJF, (c, d) at 800 hPa for SON, (e, f) at 600 hPa for DJF and (g, h) at 600
 8 hPa for SON.

1 Figure S2 shows global maps of percentage differences between MOPITT and the transformed
 2 trajectory-mapped MOZAIC-IAGOS CO climatology at 800 and 600 hPa pressure levels for DJF
 3 and SON 2001-2012. Differences are generally less than $\pm 20\%$ at 800 hPa, with a negligible
 4 overall bias, but larger at 600 hPa, with MOPITT on average 10-20% ~~higher-lower, except for a~~
 5 ~~few few places over the Caribbean, southeast Asia and central Africa.??~~ Generally, the
 6 comparisons of the CO profiles of the transformed trajectory-mapped MOZAIC-IAGOS and
 7 MOPITT for both grid cells as well as zonal mean for different latitude bands show a consistent,
 8 significant bias: MOPITT is lower from about 700 hPa to 300 hPa, but shows a negligible bias in
 9 the lowermost troposphere. Above 300 hPa, they seem to agree better, although this may be
 10 partly due to the fact that the retrieved CO values in this region are highly influenced by the
 11 MOPITT a priori data for both cases.

12 4.2 Comparison with MOPITT CO total column values

13 CO total column amounts are retrieved from the MOPITT observations in addition to the profile
 14 retrievals. The retrieved CO total column \bar{c}_{ret} (a scalar) is related to the retrieved profile x_{ret} (a
 15 vector) through the linear relation

$$16 \bar{c}_{ret} = t^T x_{ret} \quad (3)$$

17 where T indicates the transpose operation and t is the total column vectors. The CO total column
 18 averaging kernel can be calculated from the profile averaging kernels by

$$19 \alpha = t^T A \quad (4)$$

20 The column operator simply converts the mixing ratio for each retrieval level to a partial column
 21 amount. Using the hydrostatic relation, the operator \bar{t} is expressed as

$$22 \bar{t} = 2.120 \cdot 10^{13} \Delta p \quad (5)$$

23 Equation (5) is expressed in molecules/cm²/ppbv and Δp is the vector of the thicknesses of the
 24 retrieval pressure levels (in hPa). The interfaces of the retrieval layers are set at the surface, top
 25 of the atmosphere, and the midpoints between the standard nine retrieval levels. Determination
 26 of Δp required in Eq. (5) has to be made individually for each retrieval because of the variability
 27 of the surface pressure. The boundaries of the imaginary layer associated with each level are
 28 located at the pressure midpoints between the levels in the grid.

29 For example, for a surface pressure of 950 hPa, the fixed retrieval pressure grid levels along with
 30 surface pressure would be (950, 900, 800, 700, 600, 500, 400, 300, 200, 100) hPa. Hence the
 31 corresponding Δp values would be (25, 75, 100, 100, 100, 100, 100, 100, 100, 100) hPa.
 32 Column amounts are calculated from the in situ profiles according to Eq. (6) to validate the CO
 33 total column retrievals.

1 In the same manner as we have done for the retrieved CO profiles, the retrievals of CO total
2 column c_{ret} may be compared against total column values derived from in situ profiles x .
3 Utilizing Eq. (2), the retrievals of the total CO column c_{ret} found in Eq. (3) can be rewritten
4 alternatively as

$$5 \quad c_{ret} = c_a + \alpha(x - x_a) \quad (6)$$

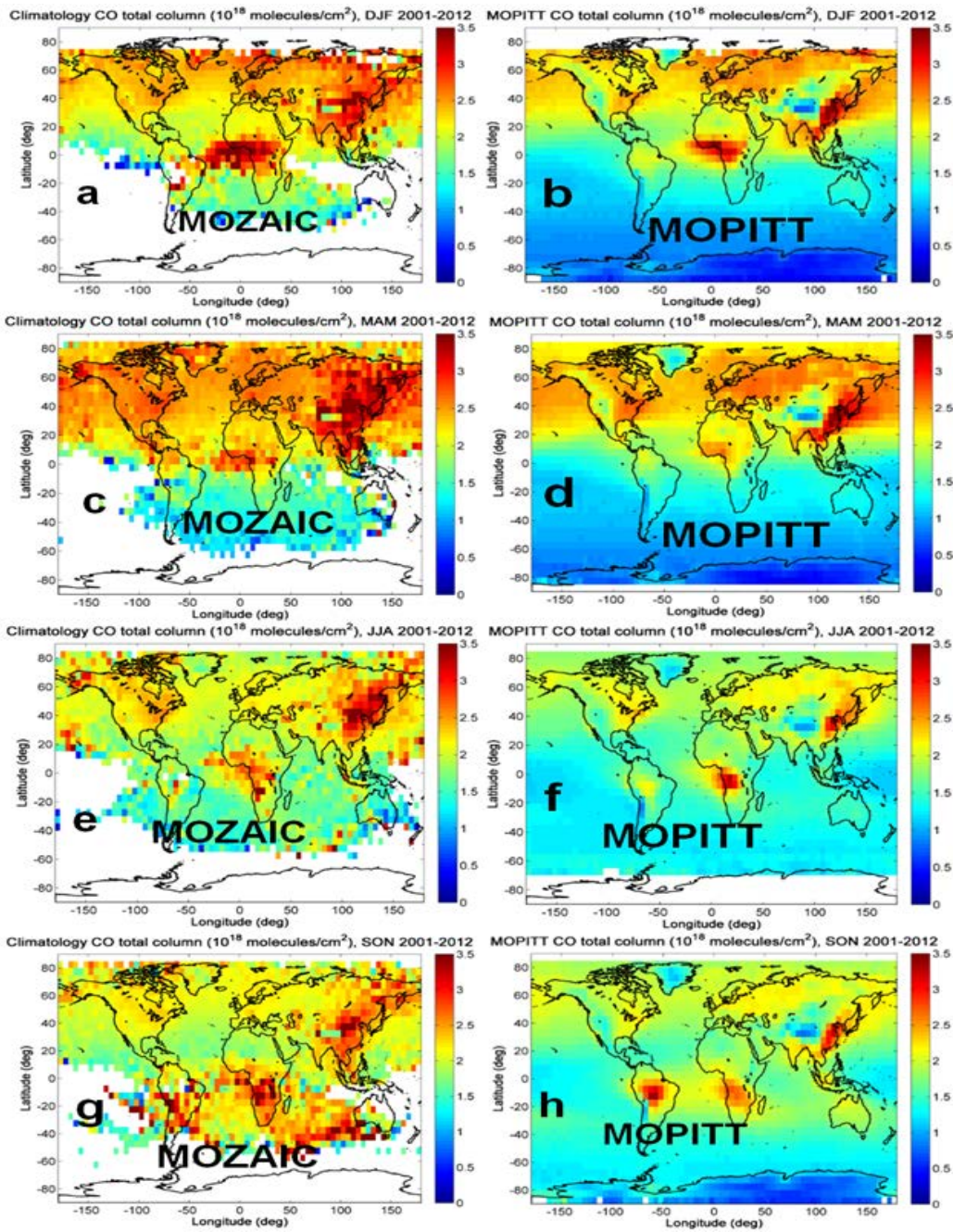
6 where $c_a = t^T x_a$ is the a priori total column value corresponding to the a priori profile x_a , α is
7 the CO total column averaging kernel and x is the in situ profile.

8 We have calculated the global total CO columns for both the MOZAIC-IAGOS CO climatology
9 (using the MOPITT a priori and averaging kernels by applying Eq. (6)) and for MOPITT CO
10 retrievals and compared different regions of the globe and different times-time intervals from
11 2001-2012. The comparisons between the climatology and the MOPITT observations agree well,
12 typically to within 10%. For most regions the MOPITT CO total columns are 10-20% slightly
13 high lower than the trajectory-mapped MOZAIC-IAGOS CO climatology total columns, with
14 larger differences while in high CO source regions MOPITT seems to underestimate CO
15 emissions. The SH shows a distinct latitude gradient, which is not evident in the NH. This is
16 likely related to the existence of major CO sources in the NH and the absence of large sources of
17 emission in the SH. Nighttime CO observations of MOPITT have not been validated and appear
18 subject to larger bias (Heald et al., 2004). Hence, we use the daytime data for comparison.

19 Figure 40-12 shows global total column CO for August 2002, December 2005, December 2011
20 and August 2012 four seasons. From Fig. 40,1 it is clear that MOPITT and the climatology are
21 similarly able to capture the CO spatial variability. In August 2002 and 2012 NH autumn,
22 elevated total column CO is seen over South America, southeast Asia and west African which is
23 due primarily to agricultural biomass burning in the regions. In both months, we see high total
24 column CO over southeast Asia and west Africa. High total column CO is also seen in all
25 seasons over eastern China, which is one of the major emission regions in the world. Northern
26 hemispheric total columns are much higher than those in the southern hemisphere, and CO is
27 somewhat more abundant in the NH winter (December), which is reasonable expected due to the
28 lower amounts of hydroxyl radical (OH) that are present in the troposphere in that season
29 (reduced oxidizing capacity). Difference plots for the CO maps shown Fig. 4012 are shown in
30 Figure S3. Generally, the MOPITT CO total column retrievals are slightly higher than the
31 trajectory mapped MOZAIC IAGOS CO climatology.

32

33

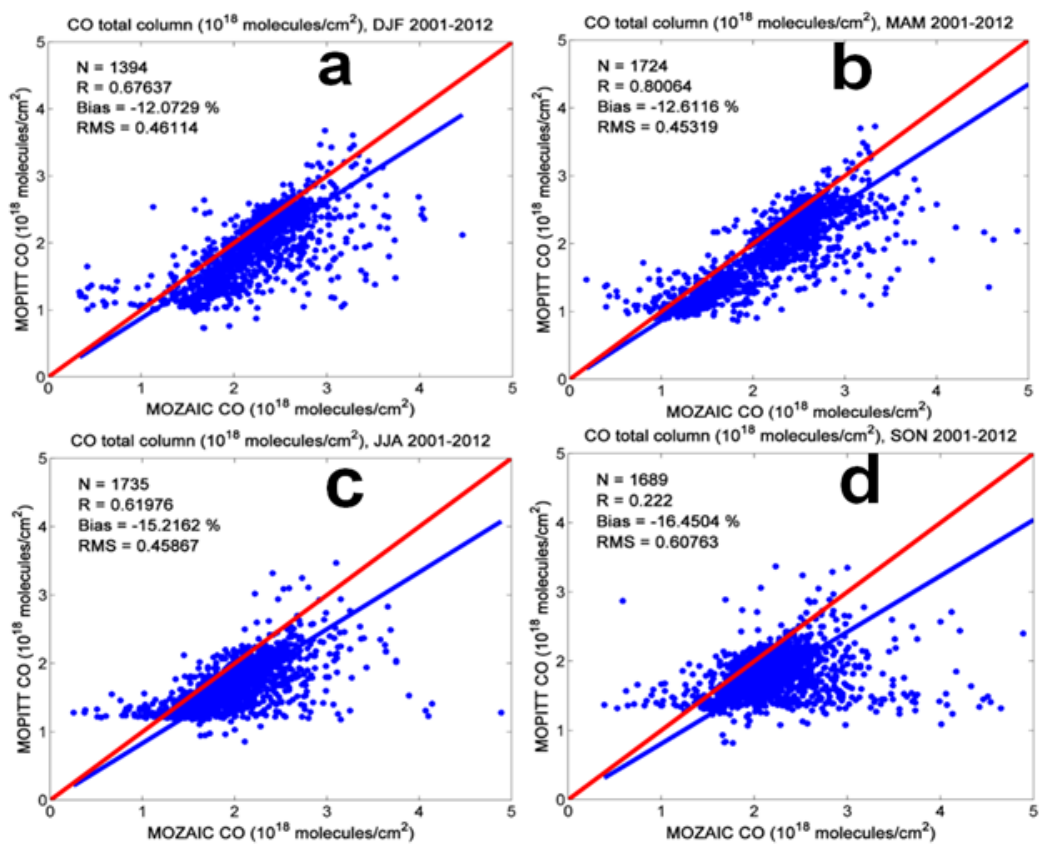


1
 2 **Fig. 4012.** Global total column CO from the transformed trajectory-mapped MOZAIK-
 3 climatogy and MOPITT data for ~~August-2002~~December-February, ~~December-2005~~March-

1 | May, December 2011 June-August and August-September-November 2001-2012. Data are
2 | averaged in 5°x5° latitude- longitude bins.

3 | Figure S3 shows global difference plots for the CO maps shown Fig. 10. Biases generally lie
4 | within ±20%, and the global mean bias between the MOPITT and MOZAIC IAGOS CO
5 | climatology total columns is typically about 5% or less. While overall bias shows MOPITT to
6 | be higher, it is also evident that the trajectory mapped MOZAIC IAGOS climatology is typically
7 | higher near major sources (eastern China, west central Africa and western South America) as
8 | well as over some areas of the oceans where aircraft data are not available. The negative biases
9 | near major sources are probably due to the limited vertical resolution of MOPITT as previously
10 | noted.

11 | Similar results are found for other years (Fig. 11-13). This figure shows scatter plots of retrieved
12 | MOPITT CO total columns against the transformed trajectory-mapped MOZAIC-IAGOS
13 | climatology for August 2008, December February, December 2008 March May, August 2012
14 | June August and December September November 2001-2012 the same periods shown in Fig.
15 | 10-12. MOPITT and the trajectory mapped climatology generally show strong correlations are
16 | strong except in SON 2001-2012, and average biases of less than 20% with MOPITT
17 | the trajectory MOZAIC-IAGOS is higher most cases. This is consistent with previous work,
18 | which also However, previous shows positive total column retrieval bias against aircraft data
19 | (Deeter et al., 2014, 2013; Emmons et al., 2009, 2007). The trajectory mapped climatology high
20 | bias might be in part associated with the effects of urban sources of CO since all airport effect;
21 | however the averaging kernels (Fig. 23) are not very sensitive to CO in the boundary layer.
22 | s are located near major urban centers.



1
2

3 **Fig. 4413.** Global MOPITT CO column retrievals versus transformed trajectory-mapped
 4 MOZAIC-IAGOS CO climatology column for ~~the months and years shown above~~ four seasons.
 5 The ~~mean difference in %bias is calculated as the difference for each grid cell, [2(MOPITT-~~
 6 ~~Clim)/(Clim+MOPITT)], is calculated for each pixel and then averaged over all pixelsgrid cells.~~
 7 The ~~blue line is the line of best fit, the red line is the 1:1 line and the correlation coefficient (R),~~
 8 total number of data points (N) and root mean square error (RMS) are ~~given~~indicated.

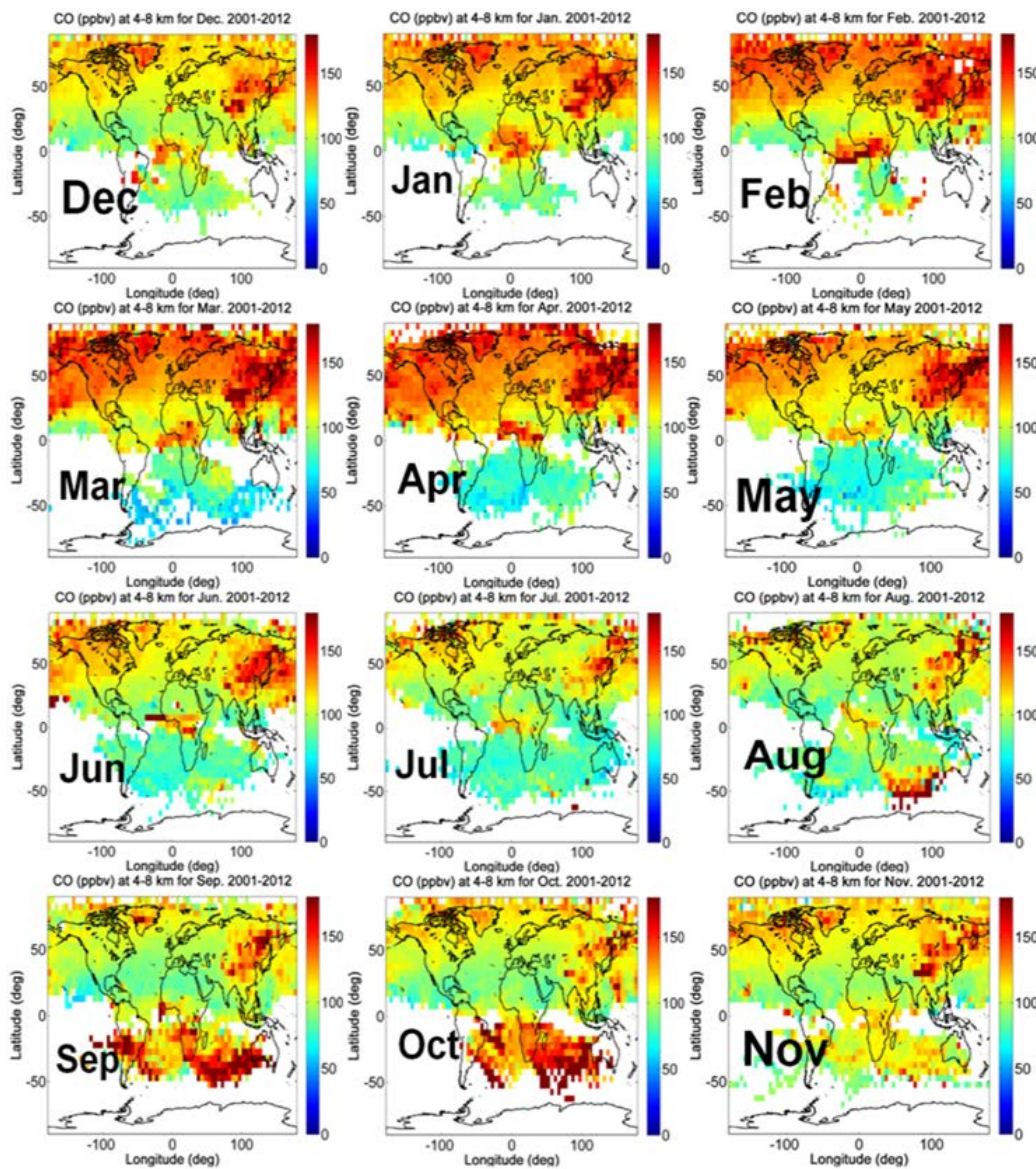
9 **5 Results**

10 **5.1 Global distribution of MOZAIC-IAGOS CO climatology**

11 ~~As an example, Fig. Figure 12-14~~ shows the monthly mean CO VMR between 4 and 8 km
 12 altitude above sea level for ~~the four seasons (i.e., December-February, March-May, June-August~~
 13 ~~and September-November) during 2001-2012.~~ The climatology is able to capture the CO spatial
 14 variability fairly well: the northern hemispheric concentrations are much higher, and the biomass

1 burning peaks are clearly visible for the NH winter and spring seasons. The climatology shows
2 more abundant CO in the NH during these seasons. This is due primarily to lower OH levels
3 during the cold season which permits a longer lifetime for CO, although there also appears to be
4 an additional source in eastern Asia. Enhanced CO concentration is observed in the tropical
5 regions where wildfire burning is typical during ~~the December/January–February season~~ April,
6 like west Africa and a large part of central Africa (Sauvage et al., 2005, 2007). At southern mid-
7 latitudes between South America, southern Africa and Australia, we observe high CO from
8 September to November, during the agricultural burning season. ~~This is accompanied by~~
9 ~~enhanced ozone in the same region (e.g. Ding et al., 2015; see also Sect. 5.2), produced via~~
10 ~~reactions R1–R5 and similar.~~ Although Fig. ~~12–14~~ shows a 12-year global map, the strong
11 enhanced CO over these regions (west Africa, South America, and southeast Asia) is clearly
12 observable as an annual feature with significant interannual variability.

13 ~~Furthermore, Fig. 12 allows us to examine the annual variation of the global distribution of CO~~
14 ~~between 4 and 8 km altitudes above sea level. Despite the limited MOZAIC-IAGOS data in the~~
15 ~~SH, the seasonal cycle of CO is clearly shown in both hemispheres. The greatest change of CO~~
16 ~~from north to south occurs around the tropics in February–April when CO levels are greatest in~~
17 ~~the NH. The reverse gradient appears with a sharp decrease across the tropics in September–~~
18 ~~October when CO levels peak in the SH. High CO levels are seen in August between Southeast~~
19 ~~Africa and Southwest Australia, which is as a result of the long range transport of CO produced~~
20 ~~from biomass burning in the tropical areas (i.e., southern Africa).~~

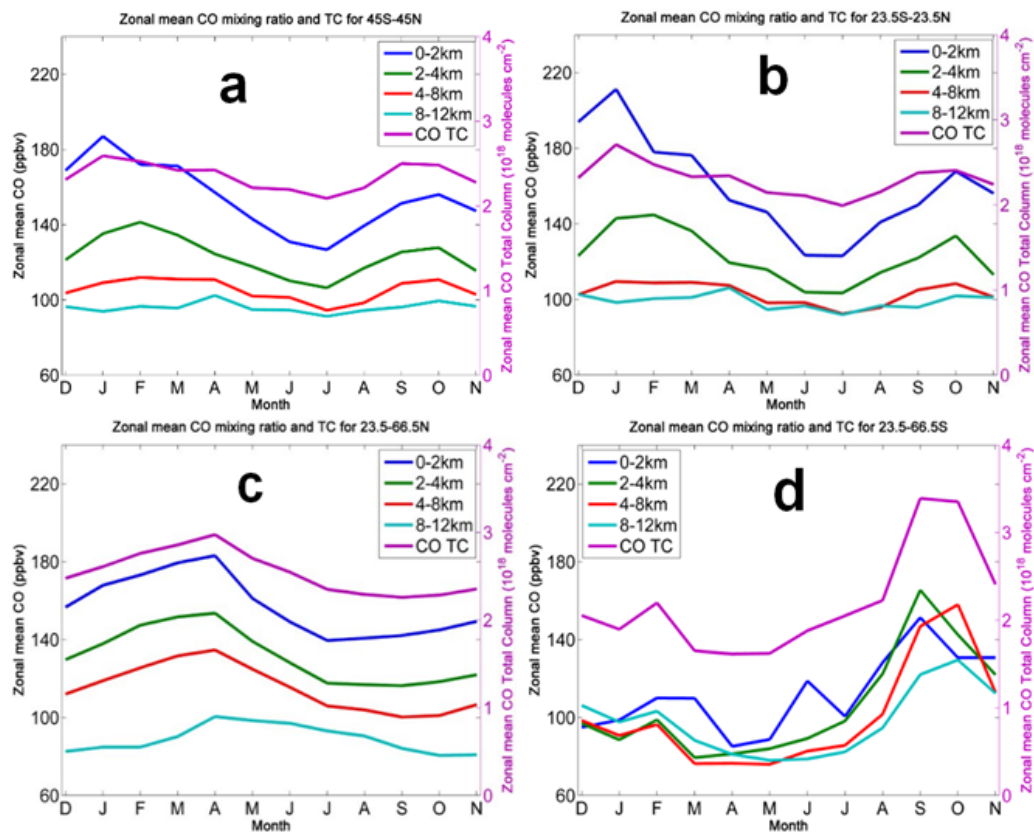


1
2

3 **Fig. 1214.** Global monthly mean CO distribution from the trajectory-mapped MOZAIC-IAGOS
 4 CO VMR as a function of latitude and longitude for January-December 2001-2012 and altitudes
 5 between 4-8 km a.s.l. The data were averaged with a bin size of $5^{\circ} \times 5^{\circ}$ latitude and longitude.

6 **5.2 Zonal distribution of MOZAIC-IAGOS CO climatology**

1 **5.2.1 Seasonal variation**



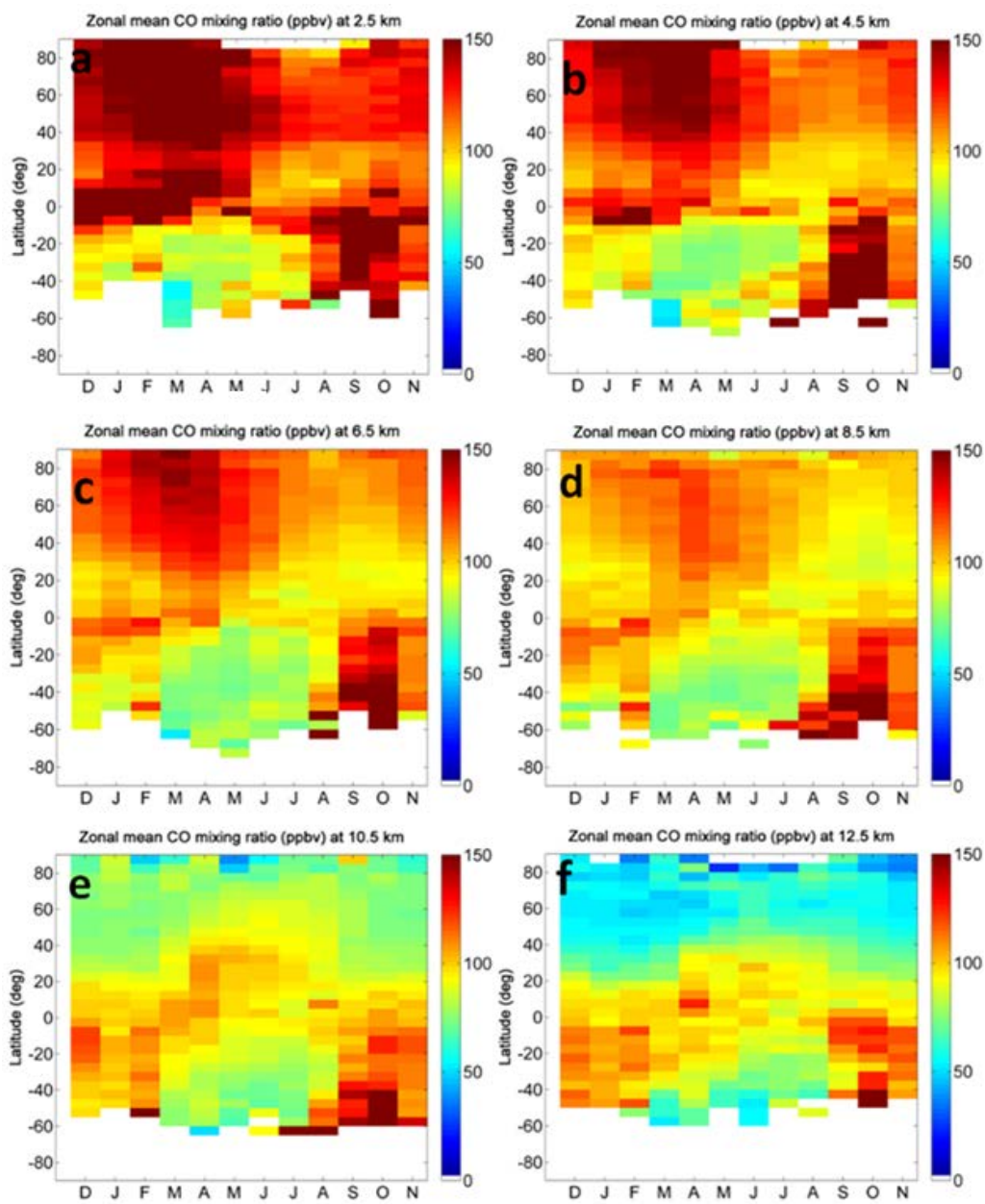
2
3 **Fig. 13.15.** Zonally averaged monthly variation of CO for the latitude bands 45°S-45°N-(a), 23.5°
4 S-23.5°-N-(b), 23.5-66.5°-N-(c) and 23.5-66.5°-S-(d). Monthly mean CO VMRs and total
5 columns were calculated for the period 2001-2012. The CO mixing ratios are shown for
6 ranges 0-2 km, 2-4 km, 4-8 km and 8-12 km, as well as total column (TC) a.s.l. The abscissa is
7 monthly mean of CO covered during 2001-2012.

8 In Fig. 13, data are grouped in three bands representing the NH extratropics (Fig. 13c), the SH
9 extratropics (Fig. 13d), the tropics (Fig. 13b) and for latitude band 45°S-45°N (Fig. 13a). The
10 zonal mean trajectory mapped MOZAIC IAGOS CO climatology for these latitude bands is
11 shown for the altitude ranges 0-2 km, 2-4 km, 4-8 km and 8-12 km.

12 As can be seen from Fig. 13.15, CO shows distinct seasonal cycles in both hemispheres. In the
13 NH extratropics (Fig. 13.15c), maximum CO VMR is observed in February-April following a
14 steady increase during fall and winter. This is followed by a rapid decrease giving rise to the
15 lowest CO levels in July-September-August. The seasonal decline of CO VMR in summer shows

1 the typical seasonal pattern of CO in the NH driven by OH increase during this time (Yurganov
2 et al., 2008; Novelli et al., 1998). In the SH extratropics (Fig. ~~13d~~15d), CO levels peak in
3 September-October. This is consistent with previous studies by Novelli et al. (1998). In the SH,
4 the annual CO maximum is earlier at lower altitudes. Rinsland et al. (2002) suggested this
5 phenomenon to be associated with the vertical and horizontal CO dispersion away from the
6 biomass burning region in the tropics. Moreover, CO shows greater seasonal variability,
7 particularly at higher altitudes, in the SH than in the NH. ~~This can also be seen in Fig. 12.~~ The
8 seasonal CO cycle in the tropics (Fig. ~~13b~~15b) and for latitude band 45°S-45°N (Fig. ~~13a~~15a)
9 both display a July minimum, and a secondary maximum in October while the primary
10 maximum is in late NH winter/early spring. ~~This~~The CO cycle in both hemispheres is controlled
11 by seasonal variations of OH; ~~as OH is the major CO sink~~ (Logan et al., 1981; Bergamaschi et
12 al., 2000; Novelli et al., 1998) and ~~the space-time distribution of its sources (Novelli et al.,~~
13 ~~1998), in particular the biomass burning either in the Tropics (largest fires occur in austral~~
14 ~~Africa and South America in SON) or and to a lesser degree at boreal latitudes (largest fires in~~
15 ~~June July August), and anthropogenic sources at northern mid-latitudes.~~

16 Figure ~~14~~16 shows zonal mean latitude-time cross-section plots of CO VMR at 2.5 km, 4.5 km,
17 6.5 km, 8.5 km, 10.5 km and 12.5 km altitudes for the period 2001-2012. The latitude-time
18 cross-section shows the seasonal cycle of zonal mean CO for different altitudes, as seen in the
19 previous figures, and also the variation of the interhemispheric CO VMR gradient throughout the
20 year. The strongest interhemispheric gradient occurs in March, at low altitude, and the smallest
21 gradients are seen in northern summer. The gradient in NH spring reverses at higher altitudes,
22 and in NH fall where it is especially strong at higher altitudes. Plots 14e, f also clearly show the
23 weak seasonal cycle in the NH upper troposphere compared to that in the SH.

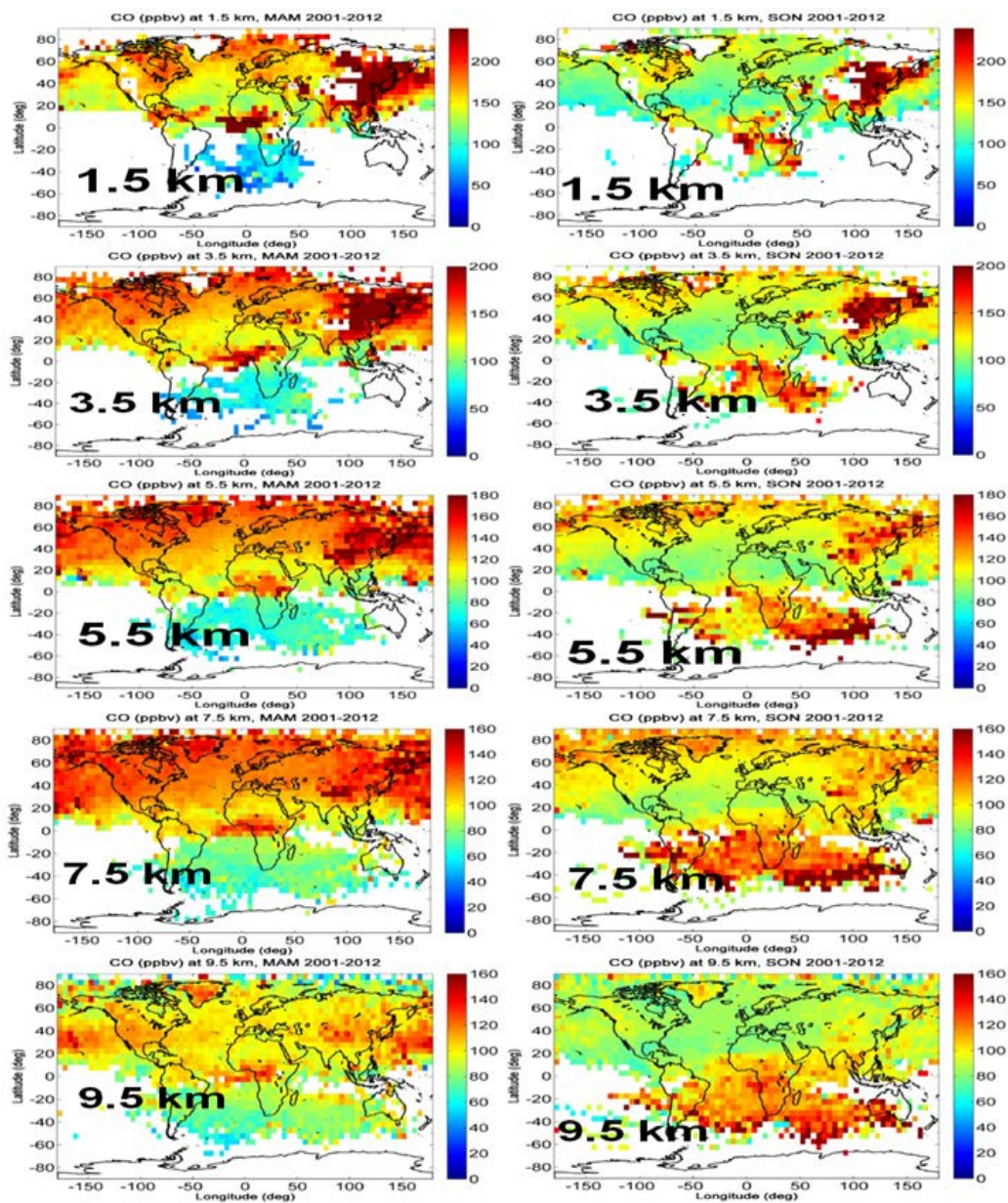


1
2
3 **Fig. 1416.** Seasonal variation of zonal monthly mean trajectory-mapped MOZAIC-IAGOS CO
4 climatology at 2.5 (a), 4.5 (b), 6.5 (c), 8.5 (d), 10.5 (e) and 12.5 (f) km altitudes a.s.l. for the
5 period 2001-2012. The zonal mean data are averaged in 5° latitude intervals.

1 5.3.2 Vertical distribution

2 Figure 45-17 illustrates the variation of CO with altitude for the seasons in which we observe
3 maximum CO levels in both the SH and NH (i.e., MAM and SON). The seasons demonstrate the
4 greatest CO VMRs are found at lower altitudes in both hemispheres, although, even though CO
5 declines with altitude in both hemispheres, it does so faster in the NH than the SH. This which
6 results in a decrease in the strength of the interhemispheric gradient (SH to NH) with altitude.
7 This result is consistent with Edwards et al. (2006) who suggested that in the absence of
8 continued CO input from the source regions (i.e., biomass burning in southern Africa and South
9 America), the aged CO is gradually distributed vertically throughout the troposphere in the SH.
10 In fact, in regions where there is deep convection this leads to an enhanced CO concentration in
11 the upper troposphere, as can be seen on the right-hand side of Fig. 45-17 and in Fig. 4618d.
12 Moreover, Liu et al. (2006) showed large horizontal CO gradients in association with vertical
13 and horizontal transport of air originated from with different chemical signatures of origin.

14 The zonal CO mean vertical profiles for February, April, July and September, averaged for
15 2001-2012 over the latitude bands 23.5-66.5°N (NH extratropics), 23.5-66.5°S (SH
16 extratropics) and 23.5°S-23.5°N (tropics), are shown in Fig. 4618. The results are displayed for
17 latitude bands 23.5-66.5°N (NH extratropics), 23.5-66.5°S (SH extratropics) and 23.5°S-23.5°N
18 (tropics). The CO profiles show strong seasonal and latitudinal variability primarily in the NH
19 extratropics. The largest VMRs of CO occur at lower altitudes in the NH extratropics in February
20 and April but the strong decline with altitude causes CO VMRs to be higher in the SH at high
21 altitudes than in the NH. In the SH in February, April, July and September, there is little
22 variation of CO with altitude. This is due to the sampling of the lower most stratosphere in the
23 NH much more frequently than in the SH. The trajectory-mapped CO in the SH extratropics is
24 mainly representative of the tropics, while unlike in the NH extratropics where there are many
25 CO measurements north poleward of 40°N. This implies that sampling of the lowermost
26 stratosphere will be more frequent in the NH than in the SH. The altitude gradients are similar in
27 July and September, with CO levels in September in the SH higher than those in the NH. This is
28 typically the influence of tropical biomass burning in South America and austral Africa, which
29 are the two regions most represented in the climatology in the SH. In the tropics, CO VMRs
30 show a rapid decrease with altitude in the lower troposphere but above approximately 4-5 km
31 changes with altitude are minor.

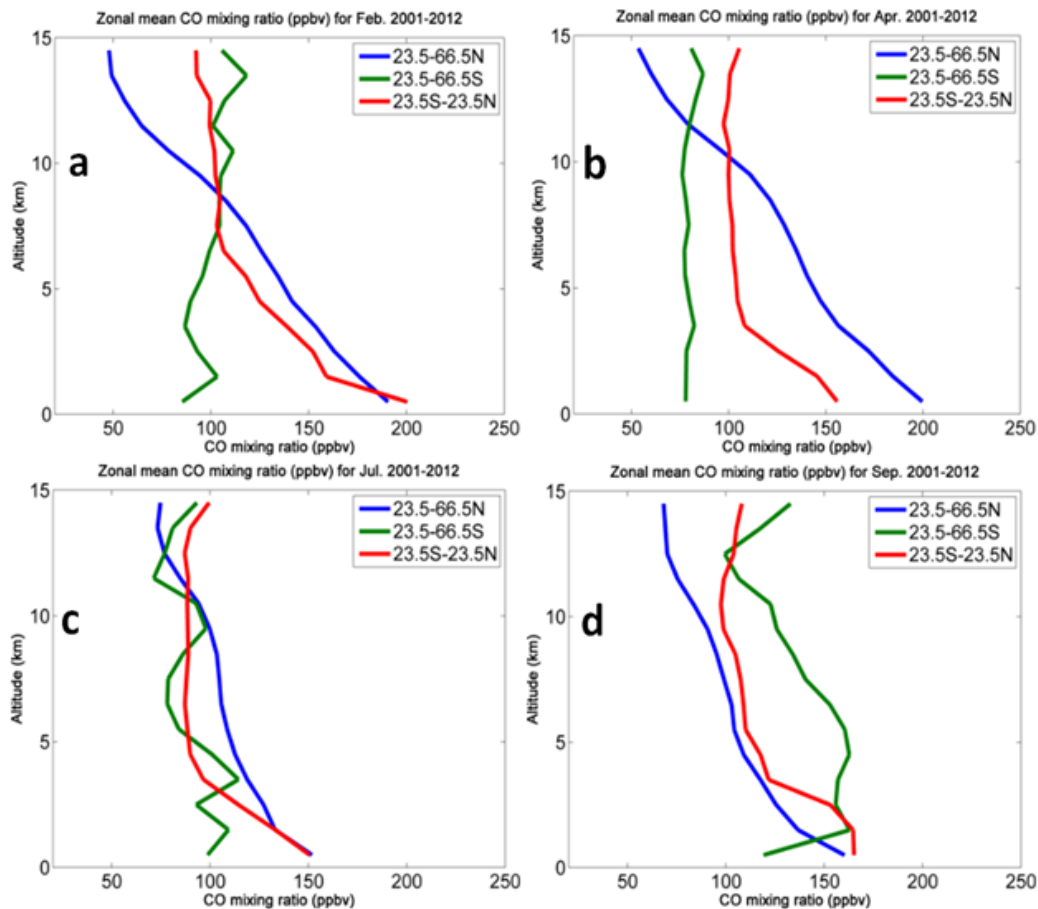


1
2

3 | **Fig. 4517.** Global distribution of seasonal (the NH spring and fall) mean trajectory-mapped
 4 | MOZAIC-IAGOS CO climatology as a function of latitude and longitude for altitudes 1.5, 3.5,
 5 | 5.5 km, 7.5 km and 9.5 km a.s.l. The left and right columns show average CO VMRs for March-

1 April-May and September-October-November, 2001-2012. The data are averaged with a bin size
2 of $5^{\circ} \times 5^{\circ}$ latitude and longitude.

3



4

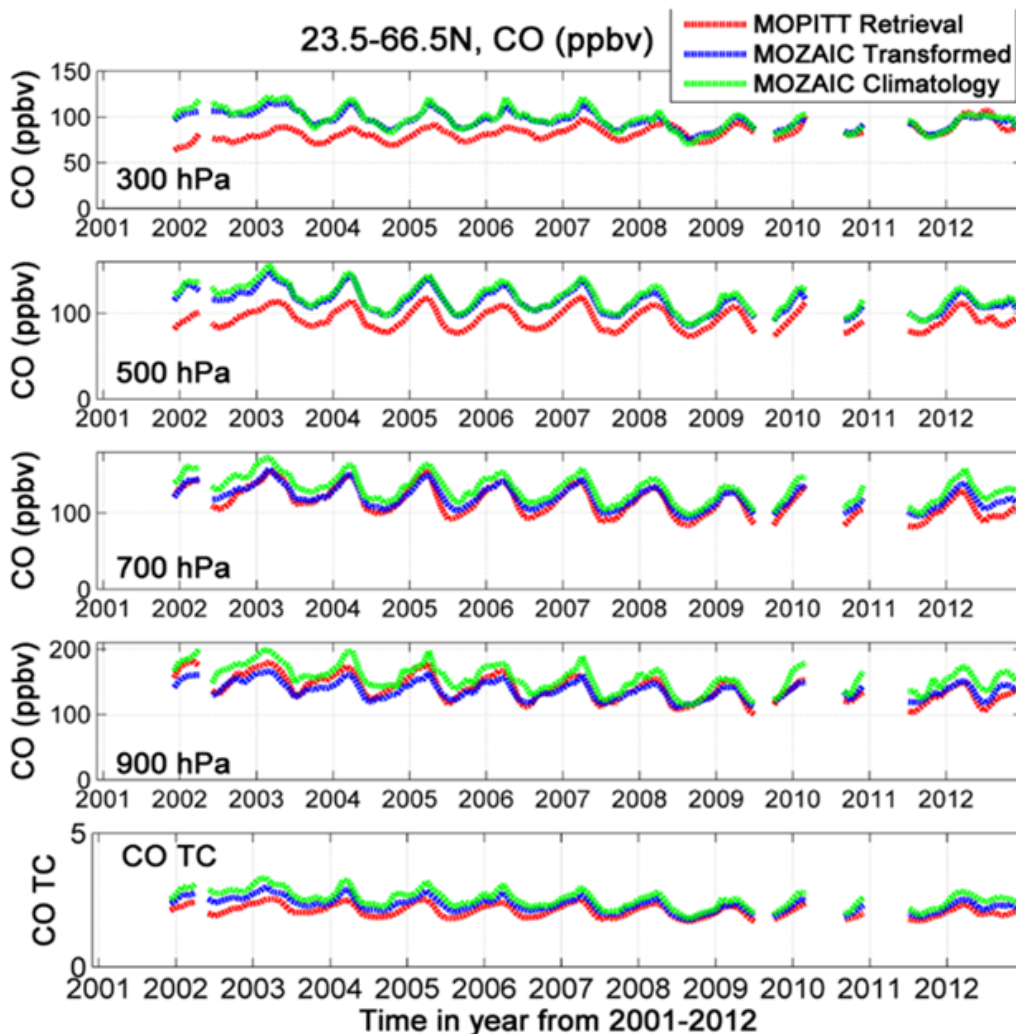
5 **Fig. 1618.** Monthly mean profiles of CO from the trajectory-mapped MOZAIC-IAGOS CO
6 climatology for February (a), April (b), July (c) and September (d) averaged for 2001-2012. The
7 different colors represent CO mean VMR for the latitude bands 23.5-66.5°N (blue), 23.5-66.5°S
8 (green) and 23.5°S-23.5°N (red).

9 6 Applications

10 6.1 Global variation and trends of CO

11 The smoothed time series of the NH extratropical zonal mean CO VMR at 900, 700, 500, and
12 300 hPa for the trajectory-mapped MOZAIC-IAGOS dataset 2001-2012 is shown in Fig. 4719.

1 For purposes of comparison we also show data from MOPITT and from the mapped MOZAIC-
2 IAGOS dataset transformed with the MOPITT averaging kernels. Gaps in the figure occur
3 whenever one data source is missing. The gaps in June-July 2001 and August-September 2009
4 were due to a cooler failure of the MOPITT instrument. MOZAIC-IAGOS began CO
5 measurement in December 2001 and there were only partial data available in 2010 and 2011. The
6 observations show an annual late winter or springtime peak in the NH extratropical zonal CO
7 loading each year, in conjunction with low wintertime OH levels. The same interannual cycle of
8 CO is captured by both trajectory-mapped MOZAIC-IAGOS (transformed and untransformed)
9 and MOPITT. They appear to track short-term changes equally well. However, while all show a
10 modest decline in the lower troposphere ~~particularity~~ until about 2008-2009 (~~and thereafter which~~
11 CO VMR seems to level off), in accordance with the trends found by Worden et al. (2013), in the
12 upper troposphere MOPITT shows a modest increase, ~~and~~ It also shows a significant bias with
13 respect to the trajectory-mapped MOZAIC-IAGOS data that decreases with time. Although the
14 untransformed trajectory-mapped MOZAIC-IAGOS CO values show a significant difference
15 against the transformed ~~at data in the~~ lower troposphere, they seem to agree well at higher levels.
16 ~~However,~~ The untransformed trajectory-mapped MOZAIC-IAGOS data shows higher CO levels
17 ~~compared to than~~ MOPITT CO retrievals ~~for at~~ all levels.



1
 2 **Fig. 1719.** Zonally averaged time series of monthly mean CO VMR, at individual levels and total
 3 columns, as retrieved measured by MOPITT CO retrievals and from the trajectory-mapped
 4 MOZAIC-IAGOS CO climatology (transformed and untransformed,) and transformed using
 5 MOPITT's averaging kernels) for the latitude band 23.5°-66.5° N.

6 Laken and Shahbaz (2014) found increasing CO trends over widespread regions of South
 7 America, Mexico, central Africa, Greenland, the eastern Antarctic, and the entire region of India
 8 and China from MOPITT data. Figure S4The SH extratropics also shows similar time series
 9 similar to those in Fig. 1719 for the SH extratropics, but the negative trend is not as clear as that
 10 in the NH due to limited data. The annual springtime peak in the SH zonal CO loading is again
 11 visible in all of the time series. This is predominantly associated with dry season biomass

1 burning emissions in South America, southern Africa, southeast Asia, and northwestern
2 Australia. In later months, the CO resulting from these emissions is generally destroyed by more
3 active photochemistry during the SH summer. At these times, the retrieved zonal CO falls to
4 background levels (around 40-50 ppbv) which are representative of the remote ocean regions
5 where CO production by methane oxidation is the dominant source (Edwards et al., 2006).

6 ~~Biases between MOPITT and MOZAIC-IAGOS are again significant at all levels, but lowest in~~
7 ~~the lower troposphere, and again decrease with time. The untransformed trajectory-mapped~~
8 ~~MOZAIC-IAGOS data again show higher CO levels than the transformed CO climatology at all~~
9 ~~levels.~~

10 ~~In Fig. S5, we display~~We looked at the time series of the zonal monthly mean of CO VMR for
11 the tropics. The biases between the MOPITT retrievals and the trajectory-mapped MOZAIC-
12 IAGOS in general show the same features as for the extratropics, both in time and vertical levels.
13 ~~The CO values show~~while the seasonal patterns ~~that~~ combine those ~~seasonal patterns~~ of the NH
14 and SH seen in Figs. ~~17-19~~and S4.

15 ~~In Sect. 4, we found significant biases between the MOPITT retrievals and the trajectory-mapped~~
16 ~~MOZAIC-IAGOS CO dataset.~~In Fig. ~~S6~~S4, we display the monthly mean time series for
17 Frankfurt from December 2001--December 2012. ~~As can be seen from the figure, These also~~
18 ~~show we notice again~~ significant biases, declining with time, between MOPITT and the
19 transformed MOZAIC-IAGOS in situ above 700 hPa, in good agreement with the result shown
20 in Fig. ~~17~~19. ~~The biases also appear to decrease similarly with time in the upper troposphere.~~
21 Furthermore, MOPITT shows a modest increase in CO levels in the upper troposphere while
22 MOZAIC-IAGOS in situ (transformed and untransformed) shows a modest decline, consistent
23 with Petetin et al. (2015), who report a similar decrease over Frankfurt. The MOPITT ~~retrievals~~
24 and MOZAIC-IAGOS (transformed and untransformed) CO values ~~also for Frankfurt~~ show the
25 same seasonal patterns as the NH extratropics (Fig. ~~17~~19). This comparison ~~indicates suggests~~
26 that a prominent bias, declining with time, exists between MOZAIC-IAGOS and MOPITT L3
27 V6 TIR/NIR products.

28 **6.2 Global distribution of O₃-CO correlations**

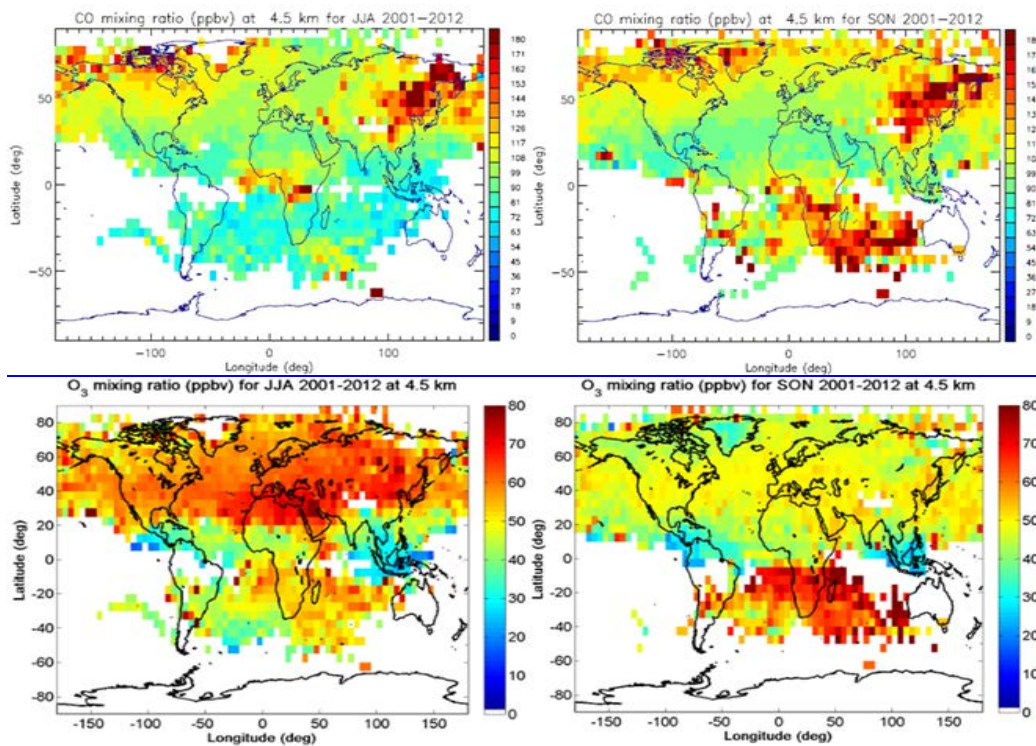
29 ~~Global O₃ datasets have been developed by trajectory mapping of ozonesonde, aircraft and~~
30 ~~satellite measurements and validated (Tarasiek et al., 2010; G. Liu et al., 2013; J. Liu et al.,~~
31 ~~2013; Osman et al., manuscript in preparation). The maps show consistent agreement with~~
32 ~~independent in situ and satellite instruments. As a potential application of such datasets (O₃ and~~
33 ~~CO maps), we present here the relationship between O₃ and CO. The O₃-CO correlations were~~
34 ~~derived from the concurrent measurements of O₃ and CO using MOZAIC-IAGOS.~~

35 ~~Since CO is involved in the production and destruction of O₃, studies of O₃-CO correlation can~~
36 ~~offer significant insight into the photochemical origin of air masses (e.g. Parrish et al., 1993;~~
37 ~~Chin et al., 1994; Zhang et al., 2008; Voulgarakis et al., 2011; Kim et al., 2013). A positive~~

1 correlation is expected in regions where CO and O₃ are related due to emissions and
2 photochemistry (for example, downwind of major CO and NO_x source regions and in the
3 presence of a significant actinic flux). However, during winter, Parrish (1993) observed that O₃-
4 CO were negatively correlated, presumably due to titration of O₃ by NO. Strong anticorrelation
5 is also expected where stratospheric intrusions are a significant source of O₃, since CO mixing
6 ratios in the stratosphere are quite low. For a remote maritime site, O₃-CO correlation would
7 only be expected during periods when the site was downwind of significant CO and NO_x
8 sources.

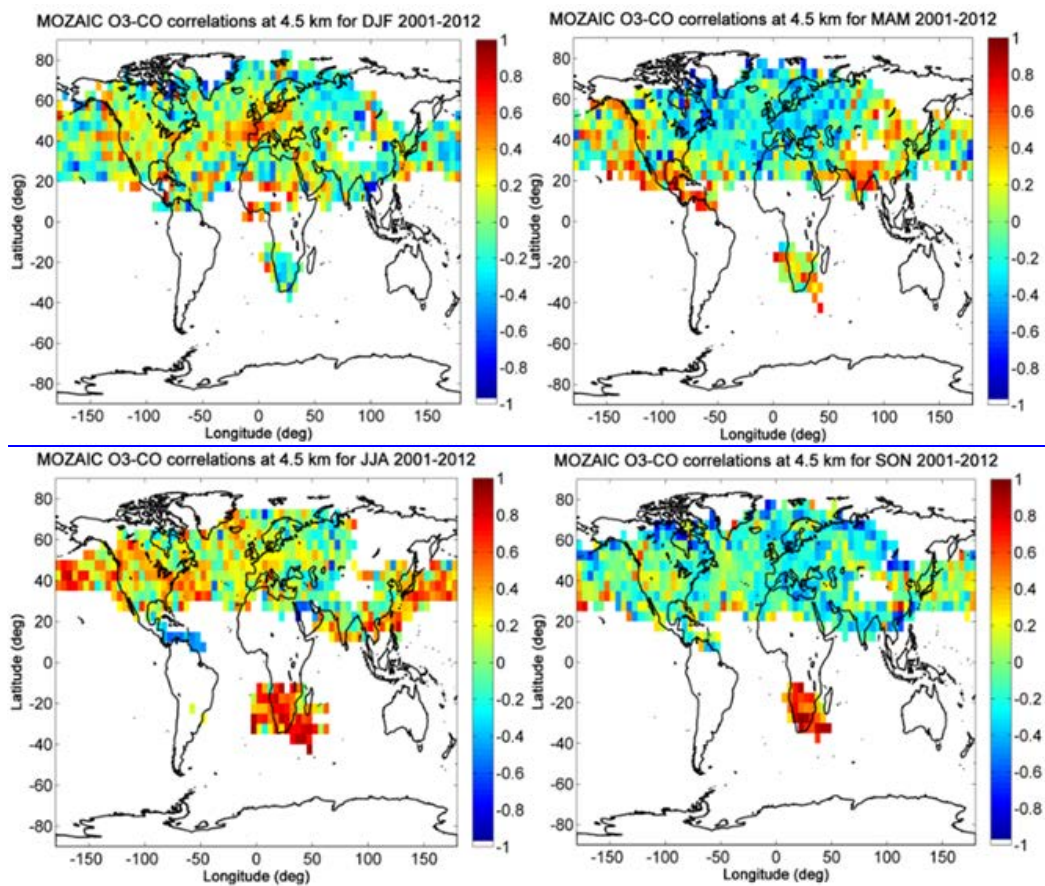
9 Although a quantitative interpretation in terms of O₃ production is complicated by sampling of
10 air masses with varying background mixing ratios (Chin et al., 1994; Mauzerall et al., 1998), the
11 correlation still provides valuable information about anthropogenic influence on O₃. Figures 19-
12 21 examine the O₃-CO correlations observed by concurrent O₃ and CO measurements using
13 MOZAIC-IAGOS instruments during the period from 2001-2012.

14 Figure 18 shows the global spatial distribution of O₃ and CO from the trajectory mapped
15 MOZAIC-IAGOS climatologies for June-August and September-November of 2001-2012 at 4.5
16 km above sea level. The right panels of Fig. 18 show significantly enhanced CO and O₃ VMRs
17 in the SH between southern Africa and Australia. In central Africa, where there is strong
18 production of CO as a result of high biomass burning, there appears to be high O₃ concentrations
19 during September-November in anthropogenically polluted and biomass burning regions. In the
20 polluted region of east China O₃ is highest in the summer when photochemical activity is at its
21 peak. The highest values of O₃ in the summertime are seen over the Middle East, north Africa
22 and central Asia. The global spatial distribution of O₃ and CO from MOZAIC-IAGOS is
23 generally consistent with previous OMI/AIRS results reported by Kim et al. (2013).

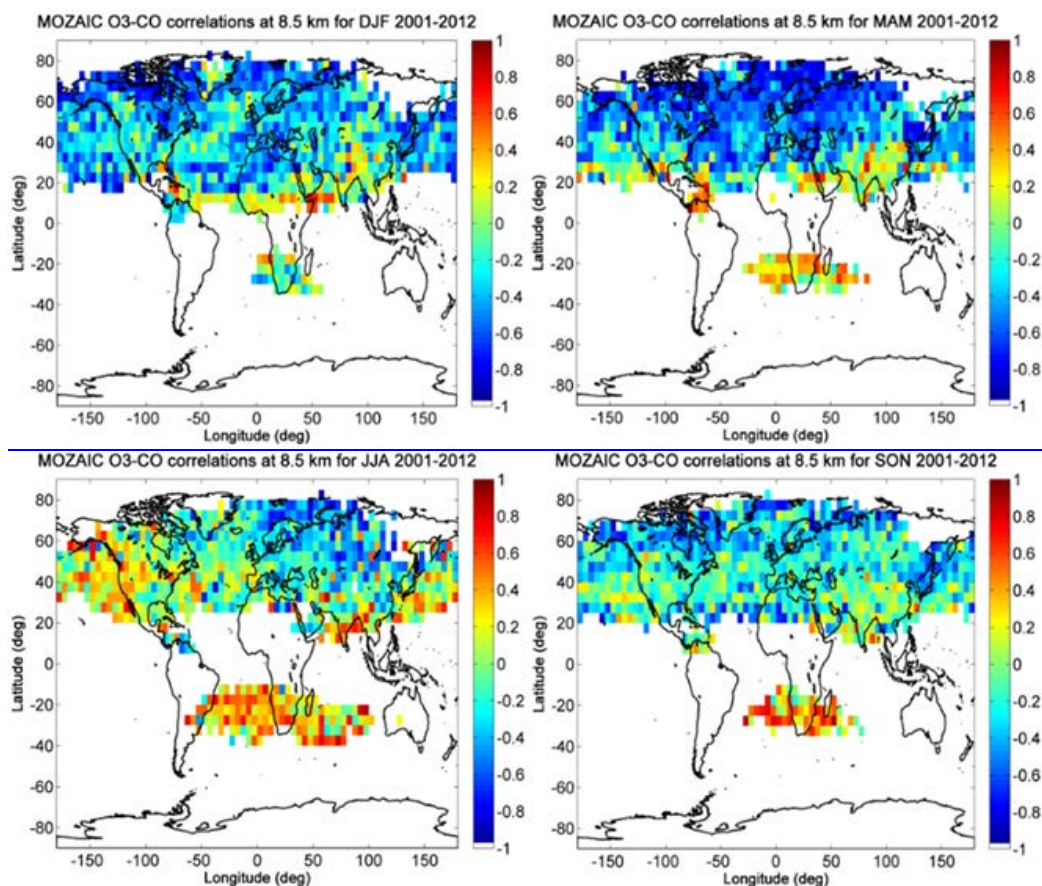


1
2 **Fig. 18.** Global distribution of seasonal (NH Winter and Fall) mean concentrations of O₃ and CO
3 from the trajectory mapped MOZAIC IAGOS climatologies as a function of latitude and
4 longitude at 4.5 km altitude above sea level. The data are binned on a 5°×5° latitude and
5 longitude grid.

6 Correlation coefficients of the trajectory mapped MOZAIC IAGOS O₃ and CO climatology
7 seasonal fields from 2001–2012 are displayed in Fig. 19. The seasonal O₃–CO correlations for
8 the three month time series (DJF, MAM, JJA, SON) of the O₃ and CO mixing ratios were
9 computed for each grid. Figure 19 shows that in June–August and September–November, the O₃–
10 CO correlation coefficients in the SH appear to be very strong positive in the southern
11 midlatitudes in winter–spring. This suggests that in the SH winter, spring (and perhaps even in
12 autumn) photochemical O₃ production is more dominant. In general, in the NH the O₃–CO
13 correlations seem to be fairly positive in all seasons except the scattered low negative correlation
14 coefficients seen in the spring (and perhaps even in autumn). This indicates that photochemical
15 O₃ production clearly dominates most of the year at lower altitudes.



1
 2 **Fig. 19.** O₃-CO correlation coefficients of seasonal means for 2001-2012 from the trajectory-
 3 mapped MOZAIC-*LAGOS* measurements at 4.5 km altitude a.s.l. The top left, top right, bottom
 4 left and bottom right panels are the O₃-CO correlation coefficients for December-February,
 5 March-May, June-August and September-November, respectively.



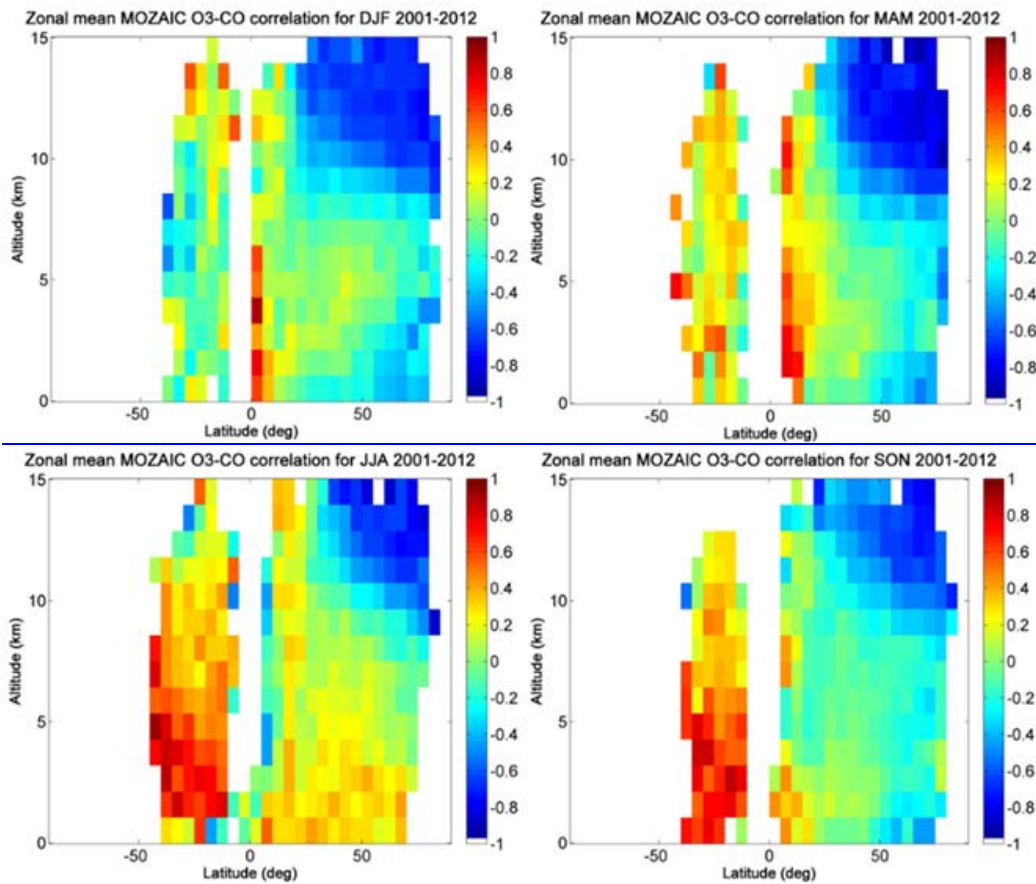
1
2 **Fig. 20.** Same as Fig. 19 but for an altitude of 8.5 km a.s.l.

3 Figure 20 shows the O_3 -CO correlation coefficients at 8.5 km altitude. In the SH strongly
 4 positive O_3 -CO correlation coefficients are notable in all seasons except December-February,
 5 which suggests that photochemical O_3 production is dominant here even at this altitude. Strong
 6 negative correlations in the NH mid and higher latitudes in December-February and March-May
 7 indicate that the stratosphere is a major O_3 source at this altitude. In the NH summer where
 8 photochemical O_3 formation is a dominant source of O_3 , positive O_3 -CO correlation coefficients
 9 are seen, consistent with previous work by Zahn et al. (2002). Moreover, the same figure shows
 10 (see also Fig. 21) that in all four seasons O_3 -CO correlation coefficients in the tropics are
 11 positive. This is consistent with model calculations that estimate the O_3 abundance in the tropical
 12 upper troposphere originating from the stratosphere to be only 5–15% (Roelofs and Lelieveld,
 13 1997; Lamarque et al., 1999). Some fraction of the extratropical CO may originate as CO
 14 transported from tropical biomass burning regions to the extratropics; however Bowman (2006)
 15 showed using MOPITT CO data that transport from the tropics to the extratropics is a

1 comparatively slow process while the zonal dispersion of air parcels within the tropics and
2 subtropics is relatively rapid.

3 As a summary, in Fig. 21 we display the distribution of the zonal mean of the O_3 -CO correlation
4 coefficients from the trajectory mapped CO and O_3 datasets as a function of latitude and altitude
5 for the period from 2001-2012. The figure shows that in the lower troposphere the O_3 -CO
6 correlations have generally positive values as photochemistry is the dominant source of O_3 , and
7 the stratospheric influence is relatively small. In the mid and upper troposphere, the influence of
8 the influx of stratospheric air depends strongly on latitude and season, but it always affects
9 calculated O_3 -CO correlation coefficients. The NH high latitudes show negative correlations in
10 winter, spring and fall, in agreement with previous studies (e.g. Voulgarakis et al., 2011; Parrish
11 et al., 1998). Due to lack of sunlight, these regions do not experience intense photochemistry and
12 are dominated by O_3 destruction or dry deposition or both (Voulgarakis et al., 2011). Even
13 though stratospheric intrusion can drive the negative correlations in the region, it is more
14 frequent in spring (Zhang et al., 2008). In the SH, strong correlations are seen at all altitudes in
15 all seasons except December-February, in agreement with those reported by Kim et al. (2013).

16 Further division of the climatology into annual averages may provide a global view of CO
17 changes and transport. As CO is involved in both the production and destruction of O_3 , O_3 -CO
18 correlations derived from the trajectory mapped MOZAIC-IAGOS CO and O_3 climatology
19 datasets presented here may provide important insights into the origin of air masses and the
20 budgets of O_3 and CO in the troposphere. Figure 21 demonstrates one aspect of the value of the
21 MOZAIC-IAGOS continuous, long term, global, vertically resolved in situ measurements. Such
22 routine commercial aircraft observations provide valuable information on atmospheric
23 composition that can improve our understanding of global and regional air quality and the
24 potential impact of greenhouse gases on climate change.



1
2 **Fig. 21.** Latitude-altitude cross-section of zonal seasonal means of the O_3 -CO correlation
3 coefficients for 2001-2012 from the trajectory mapped MOZAIC IAGOS CO and O_3
4 climatologies. The top left, top right, bottom left and bottom right panels are the O_3 -CO
5 correlation coefficients for December-February, March-May, June-August and September-
6 November, respectively.

7 Conclusions

8 We have presented a three-dimensional (i.e., latitude, longitude, altitude) gridded climatology of
9 CO developed by trajectory mapping of global MOZAIC-IAGOS data. This quasi-global
10 climatology dataset offers a complement to global satellite measurements, at significantly higher
11 vertical resolution, that facilitates visualization and comparison of different years and seasons,
12 and offers insight into the global variation and trends of CO. Even though the MOZAIC-IAGOS
13 aircraft data are unevenly distributed both in time and space across the globe, the trajectory-
14 mapped dataset is uniformly distributed on a $5^\circ \times 5^\circ \times 1$ km grid. [The trajectory-based interpolation](#)

1 ~~method confers significant advantages over linear or quadratic interpolation.~~ Major regional
2 features of the global CO distribution are clearly evident in the CO maps for different seasons
3 and altitudes. The trajectory-mapped CO shows distinct seasonal cycles with the CO annual
4 maximum occurring in September-October in the SH, coincident with the tropical biomass
5 burning season (Rinsland et al., 2002), and in April in the NH, while the tropics show distinct
6 maxima in January-February and in October. ~~We note caution that the observed result in the SH~~
7 ~~is obtained from the limited data we have from the region.~~ The interhemispheric CO gradient is
8 strongest in late winter/early spring, and smallest in northern summer. Time series analysis of the
9 climatology shows that in the NH and the tropics CO is declining with time. This is consistent
10 with ~~the~~ previous studies using ground-based, aircraft and satellite data, such as Petetin et al.
11 (2015), Worden et al. (2013), Laken and Shahbaz (2014) and Novelli et al. (1998). ~~(In the SH,~~
12 ~~due to limited MOZAIC-IAGOS data, a clear CO trend cannot be seen.)~~ The consistency of our
13 findings with those from other global datasets lends increased confidence that the CO
14 ~~climatology dataset~~ derived from trajectory mapping of global MOZAIC-IAGOS data can be
15 used for CO trend studies at regional and global scales.

16 The trajectory-mapped CO dataset has been validated by comparing maps constructed using only
17 forward trajectories and using only backward trajectories. The two methods show similar global
18 CO distribution patterns. Differences are most commonly 10% or less, and found to be less than
19 30% for almost all cases. They are typically less than 10% at northern mid-latitudes and less than
20 20% in the tropics between $\pm 30^\circ$ latitude, except in the Pacific and Atlantic oceans where it can
21 reach as large as 30%. The dataset has also been validated by comparison against in-situ
22 MOZAIC-IAGOS aircraft measurements, where the data from the validation site are excluded
23 from the trajectory-mapped data. Although the comparison shows larger differences below 2 km,
24 the profiles from the two methods agree very well between 2 and 10 km with the magnitude of
25 ~~bias differences~~ within 20%. ~~A f~~ Furthermore, comparison between the trajectory-mapped ~~result~~
26 and MOZAIC-IAGOS in situ CO cruise data, ~~which were not included in the trajectory-mapping,~~
27 shows that major regional features of the global CO distribution for different seasons are clearly
28 evident in both maps and they agree ~~very~~ well ~~qualitatively~~ in regions of overlap. This suggests
29 that the trajectory-mapped CO data performs well not only near airports but also in remote areas.
30 ~~Validation was also performed against independent data from the NOAA aircraft flask sampling~~
31 ~~program. The results suggest small or insignificant biases in the upper troposphere, but positive~~
32 ~~biases as large as 12% for MOZAIC-IAGOS in the lower troposphere. This is probably due to~~
33 ~~the “airport effect”, a sampling bias that occurs because commercial aircraft operate from large~~
34 ~~airports near large cities, with typically elevated CO levels in the boundary layer.~~

35 The trajectory-mapped CO dataset has also been extensively compared with MOPITT retrievals.
36 Between 700 and 300 hPa, a prominent bias, declining with time, exists between MOZAIC-
37 IAGOS and MOPITT L3 V6 TIR/NIR products.

38 ~~A small positive bias for CO total column is found, consistent with those previously reported for~~
39 ~~MOPITT (Deeter et al., 2014, 2013; Emmons et al., 2009, 2007).~~

1 ~~Comparison of similar maps made using the concurrent O₃ measurements by MOZAIC-IAGOS~~
2 ~~permits some insight into the sources of tropospheric O₃. The O₃-CO correlation shows a~~
3 ~~significant seasonal and latitudinal variation. In the tropics, where the influence by stratospheric~~
4 ~~air is small, generally positive correlations are seen, as photochemistry is the dominant source of~~
5 ~~O₃. In the extratropics, strong negative correlations in the NH winter, spring and autumn indicate~~
6 ~~that the influx of stratospheric air is a primary source, especially in the upper troposphere, while~~
7 ~~the picture is mixed in the summer. Strong O₃-CO correlations are noted in all seasons except~~
8 ~~December-February over southern Africa, which suggests that photochemistry is generally the~~
9 ~~predominant O₃ source in this region.~~

10 ~~Such constraints on tropospheric ozone sources can be useful for chemical transport model~~
11 ~~evaluation, as demonstrated by Kim et al. (2013).~~

12 ~~This study demonstrates one aspect of the value of the MOZAIC-IAGOS continuous, long-term,~~
13 ~~global, vertically resolved in situ measurements. Such routine commercial aircraft observations~~
14 ~~provide valuable information on atmospheric composition that can improve our understanding of~~
15 ~~global and regional air quality and the potential impact of greenhouse gases on climate change.~~
16 ~~Further division of the climatology into annual averages may~~
17 ~~of CO changes and transport as well as interannual variability.~~
18 ~~The dataset provide a global view~~
19 ~~is unique 3D CO climatology~~
20 ~~dataset presented here has the potential to be used for time series and trend analysis, and~~
21 ~~provides a quasi-global view of CO changes and transport as well as interannual variability. It~~
22 ~~will also be useful as model initial fields, and background and boundary fields. It will be~~
23 ~~especially useful as an improved a priori climatology for satellite data retrieval. The global~~
24 ~~picture it presents is also expected to be valuable for comparison and validation of model results.~~
25 ~~The data isare publically available at ftp://es-ee.tor.ec.gc.ca/pub/ftpdt/MOZAIC_output_CO/.~~

25 **Acknowledgements.** The authors acknowledge the strong support of the European Commission,
26 Airbus, and the Airlines (Lufthansa, Air-France, Austrian, Air Namibia, Cathay Pacific, Iberia
27 and China Airlines so far) who carry the MOZAIC or IAGOS equipment and perform the
28 maintenance since 1994. MOZAIC is presently funded by INSU-CNRS (France), Météo-France,
29 Université Paul Sabatier (Toulouse, France) and Research Center Jülich (FZJ, Jülich, Germany).
30 IAGOS has been additionally funded by the EU projects IAGOS-DS and IAGOS-ERI. The
31 MOZAIC-IAGOS database is supported by ETHER (CNES and INSU-CNRS). Data are also
32 available via Ether web site <http://www.pole-ether.fr>. We thank the many whose dedication
33 makes such a dataset possible. The MOPITT ~~data were obtained from the NASA Langley~~
34 ~~Research Center Atmospheric Science Data Center, team is appreciated for their datasets for~~
35 ~~validation. We acknowledge thank R. Draxler and the NOAA Air Resources Laboratory for the~~
36 ~~trajectory model HYSPLIT (Hybrid Single Particle Lagrangian Integrated Trajectory Model)~~
37 ~~from the NOAA Air Resources Laboratory (<http://www.arl.noaa.gov/ready.html>), driven by~~
38 ~~theand NCEP/NCAR for the global meteorological reanalysis data—data from the~~

1 | ~~NOAA/OAR/ESRL PSD, Boulder, Colorado, USA, at <http://www.esrl.noaa.gov/psd/>.~~ The first
2 | author is grateful to the Natural Sciences and Engineering Research Council of Canada (NSERC)
3 | and Environment Canada for a research fellowship. [Important discussions with Merritt Deeter](#)
4 | [regarding MOPITT averaging kernels are much appreciated.](#) We thank Paul Novelli and Colm
5 | [Sweeney of NOAA/Global Monitoring Division and Steven Wofsy of Harvard](#)
6 | [University/School of Engineering and Applied Sciences for providing the in situ CO profiles.](#)

7 | **References**

8 | Bergamaschi, P., R. Hein, M. Heimann, and P. J. Crutzen, Inverse modeling of the global CO
9 | cycle: 1. Inversion of CO mixing ratios, *J. Geophys. Res.*, 105(D2), 1909
10 | doi:10.1029/1999JD900818, 2000.

11 | Boden, T. A., G. Marland, and R. J. Andres, Global, Regional, and National Fossil-Fuel CO₂
12 | Emissions. Carbon Dioxide Information Analysis Center, Oak Ridge Natl. Lab., U.S. Dep. of
13 | Energy, Oak Ridge, Tenn., doi:10.3334/CDIAC/00001. (Available at
14 | <http://cdiac.ornl.gov/trends/emis/cpa.html>), (last access: 8 September 2015), 2009.

15 | ~~Bowman, K. W., Rodgers, C. D., Kulawik, S. S., Worden, J., Sarkissian, E., Osterman, G., Steck,~~
16 | ~~T., Lou, M., Eldering, A., Shephard, M., Worden, H., Lampel, M., Clough, S., Brown, P.,~~
17 | ~~Rinsland, C., Gunson, M., Beer, R., Tropospheric emission spectrometer: Retrieval method and~~
18 | ~~error analysis, *IEEE Trans. Geosci. Remote. Sens.*, 44, 1297–1307, 2006.~~

19 | Brook, J.R., T.F. Dann, E. Galarneau, D. Herod and J.-P. Charland, (2014), The State of Air
20 | Quality in Canada: National Patterns, in *Air Quality Management, Canadian Perspectives on a*
21 | *Global Issue*, Springer, Dordrecht, ISBN 978-94-007-7557-2, 43-67, doi: 10.1007/978-94-007-
22 | 7557-2

23 | Cai, H., and S. Xie, Estimation of vehicular emission inventories in China from 1980 to 2005,
24 | *Atmos. Environ.*, 44(39), 8963–8979, 2007.

25 | Carmichael, G. R., Y. Tang, G. Kurata, I. Uno, D.G. Streets, J-H Woo, H. Huang, J. Yienger, B.
26 | Lefer, R.E. Shetter, D.R. Blake, E. Atlas, A. Fried, E. Apel, F. Eisele, C. Cantrell, M.A. Avery,
27 | J.D. Barrick, G.W. Sachse, W.L. Brune, S.T. Sandholm, Y. Kondo, H.B. Singh, R.W. Talbot, A.
28 | Bandy, D. Thorton, A.D. Clarke, and B.G. Heikes, Regional-scale chemical transport modeling
29 | in support of intensive field experiments: Overview and analysis of the TRACE-P observations,
30 | *J. Geophys. Res.*, 108(D21), 8823, doi:10.1029/2002JD003117, 2003.

31 | Chameides, W., . L., P.S. Kasibhatla, J. J. Yienger, H . Levy II, and W. J. Moxim, The growth of
32 | continental-scale metro-agro-plexes, regional ozone pollution, and world food production,
33 | *Science*, 264, 74-77, 1994.

1 [Chin, M., D. J. Jacob, J. W. Munger, D. D. Parrish, and B. G. Doddridge, Relationship of ozone](#)
2 [and carbon monoxide over North America, *J. Geophys. Res.*, 99, 14,565–14,573, 1994.](#)

3 Clark H., B. Sauvage, V. Thouret, P. Nédélec, R. Blot, K.Y. Wang, H. Smit, P. Neis, A. Petzold,
4 G. Athier, D. Boulanger, J-M. Cousin, K. Beswick, M. Gallagher, D. Baumgardner, J. Kaiser, J-
5 M. Flaud, A. Wahner, A. Volz-Thomas and J-P. Cammas, The first regular measurements of
6 ozone, carbon monoxide and water vapour in the Pacific UTLS by IAGOS, *Tellus B*, 67, 28385,
7 <http://dx.doi.org/10.3402/tellusb.v67.28385>, 2015.

8 [Conway, T. J., P. P. Tans, L. S. Waterman K., W. Thoning D., R. Kitzis, K. A. Masarie, and N](#)
9 [.Zhang, Evidence for interannual variability of the carbon cycle from the NOAA/CMDL global](#)
10 [air sampling network, *J. Geophys. Res.*, 99, 22,831-22,855, 1994.](#)

11 Crutzen, P. A., A discussion of the chemistry of some minor constituents in the stratosphere and
12 troposphere, *Pure and Applied Geophysics* 106±108, 1385-1399, 1973.

13 [Deeter, M. N. \(2002\), Calculation and Application of MOPITT \(Measurements of Pollution in](#)
14 [the Troposphere\) Averaging Kernels, Available at](#)
15 http://www.acom.ucar.edu/mopitt/data/avg_krnls_app.pdf

16 Deeter, M. N., L. K. Emmons, D. P. Edwards, J. C. Gille, and J. R. Drummond, Vertical
17 resolution and information content of CO profiles retrieved by MOPITT, *Geophys. Res. Lett.*,
18 31, L15112, doi:10.1029/2004GL020235, 2004.

19 [Deeter, M. N., MOPITT \(Measurements of Pollution in the Troposphere\) Validated Version 5](#)
20 [Product User's Guide, National Center for Atmospheric Research. Available at](#)
21 http://www.acom.ucar.edu/mopitt/v5_users_guide_beta.pdf, 2011.

22 [Deeter, M., H.M. Worden, D.P. Edwards, J.C. Gille, and A.E. Andrews: Evaluation of MOPITT](#)
23 [retrievals of lower-tropospheric carbon monoxide over the United States, *J. Geophys. Res.*, 117,](#)
24 [D13306, DOI: 10.1029/2012JD017553, 2012.](#)

25 [Deeter, M. N., Edwards, D. P., Gille, J. C., Emmons, L. K., Francis, G., Ho, S.-P., Mao, D.,](#)
26 [Masters, D., Worden, H., Drummond, J. R., and Novelli, P.: The MOPITT Version 4 CO](#)
27 [Product: Algorithm Enhancements, Validation, and Long-Term Stability, *J. Geophys. Res.*, 115,](#)
28 [D07306, doi:10.1029/2009JD013005, 2010.](#)

29 Deeter, M. N., Martínez-Alonso, S., Edwards, D. P., Emmons, L. K., Gille, J. C., Worden, H. M.,
30 Pittman, J. V., Daube, B. C., and Wofsy, S. C.: Validation of MOPITT Version 5 thermal-
31 infrared, near-infrared, and multispectral carbon monoxide profile retrievals for 2000–2011, *J.*
32 *Geophys. Res.*, 118, 6710–6725, doi:10.1002/jgrd.50272, 2013.

- 1 Deeter, M. N., Martínez-Alonso, S., Edwards, D. P., Emmons, L. K., Gille, J. C., Worden, H. M.,
2 Sweeney, C., Pittman, J. V., Daube, B. C., and Wofsy, S. C.: The MOPITT Version 6 product:
3 algorithm enhancements and validation, *Atmos. Meas. Tech.*, 7, 3623-3632, 2014.
- 4 Ding, K., Liu, J., Ding, A., Liu, Q., Zhao, T. L., Shi, J., Han, Y., Wang, H., Jiang, F.:
5 Uplifting of carbon monoxide from biomass burning and anthropogenic sources to the free
6 troposphere in East Asia, *Atmos. Chem. Phys.* 15, 2843-2866, doi:10.5194/acp-15-2843-2015,
7 2015.
- 8 Draxler, R. R.: HYSPLIT4 user's guide, NOAA Tech. Memo, ERL ARL-230, NOAA Air
9 Resources Laboratory, Silver Spring, MD, 1999.
- 10 Draxler, R.R., Hess, G.D., An overview of the Hysplit_4 modeling system for trajectories,
11 dispersion, and deposition. *Australian Meteorological Magazine* 47, 295–308, 1998.
- 12 Drummond, J. R., and G. S. Mand, The Measurements of Pollution in the Troposphere
13 (MOPITT) instrument: Overall performance and calibration requirements, *J. Atmos. Oceanic*
14 *Technol.*, 13, 314– 320, 1996.
- 15 Edwards, D. P., Lamarque, J.-F., Attié, J.-L., Emmons, L. K., Richter, A., Cammas, J.-P.,
16 Gille, J. C., Francis, G. L., Deeter, M. N., Warner, J., Ziskin, D. C., Lyjak, L. V., Drummond, J.
17 R., and Burrows, J. P.: Tropospheric ozone over the tropical Atlantic: A satellite perspective, *J.*
18 *Geophys. Res.*, 108(D8), 4237, doi:10.1029/2002JD002927, 2003.
- 19 Edwards, D. P., C. Halvorson, and J. C. Gille, Radiative transfer modeling of the EOS Terra
20 Satellite Measurements of Pollution in the Troposphere (MOPITT) instrument, *J. Geophys. Res.*,
21 104, 16,755–16,775, 1999.
- 22 Edwards, D. P., G. Petron, P. C. Novelli, L. K. Emmons, J. C. Gille, and J. R. Drummond,
23 Southern Hemisphere carbon monoxide interannual variability observed by Terra/Measurement
24 of Pollution in the Troposphere (MOPITT), *J. Geophys. Res.*, 111, D16303,
25 doi:10.1029/2006JD007079, 2006.
- 26 Emmons, L. K., D. P. Edwards, M. N. Deeter, J. C. Gille, T. Campos, P. Nedelec, P. Novelli,
27 and G. Sachse, Measurements of Pollution In The Troposphere (MOPITT) validation through
28 2006, *Atmos. Chem. Phys.*, 9, 1795–1803, 2009.
- 29 Emmons, L. K., G. G. Pfister, D. P. Edwards, J. C. Gille, G. Sachse, D. Blake, S. Wofsy, C.
30 Gerbig, D. Matross, and P. Nedelec, Measurements of Pollution in the Troposphere (MOPITT)
31 validation exercises during summer 2004 field campaigns over North America, *J. Geophys. Res.*,
32 112, D12S02, doi:10.1029/2006JD007833, 2007.
- 33 Emmons, L. K., Gille, J. C., Edwards, D. P., Attié, J.-L., Warner, J., Ziskin, D., Francis, G.,
34 Khattatov, B., Yudin, V., Lamarque, J.-F., Ho, S.-P., Mao, D., Chen, J. S., Drummond, J.,

- 1 Novelli, P., Sachse, G., Coffey, M. T., Hannigan, J. W., Gerbig, C., Kawakami, S., Kondo,
2 Y., Takegawa, N., Schlager, H., Baehr, J., Ziereis, H., Validation of Measurements of Pollution
3 in the Troposphere (MOPITT) CO retrievals with aircraft in situ profiles, *J. Geophys. Res.*, 109,
4 D03309, doi:10.1029/2003JD004101, 2004.
- 5 Fishman, J., and Seiler, W., Correlative Nature of Ozone and Carbon Monoxide in the
6 Troposphere: Implications for the Tropospheric Ozone Budget, *J. Geophys. Res.*, 88, C6, 3662-
7 3670, 1983.
- 8 Galanter, M., H. Levy II, and G. R. Carmichael, Impacts of biomass burning on tropospheric CO,
9 NO_x, and O₃, *J. Geophys. Res.*, 105, 6633-6653, 2000.
- 10 Granier, C., Bessagnet, B., Bond, T., D'Angiola, A., v. d. Gon, H. D., Frost, G. J., Heil, A.,
11 Kaiser, J. W., Kinne, S., Klimont, Z., Kloster, S., Lamarque, J.-F., Lioussé, C., Masui, T.,
12 Meleux, F., Mieville, A., Ohara, T., Raut, J.-C., Riahi, K., Schultz, M. G., Smith, S. J., Thomson,
13 A., v. Aardenne, J., v. d. Werf, G. R., and v. Vuuren, D. P.: Evolution of anthropogenic and
14 biomass burning emissions of air pollutants at global and regional scales during the 1980–2010
15 period, *Clim. Change*, 109, 163–190, doi:10.1007/s10584-011-0154-1, 2011.
- 16 Gregg, J. S., R. J. Andres, and G. Marland, China: Emissions pattern of the world leader in CO₂
17 emissions from fossil fuel consumption and cement production, *Geophys. Res. Lett.*, 35, L08806,
18 doi:10.1029/2007GL032887, 2008.
- 19 Heald, C. L., Jacob, D. J., Jones, D. B. A., Palmer, P. I., Logan, J. A., Streets, D. G., Sachse, G.
20 W., Gille, J. C., Hoffman, R. N., and Nehr Korn, T.: Comparative inverse analysis of satellite
21 (MOPITT) and aircraft (TRACE-P) observations to estimate Asian sources of carbon monoxide,
22 *J. Geophys. Res.*, 109, D15S04, doi:10.1029/2004JD005185, 2004.
- 23 Holloway, T., Levy II, H., Kasibhatla, P., Global distribution of carbon monoxide. *J. Geophys.*
24 *Res.*, 105, 12123e12147, 2000.
- 25 Hoor, P., Gurk, C., Brunner, D., Hegglin, M. I., Wernli, H., and Fischer, H.: Seasonality and
26 extent of extratropical TST derived from in-situ CO measurements during SPURT, *Atmos.*
27 *Chem. Phys.*, 4, 1427–1442, 2004.
- 28 Hubler, G., Montzka, D. D., Norton, R. B., Murphy, P. C., Fehsenfeld, F. C., Liu, S. C., Ridley,
29 B. A., Walega, J. G., Atlas, E., Grahek, F. E., Heidt, L. E., Merrill, J., Huebert, B. J., and
30 Bodhaine, B. A.: Total reactive oxidized nitrogen (NO_y) in the remote Pacific troposphere and
31 its correlation with O₃ and CO: Mauna Loa Observatory Photochemistry Experiment 1988, 25, *J.*
32 *Geophys. Res.*, 97, 10 427–10 447, 1992.
- 33 [IPCC, 2013 \(IPCC AR5\): Climate Change 2013: The Physical Science Basis. Contribution of](#)
34 [Working Group I to the Fifth Assessment Report of the Intergovernmental Panel on Climate](#)
35 [Change \[Stocker, T.F., D. Qin, G.-K. Plattner, M. Tignor, S.K. Allen, J. Boschung, A. Nauels, Y.](#)

- 1 [Xia, V. Bex and P.M. Midgley \(eds.\)\]. Cambridge University Press, Cambridge, United](#)
2 [Kingdom and New York, NY, USA, 1535 pp.](#)
- 3 Jacob, D. J., Crawford, J. H., Kleb, M. M., Connors, V. S., Bendura, R. J., Raper, J. L., Sachse,
4 G. W., Gille, J. C., Emmons, L., and Heald, C. L.: Transport and Chemical Evolution over the
5 Pacific (TRACE-P) aircraft mission: Design, execution, and first results, *J. Geophys. Res.*,
6 108(D20), 9000, doi:10.1029/2002JD003276, 2003.
- 7 Jaffe, D.A., R.E. Honrath, L. Zhang, H. Akimoto, A. Shimizu, H. Mukai, K. Murano, S.
8 Hatakeyama, and J. Merrill, Measurements of NO, NO_y, CO, and O₃ and estimation of the
9 ozone production rate at Oki Island, Japan during PEM-West, *J. Geophys. Res.*, 101, 2037-2048,
10 1996.
- 11 Kalnay, E., Kanamitsu, M., Kistler, R., Collins, W., Deaven, D., Gandin, L., Iredell, M., Saha,
12 S., White, G., Woollen, J., Zhu, Y., Leetmaa, A., Reynolds, R., Chelliah, M., Ebisuzaki, W., 30
13 Higgins, W., Janowiak, J., Mo, K. C., Ropelewski, C., Wang, J., Jenne, R., and Joseph, D.: The
14 NCEP/NCAR 40-year reanalysis project, *B. Am. Meteorol. Soc.*, 77, 437–471, 1996.
- 15 Khalil, M. A. K., and R. A. Rasmussen, Carbon monoxide in the Earth's atmosphere: Indications
16 of a global increase, *Nature*, 332, 242-245, 1988.
- 17 Khalil, M. A. K., and R. A. Rasmussen, Global decrease in atmospheric carbon monoxide
18 concentration, *Nature*, 370, 639-641, 1994.
- 19 Kim, P. S., D. J. Jacob, X. Liu, J. X. Warner, K. Yang, K. Chance, V. Thouret, and P. Nedelec,
20 Global ozone–CO correlations from OMI and AIRS: constraints on tropospheric ozone sources,
21 *Atmos. Chem. Phys.*, 13, 9321–9335, 2013.
- 22 Laken, B., Shahbaz, T., Satellite-Detected Carbon Monoxide Pollution during 2000–2012:
23 Examining Global Trends and also Regional Anthropogenic Periods over China, the EU and the
24 USA, *Climate*, 2(1), 1-16; doi:10.3390/cli2010001, 2014.
- 25 [Lang, P.M., L. P. Steele, L. S. Waterman, R. C. Martin, K. A. Masarie, and E. J. Dlugokencky](#)
26 [NO AA/CMDL atmospheric methane data for the period 1983-1990 from shipboard flask](#)
27 [sampling NOAA Tech. Memo., ERL CMDL-4, 88 pp., 1992.](#)
- 28 ~~[Lamarque, J. F., P. G. Hess, and X. X. Tie, Three dimensional model study of the influence of](#)~~
29 ~~[stratosphere–troposphere exchange and its distribution on tropospheric chemistry, *J. Geophys.*](#)~~
30 ~~[Res., 104, 26,363–26,372, 1999](#)~~
- 31 Law, K. S., and J. A. Pyle, Modeling trace gas budgets in the troposphere 2. CH₄ and CO, *J.*
32 *Geophys. Res.*, 98, 18401–18412, doi:10.1029/93JD01480, 1993.
- 33 Lelieveld, J., P. J. Crutzen, V. Ramanathan, M. O. Andreae, C. A. M. Brenninkmeijer, T.
34 Campos, G. R. Cass, R. R. Dickerson, H. Fischer, J. A. de Gouw, A. Hansel, A. Jefferson, D.

1 Kley, A. T. J. de Laat, S. Lal, M. G. Lawrence, J. M. Lobert, O. L. Mayol-Bracero, A. P. Mitra, T.
2 Novakov, S. J. Oltmans, K. A. Prather, T. Reiner, H. Rodhe, H. A. Scheeren, D. Sikka, J.
3 Williams, The Indian Ocean Experiment: Widespread air pollution from south and Southeast
4 Asia, *Science*, 291, 1031–1036, 2001.

5 Liu, G., D. W. Tarasick, V. E. Fioletov, C. E. Sioris, and Y. J. Rochon, Ozone correlation lengths
6 and measurement uncertainties from analysis of historical ozonesonde data in North America and
7 Europe, *J. Geophys. Res.*, 114, D04112, doi:10.1029/2008JD010576, 2009.

8 Liu, G., J. Liu, D. W. Tarasick, V. E. Fioletov, J. Jin, O. Moeini, X. Liu, and C. E. Sioris, A
9 global tropospheric ozone climatology from trajectory-mapped ozone soundings, *Atmos. Chem.*
10 *Phys.* 13, 10659–10675, doi:10.5194/acp-13-10659-2013, 2013.

11 Liu, H., D. J. Jacob, I. Bey, R. M. Yantosca, B. N. Duncan, and G. W. Sachse, Transport
12 pathways for Asian combustion outflow over the Pacific: Interannual and seasonal variations, *J.*
13 *Geophys. Res.*, 108(D20), 8786, doi:10.1029/2002JD003102, 2003.

14 Liu, J., D. W. Tarasick, V. E. Fioletov, C. McLinden, T. Zhao, S. Gong, C. Sioris, J. J. Jin, G.
15 Liu, and O. Moeini, A global ozone climatology from ozone soundings via trajectory mapping: a
16 stratospheric perspective, *Atmos. Chem. Phys. Discuss.*, 13, 16831–16883, 2013.

17 Liu, J., J. R. Drummond, D. B. A. Jones, Z. Cao, H. Bremer, J. Kar, J. Zou, F. Nichitiu, and J. C.
18 Gille, Large horizontal gradients in atmospheric CO at the synoptic scale as seen by spaceborne
19 Measurements of Pollution in the Troposphere, *J. Geophys. Res.*, 111, D02306,
20 doi:10.1029/2005JD006076, 2006.

21 Liu, J., J. R. Drummond, Qinbin Li, John C. Gille, Daniel C. Ziskin, Satellite mapping of CO
22 emission from forest fires in Northwest America using MOPITT measurements, *Remote Sens.*
23 *Environ.*, 95, 502–516, 2005

24 Logan, J. A., M. J. Prather, S.C. Wofsy, and M. B. McElroy, Tropospheric chemistry: A global
25 perspective, *J. Geophys. Res.*, 86, 7210–7254, 1981.

26 Luo, M., C. P. Rinsland, C. D. Rodgers, J. A. Logan, H. Worden, S. Kulawik, A. Eldering, A.
27 Goldman, M. W. Shephard, M. Gunson, and M. Lampel, Comparison of carbon monoxide
28 measurements by TES and MOPITT: Influence of a priori data and instrument characteristics on
29 nadir atmospheric species retrievals, *J. Geophys. Res.*, 112, D09303,
30 doi:10.1029/2006JD007663, 2007.

31 Marengo, A., Thouret, V., Nedelec, P., Smit, H., Helten, M., Kley, D., Karcher, F., Simon, P.,
32 Law, K., Pyle, J., Poschmann, G., Wrede, R. V., Hume, C., and Cook, T.: Measurements of
33 ozone and water vapour by Airbus in-service aircraft: The MOZAIC airborne program, An
34 overview, *J. Geophys. Res.*, 103, 25631–25642, 1998.

- 1 Mauzerall, D. L., D. J. Jacob, S.-M. Fan, J. D. Bradshaw, G. L. Gregory, G. W. Sachse, and D.
2 R. Blake, Origin of tropospheric ozone at remote high northern latitudes in summer, *J. Geophys.*
3 *Res.*, 101, 4175–4188, 1996.
- 4 Mauzerall, D. L., D. Narita, H. Akimoto, L. Horowitz, S. Walters, D. A. Hauglustaine, and G.
5 Brasseur, Seasonal characteristics of tropospheric ozone production and mixing ratios over East
6 Asia: A global three dimensional chemical transport and model analysis, *J. Geophys. Res.*, 105,
7 17,895– 17,910, 2000.
- 8 ~~Mauzerall, D. L., J. A. Logan, D. J. Jacob, B. E. Anderson, D. R. Blake, J. D. Bradshaw, B.~~
9 ~~Heikes, G. W. Sachse, H. Singh, B. Talbot, Photochemistry in biomass burning plumes and~~
10 ~~implications for tropospheric ozone over the tropical South Atlantic, *J. Geophys. Res.*, 103,~~
11 ~~8401– 8423, 1998.~~
- 12 McKee, D. J. (Ed.): Tropospheric Ozone: Human Health and Agricultural Impacts, Boca Raton,
13 Fla.: Lewis Publishers, 39-208, 1993.
- 14 Nedelec P., Cammas J. P., Thouret V., Athier G., Cousin J. M., Legrand C., Abonnel C., Lecoer
15 F., Cayez G. and Marizy C., An Improved Infra-Red Carbon Monoxide Analyser for Routine
16 Measurements aboard Commercial Airbus Aircraft : Technical Validation and First Scientific
17 Results of the MOZAIC III Program, *Atmos. Chem. And Phys.*, Vol. 3, pp 1551-1564, 2003.
- 18 Nédélec P., Thouret V., Brioude J., Sauvage B., and Cammas J.-P., Sthol A. : Extreme CO
19 concentrations in the upper troposphere over North-East Asia in June 2003 from the in-situ
20 MOZAIC aircraft data. *Geophysical Research Letters*, 32, L14807, doi:10.1029/2005GL023141,
21 2005.
- 22 Nédélec, P., R. Blot, D. Boulanger, G. Athier, J.-M. Cousin, B. Gautron, A. Petzold, A. Volz-
23 Thomas and V. Thouret, Instrumentation on commercial aircraft for monitoring the atmospheric
24 composition on a global scale: the IAGOS system, technical overview of ozone and carbon
25 monoxide measurements, *Tellus B*, 67, 27791, <http://dx.doi.org/10.3402/tellusb.v67.27791>,
26 2015.
- 27 [Novelli, P. C., L. P. Steele, and P. P. Tans, Mixing ratios of carbon monoxide in the troposphere,](#)
28 [J. Geophys. Res., 97, 20,731-20,750, 1992.](#)
- 29 Novelli, P. C., K. A. Masarie, P. P. Tans, and P. M. Lang, Recent changes in atmospheric carbon
30 monoxide, *Science*, 263, 1587-1590, 1994.
- 31 Novelli, P. C., K. A. Masarie, P. M. Lang, B. D. Hall, R. C. Myers, and J. W. Elkins, Reanalysis
32 of tropospheric CO trends: Effects of the 1997–1998 wildfires, *J. Geophys. Res.*, 108(D15),
33 4464, doi:10.1029/2002JD003031, 2003.

- 1 Novelli, P.C., Masarie, K.A., Lang, P.M., Distributions and recent changes of carbon monoxide
2 in the lower troposphere, *J. Geophys. Res.*, 103 (D51), 19015–19033, 1998.
- 3 Osman, M., D. W. Tarasick, J. Liu, V. Thouret, V. E. Fioletov, O. Moeini, C. McLinden, C.
4 Sioris, M. Parrington and P. Nédélec: Ozone climatology derived from the Trajectory Mapping
5 of Global aircraft (MOZAIC-IAGOS), satellite (ACE-FTS, SAGE) and extended ozonesonde
6 data, in preparation, [20152016](#).
- 7 Pan, L. L., Konopka, P., and Browell, E. V.: Observations and model simulations of mixing near
8 the extratropical tropopause, *J. Geophys. Res.*, 111(D05106), doi:10.1029/2005JD006480, 2006.
- 9 ~~Parrish, D. D., Carbon monoxide and light alkanes at tropospheric tracers of anthropogenic
10 ozone, *The Tropospheric Chemistry of Ozone in the Polar Regions*, edited by H. Niki and K.H.
11 Becker, 155–169, Springer Verlag, Berlin, 1993.~~
- 12 ~~Parrish, D. D., J. S. Holloway, M. Trainer, P. C. Murphy, G. L. Forbes, and F. C. Fehsenfeld,
13 Export of North American ozone pollution to the North Atlantic Ocean, *Science*, 259, 1436–
14 1439, 1993.~~
- 15 Parrish, D. D., M. Trainer, J. S. Holloway, J. E. Yee, M. S. Warshawsky, F. C. Fehsenfeld, G. L.
16 Forbes, and J. L. Moody, Relationships between ozone and carbon monoxide at surface sites in
17 the North Atlantic region, *J. Geophys. Res.*, 103, 13,357– 13,376, 1998.
- 18 Parrish, D. D., M. Trainer, M.P. Buhr, B. A. Watkins, and F. C. Fehsenfeld, Carbon monoxide
19 concentrations and their relation to concentrations of total reactive oxidized nitrogen at two rural
20 U.S. sites, *J. Geophys. Res.*, 96, 9309–9320, 1991.
- 21 Petetin, H., Thouret, V., Fontaine, A., Sauvage, B., Athier, G., Blot, R., Boulanger, D., Cousin,
22 J.-M., and Nedelec, P.: Characterizing tropospheric ozone and CO around Frankfurt between
23 1994–2012 based on MOZAIC-IAGOS aircraft measurements, *Atmos. Chem. Phys. Discuss.*,
24 15, 23841–23891, doi:10.5194/acpd-15-23841-2015, 2015.
- 25 Petzold, A., V. Thouret, C. Gerbig, A. Zahn, C.A.M. Brenninkmeijer, M. Gallagher, M.
26 Hermann, M. Pontaud, H. Ziereis, D. Boulanger, J. Marshall, P. Nédélec, H.G.J. Smit, U. Frieß,
27 J.-M. Flaud, A. Wahner, J.-P. Cammas, A. Volz-Thomas, and IAGOS Team., Global-scale
28 atmosphere monitoring by in-service aircraft – current achievements and future prospects of the
29 European research infrastructure IAGOS. *Tellus B*, 67,
30 <http://dx.doi.org/10.3402/tellusb.v67.28452>, 2015.
- 31 Ploeger, F., Konopka, P., Günther, G., Groß, J.-U., and Müller, R.: Impact of the vertical
32 velocity scheme on modeling transport across the tropical tropopause layer, *J. Geophys. Res.*,
33 115, D03301, doi: 10.1029/2009JD012023, 2010.

- 1 Ploeger, F., Konopka, P., M'uller, R., G'unther, G., Grooß, J.-U., Schiller, C., Ravegnani, F.,
2 Ulanovski, A., and Riese, M.: Backtrajectory reconstruction of water vapour and ozone in-situ
3 observations in the TTL, Meteorol. Z., 21(3), 239–244, 2012.
- 4 Pommrich, R., M'uller, R., Grooß, J.-U., Konopka, P., Ploeger, F., Vogel, B., Tao, M., Hoppe,
5 C. M., G'unther, G., Spelten, N., Hoffmann, L., Pumphrey, H.-C., Viciani, S., D'Amato, F.,
6 Volk, C. M., Hoor, P., Schlager, H., and Riese, M.: Tropical troposphere to stratosphere transport
7 of carbon monoxide and long-lived trace species in the Chemical Lagrangian Model of the
8 Stratosphere (CLaMS), Geosci. Model Dev., 7, 2895–2916, doi:10.5194/gmd-7-2895-2014,
9 2014.
- 10 Reichle, H. G., Jr., H. G. Reichle Jr., B. E. Anderson, V. S. Connors, T. C. Denkins, D. A.
11 Forbes, B. B. Gormsen, R. L. Langenfelds, D. O. Neil, S. R. Nolf, P. C. Novelli, N. S.
12 Pougatchev, M. M. Roell, L. P. Steele., Space shuttle based global CO measurements during
13 April and October 1994, MAPS instrument, data reduction, and data validation, J. Geophys.
14 Res., 104, 21,443–21,454, 1999.
- 15 Reichle, H. G., Jr., V. S. Connors, J. A. Holland, R. T. Sherrill, H. A. Wallio, J. C. Casas, E. P.
16 Condon, B. B. Gormsen, W. Seiler, The distribution of middle tropospheric carbon monoxide
17 during early October 1984, J. Geophys. Res., 95(D7), 9845-9856, 1990.
- 18 Rinsland, C .P., and J.S. Levine, Free tropospheric carbon monoxide concentrations in 1950 and
19 1951 deduced from infrared total column amount measurements, Nature, 318, 250-254, 1985.
- 20 Rinsland, C. P., Jones, N. B., Connor, B. J., Wood, S. W., Goldman, A., Stephen, T. M.,
21 Murcray, F. J., Chiou, L. S., Zander, R. & Mahieu, E., Multiyear infrared solar spectroscopic
22 measurements of HCN, CO, C2H6, and C2H2 tropospheric columns above Lauder, New Zealand
23 (45 S Latitude). J. Geophys. Res., 107 (D14), 1-12, 2002.
- 24 Rodgers, C. D., Inverse Methods for Atmospheric Sounding: Theory and Practice, World Sci.,
25 Hackensack, N. J., 2000.
- 26 ~~Roelofs, G. J., and J. Lelieveld, Model study of the influence of cross tropopause O3 transports~~
27 ~~on tropospheric O3 levels, Tellus, 49B, 38–55, 1997.~~
- 28 -Sauvage B., V. Thouret, J.-P. Cammas, F. Gheusi, G. Athier, P. Nédélec, Tropospheric ozone
29 over Equatorial Africa : regional aspects from the MOZAIC data. Atmospheric Chemistry and
30 Physics, Vol. 5, pp 311-335, 2005.
- 31 Sauvage, B., F. Gheusi, V. Thouret, J.-P. Cammas, J. Duron, J. Escobar, C. Mari, P. Mascart, and
32 V. Pont, Medium-range mid-tropospheric transport of ozone and precursors over Africa: two
33 numerical case-studies in dry and wet seasons, Atmos. Chem. Phys., 7, 5357-5370, 2007.

1 Schoeberl, M. R., Douglass, A. R., Zhu, Z. X., and Pawson, S.: A comparison of the lower
2 stratospheric age spectra derived from a general circulation model and two data assimilation
3 systems, *J. Geophys. Res.*, 108, 4113, DOI: 10.1029/2002JD002652, 2003.

4 Shindell, D.T., G. Faluvegi, D.S. Stevenson, M.C. Krol, L.K. Emmons, J.-F. Lamarque, G.
5 Pétron, F.J. Dentener, K. Ellingsen, M.G. Schultz, O. Wild, M. Amann, C.S. Atherton, D.J.
6 Bergmann, I. Bey, T. Butler, J. Cofala, W.J. Collins, R.G. Derwent, R.M. Doherty, J. Drevet,
7 H.J. Eskes, A.M. Fiore, M. Gauss, D.A. Hauglustaine, L.W. Horowitz, I.S.A. Isaksen, M.G.
8 Lawrence, V. Montanaro, J.-F. Müller, G. Pitari, M.J. Prather, J.A. Pyle, S. Rast, J.M.
9 Rodriguez, M.G. Sanderson, N.H. Savage, S.E. Strahan, K. Sudo, S. Szopa, N. Unger, T.P.C.
10 van Noije, and G. Zeng, Multi-model simulations of carbon monoxide: Comparison with
11 observations and projected near-future changes. *J. Geophys. Res.*, 111, D19306,
12 doi:10.1029/2006JD007100, 2006.

13 Stein, O., M. G. Schultz, I. Bouarar, H. Clark, V. Huijnen, A. Gaudel, M. George, and C.
14 Clerbaux, On the wintertime low bias of Northern Hemisphere carbon monoxide found in global
15 model simulations, *Atmos. Chem. Phys.*, 14, 9295–9316, 2014.

16 Stohl, A. and Seibert, P., Accuracy of trajectories as determined from the conservation of
17 meteorological tracers, *Q. J. R. Meteorol. Soc.*, 125: 1465–1484, 1998.

18 Stohl, A., Computation, accuracy and applications of trajectories - review and bibliography,
19 *Atmos. Environ.* 32, 947-966, 1998.

20 Stohl, A., James, P., Forster, C., and Spichtinger, N.: An extension of Measurement of Ozone
21 and Water Vapour by Airbus-In-service aircraft (MOZAIC) ozone climatologies using trajectory
22 statistics, *J. Geophys. Res.*, 106, D21, 27,757-27,768, doi:10.1029/2001JD000749, 2001.

23 Tan, Q., Chameides, W. L., Streets, D., Wang, T., Xu, J., Bergin, M., and Woo, J.: An evaluation
24 of TRACE-P emission inventories from China using a regional model and chemical
25 measurements, *J. Geophys. Res.*, 109, D22305, doi:10.1029/2004JD005071, 2004.

26 Tarasick, D. W., Jin, J. J., Fioletov, V. E., Liu, G., Tompson, A. M., Oltmans, S. J., Liu, J.,
27 Sioris, C. E., Liu, X., Cooper, O. R., Dann, T., and Thouret, V.: High-resolution tropospheric
28 ozone fields for INTEX and ARCTAS from IONS ozonesondes, *J. Geophys. Res.*, 115, D20301,
29 doi:10.1029/2009JD012918, 2010.

30 Thompson, A. M.: The oxidizing capacity of the Earth's atmosphere-Probable past and future
31 changes, *Science*, 256, 1157–1165, doi:10.1126/science.256.5060.1157, 1992.

32 Tie, X., G. P. Brasseur, C. Zhao, C. Granier, S. Massie, Y. Qin, P. Wang, G. Wang, P. Yang, A.
33 Richterg, Chemical characterization of air pollution in eastern China and the eastern United
34 States, *Atmos. Environ.*, 40, 2607–2625, 2006.

- 1 Vogel, B., Pan, L. L., Konopka, P., Günther, G., Müller, R., Hall, W., Campos, T., Pollack, I.,
2 Weinheimer, A., Wei, J., Atlas, E. L., and Bowman, K. P.: Transport pathways and signatures of
3 mixing in the extratropical tropopause region derived from Lagrangian model simulations, *J.*
4 *Geophys. Res.*, 116, D05306, doi:10.1029/2010JD014876, 2011.
- 5 Volz-Thomas A., Berg M., Heil T., Houben N., Lerner A., Petrick W., Raak D., Pätz H. -W.,
6 Measurements of total odd nitrogen (NO_y) aboard MOZAIC in-service aircraft: instrument
7 design, operation and performance, *Atmospheric Chemistry and Physics*, Vol. 5, pp 583-595,
8 2005
- 9 ~~Voulgarakis, A., P.J. Telford, A.M. Aghedo, P. Braesicke, G. Faluvegi, N.L. Abraham, K.W.~~
10 ~~Bowman, J.A. Pyle, and D.T. Shindell: Global multi year O₃ CO correlation patterns from~~
11 ~~models and TES satellite observations. *Atmos. Chem. Phys.*, 11, 5819–5838, doi:10.5194/acp-11-~~
12 ~~5819-2011, 2011.~~
- 13 Wang, T., K. S. Lam, L. Y. Chan, M. A. Carroll, A. S.Y. Lee, Trace gas measurements in coastal
14 Hong Kong during the PEM-WEST (B), *J. Geophys. Res.* Vol. 102, 28,575-28,588, 1997.
- 15 Wang, T., M. A. Carroll, G. M. Alber, K. R. Owens, K. A. Duderstadt, and A. Markevitch, D.
16 Parrish, J. Holloway, and F. C. Fehsenfeld, G. Forbes and J. Ogren, Ground-based measurements
17 of NO_x and total reactive oxidized Nitrogen (NO_y) at Sable Island, Nova Scotia during the
18 NARE 1993 Summer Intensive, *J. Geophys. Res.*, 101, 28,991-29,004, 1996
- 19 Wang, Y. X., McElroy, M. B., Wang, T., and Palmer, P. I.: Asian emissions of CO and NO_x:
20 Constraints from aircraft and Chinese station data, *J. Geophys. Res.*, 109, D24304,
21 doi:10.1029/2004JD005250, 2004.
- 22 [WHO, Air quality guidelines for Europe, 2nd ed. Copenhagen, World Health Organization](#)
23 [Regional Office for Europe, 2000 \(WHO Regional Publications, European Series No. 91\), 2000](#)
- 24 [Worden, H. M., Deeter, M. N., Edwards, D. P., Gille, J. C., Drummond, J. R., and Nedelec, P.](#)
25 [P.: Observations of near-surface carbon monoxide from space using MOPITT multispectral](#)
26 [retrievals, *J. Geophys. Res.*, 115, D18314, doi:10.1029/2010JD014242, 2010.](#)
- 27 Worden, H. M., M. N. Deeter, C. Frankenberg, M. George, F. Nichitiu, J. Worden, I. Aben, K.
28 W. Bowman, C. Clerbaux, P. F. Coheur, A. T. J. de Laat, R. Detweiler, J. R. Drummond, D. P.
29 Edwards, J. C. Gille, D. Hurtmans, M. Luo, S. Martínez-Alonso, S. Massie, G. Pfister, and J. X.
30 Warner,, Decadal record of satellite carbon monoxide observations, *Atmos. Chem. Phys.*, 13,
31 837–850, doi:10.5194/acp-13-837-2013, 2013.
- 32 Yurganov, L. N., McMillan, W., Dzhola, A. V., Grechko, E. I., Jones, N. B. & van der Werf, G.
33 R., Global AIRS and MOPITT CO measurements: validation, comparison, and links to biomass
34 burning variations and carbon cycle. *J. Geophys. Res.*, 113 (D9), 1-14, 2008).

1 ~~Zahn, A., C. A. M. Brenninkmeijer, W. A. H. Asman, P. J. Crutzen, G. Heinrich, H. Fischer, J.~~
2 ~~W. M. Cuijpers, and P. F. J. van Velthoven, Budgets of O₃ and CO in the upper troposphere:~~
3 ~~CARIBIC passenger aircraft results 1997–2001, J. Geophys. Res., 107(D17), 4337,~~
4 ~~doi:10.1029/2001JD001529, 2002.~~

5 Zander, R., P. Demoulin, D.H. Ehhalt, U. Schmidt, and C.P. Rinsland, Secular increase of the
6 total vertical column abundance of carbon monoxide above central Europe since 1950, J.
7 Geophys. Res., 94, 11, 021-11,028, 1989.

8 ~~Zbinden, R. M., V. Thouret, P. Ricaud, F. Carminat¹, J.-P. Cammas, P. Nédélec, Climatology of~~
9 ~~pure tropospheric profiles and column contents of ozone and carbon monoxide using MOZAIC~~
10 ~~in the mid-northern latitudes (24° N to 50° N) from 1994 to 2009, doi:10.5194/acp-13-12363-~~
11 ~~2013, 2013.~~

12 Zeng, G., Wood, S. W., Morgenstern, O., Jones, N. B., Robinson, J. & Smale, D., Trends and
13 variations in CO, C₂H₆, and HCN in the Southern Hemisphere point to the declining
14 anthropogenic emissions of CO and C₂H₆, Atmos. Chem. Phys., 12 (16), 7543-7555, 2012.

15 ~~Zhang, L., Jacob, D. J., Boersma, K. F., Jaffe, D. A., Olson, J. R., Bowman, K. W., Worden, J.~~
16 ~~R., Thompson, A. M., Avery, M. A., Cohen, R. C., Dibb, J. E., Flock, F. M., Fuelberg, H. E.,~~
17 ~~Huey, L. G., McMillan, W. W., Singh, H. B., and Weinheimer, A. J.: Transpacific transport of~~
18 ~~ozone pollution and the effect of recent Asian emission increases on air quality in North~~
19 ~~America: an integrated analysis using satellite, aircraft, ozonesonde, and surface observations,~~
20 ~~Atmos. Chem. Phys., 8, 6117–6136, doi:10.5194/acp-8-6117-2008, 2008.~~

21 Zhang, L., Jacob, D. J., Liu, X., Logan, J. A., Chance, K., Eldering, A., and Bojkov, B. R.:
22 Intercomparison methods for satellite measurements of atmospheric composition: application to
23 tropospheric ozone from TES and OMI, Atmos. Chem. Phys., 10, 4725–4739, doi:10.5194/acp-
24 10-4725-2010, 2010.

25